

Synoptic Systems

Lead authors: Rosalind Cornforth^a, Zilore Mumba^b and Douglas J. Parker^f

Contributing authors: Gareth Berry^d, Nicolas Chapelon^e, Kone Diakaria^f, Mariane Diop^g, Kane^g, Volker Ermert^h, Andreas H. Finkⁱ, Peter Knippertzⁱ, Jean Philippe Laforeⁱ, Arlene Laing^k, Serge Lepape^e, Ross Maidment^m, John Methvenⁿ, Ben Orji^o, David Osika^p, Emmanuel Poan^j, Rémy Roca^f, Simon Rowellⁿ, Roger Smith^t, Thomas Spengler^u, Christopher M. Taylor^v, Chris Thorncroft^w, Jean^x Christoph Vincendon^e and Charles Yorke^p

Reviewer: Chris Thorncroft (University at Albany, State University of New York, USA)

^a Walker Institute, University of Reading, Reading, UK

^b Department of Mathematics and Statistics, University of Zambia, Lusaka, Zambia

^c School of Earth and Environment, University of Leeds, Leeds, UK

^d School of Mathematical Sciences, Monash University, Clayton, VIC, Australia

^e Commandement Interarmées de l'Espace (CISMF), Institut National Polytechnique de Toulouse (INP^xToulouse), Toulouse, France

^f Agence pour la Sécurité de la Navigation Aérienne en Afrique et à Madagascar (ASECNA), Abidjan, Côte d'Ivoire

^g Agence Nationale de l'Aviation Civile et de la Météorologie du Sénégal (ANACIM), Dakar, Sénégal

^h Institute of Geophysics and Meteorology, University of Cologne, Cologne, Germany

ⁱ Institute of Meteorology and Climate Research, Karlsruhe Institute for Technology, Karlsruhe, Germany

^j Centre National de Recherches Météorologiques (CNRM-UMR3589), Météo^xFrance and CNRS, Toulouse, France

^k Cooperative Institute for Research in the Atmosphere (CIRA), Colorado State University, Fort Collins, Colorado, USA

^m TAMSAT, Department of Meteorology, University of Reading, Reading, UK

ⁿ Department of Meteorology, University of Reading, Reading, UK

^o Regional Training Centre, Nigerian Meteorological Agency, Oshodi^xLagos, Nigeria

^p Ghana Meteorological Agency, Accra, Ghana

^q LMD/IPSL, CNRS, Université Pierre et Marie Curie, Paris, France

^r Meteorological Institute, University of Munich, Munich, Germany

^s Geophysical Institute, University of Bergen and Bjerknes Centre for Climate Research, Bergen, Norway

^t Centre for Ecology and Hydrology, Wallingford, UK

^u Atmospheric and Environmental Sciences, University at Albany, SUNY, Albany, NY, USA

2.1 Scientific Background

2.1.1 Introduction

The synoptic meteorology of West Africa has been studied for many decades. Since the 1930s at least, it has been known that coherent synoptic weather systems exist in the region, in the form of African easterly waves (AEWs; e.g. Piersig, 1944[1936]). More recently we have developed synoptic models of the Saharan heat low (SHL; e.g. Rácz and Smith, 1999; Parker *et al.*, 2005b; Lavaysse *et al.*, 2010, 2011; Smith and Spengler, 2011), the intertropical discontinuity (ITD; Flamant *et al.*, 2007), and various kinds of waves (e.g. Thorncroft and Hoskins, 1994; Mounier *et al.*, 2007; Mekonnen and Rossow, 2011; Ventrice and Thorncroft, 2013; Wu *et al.*, 2013) and vortices in the region (e.g. Tyner and Aiyer, 2012). Understanding such coherent weather systems, which evolve in a familiar pattern over periods of a couple

of days, helps the analysis and forecasting of the weather (Davis *et al.*, 2012). However, unlike mid-latitude regions, in West Africa the rainfall, dominated by cumulonimbus rainstorms, tends to be much less closely controlled by the prevailing synoptic conditions, being more strongly conditioned by the diurnal cycle of stability (e.g. Laing *et al.*, 2008; Bouniol *et al.*, 2012) and the land-surface forcing. Because rainfall is controlled by a combination of synoptic state, time of day and surface forcing, the relationships between synoptic state and rainfall can be difficult to evaluate (e.g. Hsieh and Cook, 2005; Cornforth *et al.*, 2009; Poan *et al.*, 2015). Probably for these reasons, the description of some aspects of the synoptic meteorology remains incomplete, in the literature and in teaching. Recent years have seen substantial progress, not least through the enhanced observational efforts and related modelling and forecasting improvements achieved during the African Monsoon Multidisciplinary Analysis

(AMMA) field campaigns (e.g. Janicot *et al.*, 2008; Lebel *et al.*, 2010; Lafore *et al.*, 2011). Here, we present a consensus of current thinking on synoptic weather systems in West Africa.

Synoptic meteorology is an important area of weather forecasting in West Africa, where the role of the human forecaster is particularly important (Fink *et al.*, 2011), relative to numerical model forecasts. From the enhanced observations of the AMMA period, we know that numerical weather prediction (NWP) models have some useful skill in representing the synoptic state over West Africa, but we also know that there remain some gross errors, notably in the representation of rainfall (e.g. Diallo *et al.*, 2014). Through a knowledge of synoptic dynamics and conceptual models, the forecaster can use NWP products alongside observations, to improve the quality of short-range forecasts in their region.

On any given day, the synoptic conditions are determined by a combination of remote atmospheric dynamics, subseasonal patterns such as Kelvin waves, regional circulations, and local responses of the weather to the synoptic state (e.g. Mekonnen and Rossow, 2011). In this chapter we focus on discussing the synoptic circulations that occur within the West Africa region, encompassing scales of a few thousand kilometres, and on timescales of 1–10 days. The larger scale circulations controlling the synoptic environment, and their seasonal variations, have already been introduced, in Chapter 1. Convectively coupled Kelvin waves also fall within this 1–10-day timescale, but are discussed in Section 7.1.4. The specific weather patterns developed within a given synoptic state are discussed in Chapters 3, 4 and 5, which address convective rainfall, local weather and atmospheric dust respectively. Here, in this chapter, we begin by presenting synoptic features on the continental scale, which drive variability. In particular, we introduce those features that need to be analysed by a forecaster on a day-to-day basis; rules for plotting the features on a synoptic chart are presented in Chapter 11. The SHL is just such a feature. The variability of the SHL influences synoptic dynamics in West Africa, as well as the occurrence of wind-blown dust; we also discuss the structure of the African easterly jet (AEJ) and the monsoon layer. In Section 2.1.3 we then address the most important synoptic patterns in this region – AEWs, extratropical wave intrusions and Guinea Coast weather systems.

2.1.2 Continental-scale Synoptic Features

The continental-scale features that have been introduced in Chapter 1 show significant synoptic variability. As explained in Chapter 11, these features are vitally important to plot on a synoptic chart. It is important for forecasters to be aware of how these features vary on intraseasonal and diurnal timescales. Subseasonal

variability in these features is particularly important because of the associated change in environment that supports or interacts with known synoptic disturbances. Diurnal variability in the continental-scale features is important as this can significantly impact the nature and impact of the known synoptic disturbances on local weather.

2.1.2.1 Saharan Heat Low

Heat lows and heat troughs are prominent climatological features in many arid land areas of the world during the warmer months, especially in low latitudes where insolation is at its peak. Such regions include the Saudi Arabian Peninsula, northwestern and northeastern Australia, northern and southwestern Africa, West Pakistan and northern India, the Qinghai-Xizang plateau in China, southwestern North America and the Iberian Peninsula. Some authors refer to these systems as thermal lows or thermal troughs. One of the most prominent examples is the summer heat low over the Sahara Desert. Although the SHL lies in the extreme north of the West African region in summer, its dynamics and intraseasonal variability are very important in their influence on the region's diurnal and synoptic circulations.

Heat lows are warm-cored, surface-based low pressure systems situated over land, and are generally contained within the lower troposphere below about 600 hPa. The theoretical study by Rácz and Smith (1999) used an idealised model to understand the essential dynamical features of a continental-scale heat low that forms over an idealised land mass, when that region is subjected to a diurnal cycle of heating and cooling. It was shown that many of the basic features of observed heat-low circulations, such as the effects associated with the coastal sea breezes and the nocturnal low-level jet, are explained by the diurnal cycle of boundary layer stability (Section 4.1.3). These concepts have been found subsequently to explain important aspects of the West African monsoon (WAM) system and the SHL (Parker *et al.*, 2005b; Lothon *et al.*, 2008; Grams *et al.*, 2010; Schuster *et al.*, 2013).

Some of the key features of the SHL can be gleaned from Figure 2.1 (see also Figure 1.33), which shows selected time-mean fields for the June–July–August season during the period from 1989 until 2009. The SHL is evident as an area of low mean sea-level pressure (MSLP) (Figure 2.1a) centred at about 22°N, 3°W. The heat low is discernible in the 850 hPa and 2 m temperature fields also (Figure 2.1b and c respectively), with maxima coinciding approximately with the local pressure minimum. The low is bounded by mountain ranges to the north (Atlas) and east (Ahaggar), and by the Atlantic Ocean to the west (see Figure 2.1d). It is reasonable to surmise that the occurrence of the heat low in that area is a result of the interplay between the orography as well as distribution of sea surface temperature (SST) and the prevailing broad-scale flow conditions.

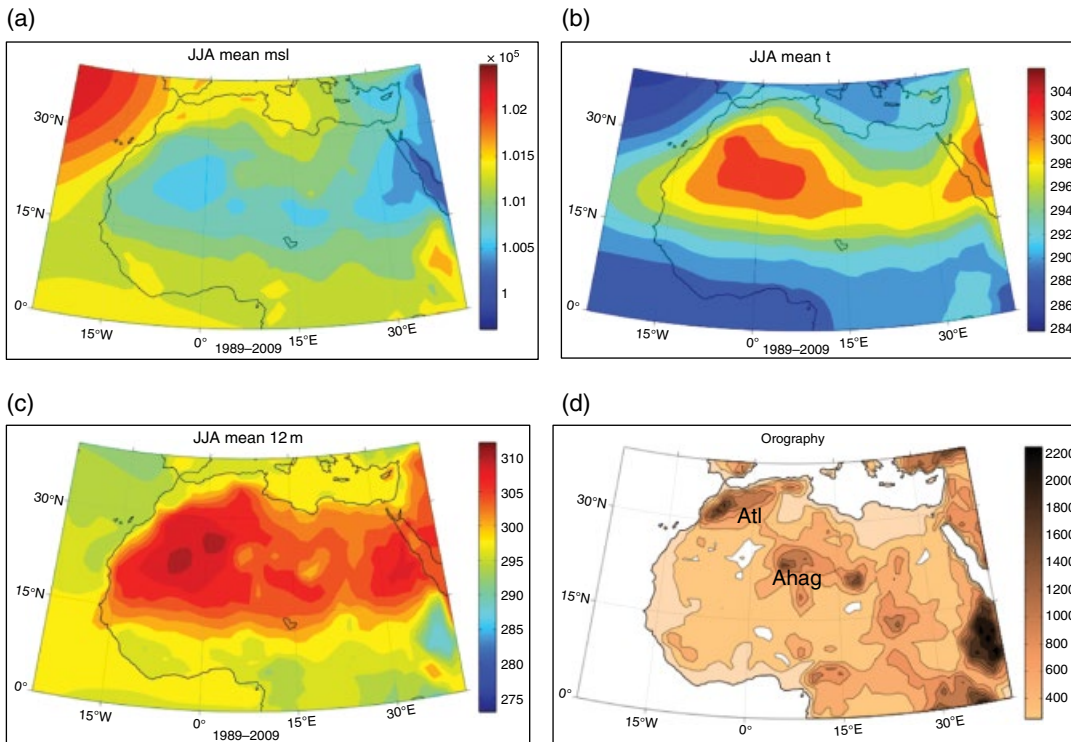


Figure 2.1 Characteristics of the SHL seen in ECMWF ERA Interim climatological mean (1989–2009) fields for June–July–August for (a) mean sea level pressure (MSLP), (b) temperature at 850 hPa, (c) 2 m temperature and (d) orographic height.

On subseasonal and synoptic timescales, the SHL migrates around the location shown in Figure 2.1 (Lavaysse *et al.*, 2009) and pulsates in strength (Lavaysse *et al.*, 2010) as it interacts with mid-latitude weather systems (Thorncroft and Flocas, 1997; Chauvin *et al.*, 2010; Roehrig *et al.*, 2011; see Section 7.1.5.1).

A prominent feature of idealised models of the heat low is the large diurnal variation in the low-level cyclonic circulation, as found by Rácz and Smith (1999) and Spengler *et al.* (2005). The mean winds are relatively calm throughout the day, while the growth of a nocturnal low-level jet leads to strong convergence and the formation of a super-geostrophic low-level cyclonic circulation during the night. Under the influence of large-scale background flows the nocturnal convergent flow can also be strongly frontogenetic (Spengler *et al.*, 2005) and, therefore, may contribute to the nocturnal intensification of the intertropical front (ITF). The formation of the cyclonic circulation can be understood through the inertial turning of the unbalanced low-level flow toward the low-pressure centre (e.g. see Blackadar (1957); Section 4.1.3.2). Therefore, while the minimum surface pressure in the idealised model occurs at 1700h, the maximum tangential wind speed at low levels is attained around 0530h and the minimum at 1600h. Although the surface low is most intense in late afternoon, the cyclonic winds weaken during the daytime and restrengthen again at night. The behaviour at low

levels is in stark contrast to that aloft, where there is almost no diurnal variation in the strength of the anticyclone (less than 2 m s^{-1}).

The nocturnal low-level jet can yield high values of vertical low-level shear that might be hazardous for air traffic (Sections 4.1.3.2 and 6.2.3). Over northern Africa, the effect of a nocturnal increase of the low-level convergence is also important for the advection of moisture into the Sahel region (Parker *et al.*, 2005b; Lothon *et al.*, 2008), particularly during the monsoon onset period in June.

The diurnal variability at low levels is in contrast to the quasi-stationary flow behaviour at the mid to upper tropospheric levels (Spengler and Smith, 2008). The low-level cyclone is surmounted by an upper-level anticyclone in the upper levels of the Saharan boundary layer, around 700–500 hPa. The anticyclone is associated with the divergent branch of the overturning circulation due to the warm Saharan boundary layer, in conjunction with the approximate conservation of absolute angular momentum. The anticyclone extends through much of the troposphere, but has its maximum strength in the lower troposphere in the upper levels of the Saharan boundary layer. To the south of the SHL, the easterly winds associated with this anticyclonic circulation correspond to the AEJ. Thorncroft and Blackburn (1999) stressed the importance of the mean state of the SHL on the AEJ.

Forecasters in the Sahel and Guinea Coast zone often look to the synoptic station temperatures in Mauritania, Mali and Niger as indicators of a likely strengthening of the monsoon circulation in subsequent days, due to stronger south–north temperature and pressure gradients. Practice has been confirmed by theory – Parker *et al.* (2005b) confirmed that the strength of the thermal anomalies in the heat low region is correlated with strengthening nocturnal monsoon winds further south.

Further impacts of the variability of the SHL have been shown by Chauvin *et al.* (2010) and Roehrig *et al.* (2011). On timescales of 10–25 days, variability in the SHL (with some extratropical influences) can be strongly related to subsequent anomalies of rainfall in the Sahel about 5 days later. ‘Ventilation’ of the SHL by cool advection from the Mediterranean can weaken the Sahelian pressure gradient and reduce subsequent rainfall over the Sahel.

Ventilation (see Chou *et al.* (2001)) of the heat low can occur from all of its flanks, in association with different kinds of weather systems. For instance, Grams *et al.* (2010) showed how a synoptically varying ‘Atlantic inflow’ around Mauritania and Sénégal interacts with the strength of the SHL in this western region, while convective cold pools emerging from storms over the Atlas Mountains of Morocco commonly bring cool air into the desert from the northwest. The interaction between the SHL and the cool ventilation from the south, in the monsoon flow and in embedded convective cold pools within the monsoon is of particular dynamical interest, as described in Section 2.1.2.2. Observations and data-assimilation results (Garcia-Carreras *et al.*, 2013) and model sensitivity studies (Marsham *et al.*, 2013) are consistent in showing that the convective cold pools from within the monsoon make a substantial contribution to the thermodynamic budget of the SHL. This raises an important possibility of feedback between the SHL and the monsoon. An intense SHL leads, for example, to a stronger monsoon circulation and increased convection in the Sahel in the subsequent days. The result of this convection is to drive stronger cold pools, which then act to ventilate the Saharan boundary layer. The relationship between these processes, which are not well captured in general circulation models (GCMs), remains an interesting area of research. Some of these mechanisms are discussed in more detail in Section 7.1.6.

2.1.2.2 The Intertropical Discontinuity or Intertropical Front

The ITD or ITF (henceforward ITD) is a zone of confluence of the winds, and an air-mass boundary, which separates the hot, dry Saharan air from the cooler, moist monsoonal air in the spring and summer months. Despite its name, the ITD is neither a true discontinuity nor a simple ‘front’, because it has a very mobile and dynamic structure, related to the diurnal variability of

‘zone B’ in the mean climatic section (Section 1.1 and Figure 1.1). It is one of the key features used by forecasters to analyse the state of the monsoon on a synoptic chart, since it maps the northward extent of the moist monsoon air (Figure 1.1, and guidance in Section 11.2 for plotting this feature).

On a daily basis the ITD is governed by the same physical processes that control the heat low. At night, when boundary-layer mixing is very weak, the cool monsoonal air to the south of the ITD accelerates northward, into the low pressure of the heat low. This means that the ITD can surge northward by several hundred kilometres overnight. Stations in the northern Sahel/southern Sahara that have experienced a hot, dry afternoon with light winds can experience cooler, moister winds with a southerly component arriving overnight. The nocturnal surge of the ITD also tends to involve a sharpening of its front, into a form of gravity current (see Section 4.1.4), which can be strong enough to lift dust and reduce visibility (Bou Karam *et al.*, 2008). The nocturnal surge of the ITD is followed by a rather shallow monsoon layer, perhaps 1000 m deep, resembling a gravity current.

During the following day, the air in the shallow monsoon layer is mixed by dry convection in the boundary layer, and eventually through the morning and into the afternoon will be mixed into the residual Saharan boundary layer (or Saharan air layer (SAL)). This cycle brings moisture into the southern margins of the Sahara. Temperature increases and humidity decreases at stations in the southern Sahara, as the cool moist monsoonal air becomes mixed with the hot and dry SAL, and conversely the SAL is moistened by this process, so that altocumulus clouds are common at the top of the SAL, around 550 hPa (Parker *et al.*, 2005a; Stein *et al.*, 2011). The dry convective mixing weakens the daytime winds, so that they become relatively light and typically gain a northeasterly component through mixing with the SAL winds.

As the day proceeds, the ITD diagnosed in synoptic station data retreats southward – the cool, moist air is mixed up with Saharan air from above, and the confluence zone also moves southward as the winds in the northern region become more northerly. It is important to realise that the southward retreat of the ITD during the day is not a material process – the air itself is not moving southward at this time – but a process due to the change in the thermodynamic characteristics of the air to the south of the ITD as it is mixed up, and changes from ‘monsoonal’ to more ‘Saharan’. This is in contrast to the nocturnal ITD surge, when air moves materially northward at low levels.

The dynamical nature of the ITD is further complicated by the role of convective cold pools, emerging from convective storms in the monsoon air to the south of the ITD. These cold pools are generated by evaporative cooling of precipitation within the storms (Section 3.1.2.2)

and also propagate as gravity currents. The convective cold pools commonly surge northward, in the late afternoon and overnight, travelling several hundred kilometres. As the cold pools enter the ITD region, they tend to merge with the ITD itself (which may be forming a sharp front around this time anyway) and then be indistinguishable from the ITD in routine observations (Flamant *et al.*, 2007, 2009; Marsham *et al.*, 2008). Thus, we see that when deep convective storms are active just to the south of the ITD, a northward surge of the ITD through the arrival of convective cold pools can be expected in that region in the coming hours.

2.1.2.3 African Easterly Jet

The AEJ is a distinct and robust feature of the tropical North African climate which has a significant influence on synoptic variability, and in particular AEWs. The AEJ is characterised by a peak in the zonal easterly wind of about 15 m s^{-1} around 600–700 hPa that is in approximate thermal wind balance with the lower tropospheric temperature gradient from south to north (or baroclinicity; Cook, 1999; see Figure 2.2). Consistent with thermal wind balance, the baroclinicity (south–north temperature gradient) reduces to zero between the surface and the level of the AEJ. Thorncroft and Blackburn (1999) showed that the reduction in baroclinicity with height is consistent with north–south variations in convection; with moist convection predominant equatorward of the AEJ and dry convection predominant poleward of the AEJ. Parker *et al.* (2005a) analysed observations from the JET2000 experiment (Thorncroft *et al.*, 2003) to highlight, in some detail, the meridional variations in convection and associated thermodynamic profiles in the AEJ region, and the schematic of the AEJ shown in Figure 2.2 is based on this work. While deep moist convection and a peak mean rainfall are located just south

of the AEJ peak and dry convection and the associated SAL are located north of the AEJ, there is an important transition zone between. In this transition zone the shallow monsoon layer undercuts the SAL that sits above it (see Figure 2.2). The relatively warm SAL air sitting above the moist monsoon air is associated with significant convective inhibition (CIN) and the build-up of convective available potential energy (CAPE) in the boundary layer in these regions. Combined with the vertical shear of the AEJ and the dryness of the SAL, which favours intense convective downdraughts (Section 3.1.2.2), the region just poleward of the AEJ is favourable for the establishment of tropical squall lines. While these convective systems are included in Figure 2.2 we do not expect convection to occur to the north of the AEJ as frequently as the region south of the AEJ (which has lower CIN).

Consistent with the meridional contrasts in moist and dry convection highlighted earlier, the AEJ is characterised by two distinctive potential vorticity (PV) anomalies. A negative PV anomaly is established in the vicinity of the SAL, poleward of the AEJ (consistent with the low stability in the SAL) and a positive PV anomaly is established equatorward of the AEJ in association with moist convection (e.g. Thorncroft and Blackburn, 1999). The positive PV anomaly is predominantly at the level of the AEJ, which is consistent with a dominant contribution from stratiform rainfall and the frequent generation of mesoscale convective vortices (MCVs) there. The so-called monsoon trough at 850 hPa (see Sections 1.1 and 2.1.3.3) is viewed here as a downward reflection of the mid-level PV peak and associated vorticity, and may represent a focal zone for MCVs.

The distinctive PV anomalies linked to the AEJ are associated with different-signed meridional gradients in PV. Combined with the meridional gradients of surface temperature, the AEJ satisfies the necessary conditions for both barotropic and baroclinic instability

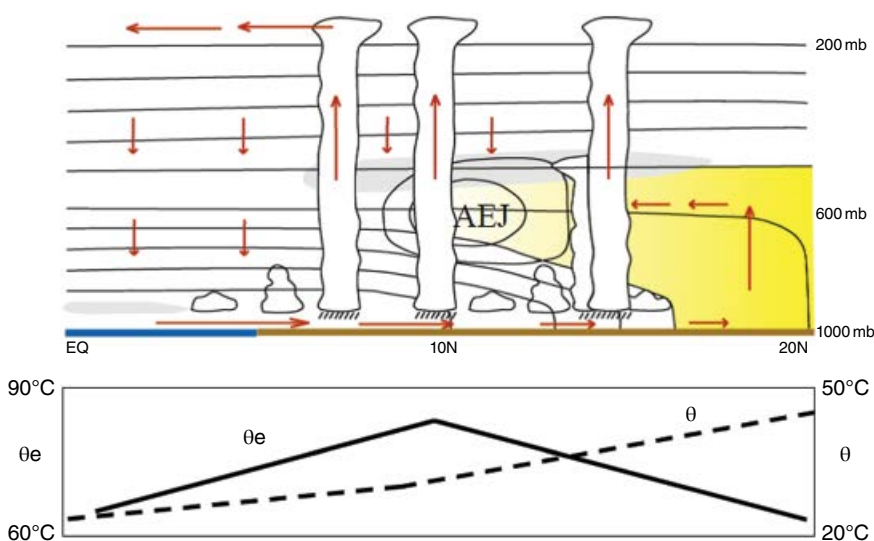


Figure 2.2 Schematic south–north vertical cross-section along the Greenwich Meridian, highlighting the SHL–AEJ–ITCZ system and SAL (shaded yellow), with meridional variations in atmospheric boundary layer potential temperature θ (contoured in upper panel) and equivalent potential temperature θ_e . The monsoon trough is located just to the south of the AEJ. Source: adapted from Figure 10 of Parker *et al.* (2005a) for the AMMA International Science Plan (http://ammainternational.org/library/docs/AMMA_ISP_May2005.pdf), and to be compared with Figures 1.1 and 1.34. Used with permission.

(e.g. Pytharoulis and Thorncroft, 1999). While recent studies have questioned the extent to which observed AEWs owe their existence to a linear instability mechanism (Hall *et al.*, 2006; Thorncroft *et al.*, 2008); the presence of these PV gradients is still essential for the development of AEWs and should be monitored.

2.1.3 African Easterly Waves

2.1.3.1 Background

AEWs develop and propagate on the AEJ over tropical North West Africa during the northern hemisphere summer. Their presence was recognised during the first half of the twentieth century from African rain gauge data that showed a distinct periodicity at around a 3-day timescale (Piersig, 1944[1936]). It was then noted by forecasters (e.g. Simpson *et al.*, 1968) that the same disturbances that brought about this periodicity were moving westward into the Atlantic basin and, in some cases, developing into tropical cyclones. Further studies have revealed that AEWs are the dominant synoptic-scale weather phenomena within the WAM system and tropical Atlantic during boreal summer. They can be observed between May and October, and peak in intensity during August and September (e.g. Carlson, 1969a,b; Burpee, 1974; Karyampudi and Carlson, 1988; Ross, 1991) and are one of the best known examples of a coherent, synoptic weather pattern in the tropics.

In the scientific literature there has been some inconsistency in the way in which AEW structures are described, and the theoretical models do not always agree with the experience of operational forecasters. It has become clear that AEWs are variable, from case to case, according to geographical location, and varying through the lifecycle of a single wave. For these reasons, we describe here some key observations and analyses of AEWs in Section 2.1.3.2, followed by a consensus description of the elements making up an AEW, and by which AEW structure may be objectively defined (in Section 2.1.3.3).

2.1.3.2 Observed Synoptic Structure of African Easterly Waves, Analyses and Statistical Composites

AEWs are most prominent in the lower troposphere, peaked at the AEJ level at around 650 hPa (approximately 3.5 km) over tropical North Africa and are characterised by periodicities of 2–6 days and wavelengths of 2000–5000 km (Reed *et al.*, 1977). Carlson (1969a,b) conducted synoptic analyses of several AEWs from the summer of 1967 and noted the presence of a wave-like perturbation to the wind field at 10,000 ft (approximately 3 km, or 700 hPa), along with two cyclonic vortices at 2000 ft (approximately 0.75 km, or 925 hPa), either side of the AEJ. Most AEWs tend to form somewhere between 15°E and 30°E over central or eastern Africa, and propagate westward through the WAM and into the tropical

Atlantic, where they are a common precursor of tropical cyclones (e.g. Carlson, 1969a; Avila and Pasch, 1992; Mekonnen *et al.*, 2006). In some instances AEWs have been observed to propagate coherently as far west as the eastern Pacific Ocean (e.g. Avila and Pasch, 1992). The AEW structure evolves as it moves westward. Before reaching the coast of West Africa, the AEWs that develop into tropical cyclones have a distinctive cold-core structure below the level of the AEJ, consistent with a vorticity maximum at the level of the AEJ (e.g. Reed *et al.*, 1977; Kwon and Mak, 1990; Hopsch *et al.*, 2007). They often begin to transform toward more warm-core structures as they move toward the Guinea Highlands region (5–13°N, 8–15°W), with regions of deep convection becoming more confined to the trough, as shown by Hopsch *et al.* (2010). The wave trough often slopes eastward with height below the AEJ level (Reed *et al.*, 1977), as expected for baroclinic growth on an easterly jet.

Kiladis *et al.* (2006), based on a regression analysis, highlighted the typical coherent synoptic evolution of AEWs as they grow and propagate across tropical North Africa and into the East Atlantic. The regression is keyed on a space–time, filtered time-series of outgoing longwave radiation (OLR) at 10°N, 10°W in the so-called ‘tropical depression’ band. The day-0 analysis in Figure 2.3 shows the regressed OLR together with streamfunction and wind vectors at 850 hPa and indicates a very coherent structure. The AEW trough–ridge structures are tilted against the horizontal shear north and south of the jet, consistent with AEWs that are undergoing barotropic growth (Section 2.1.3.5). It is also apparent in this figure that AEWs typically have a dynamical influence that crosses the Equator (Section 1.7; Figure 1.33) and also reaches as far north as 25–30°N. Given the meridional extent of the AEWs, we should expect them to interact with known convectively coupled equatorial waves to the south (Section 7.1.4) and mid-latitude weather systems to the north (Section 2.1.4). At day-0 the peak in convection, depicted by a minimum in OLR, is located in the AEW trough.

Figure 2.3 depicts the evolution of the AEWs through considering negative and positive time lags. The first indication of the AEW that reaches 10°N, 10°W at day-0 is a region of anomalous convection in the Darfur region at day-4. This is consistent with the hypothesis that AEWs are triggered by finite-amplitude disturbances such as deep convection (see Hall *et al.* (2006) and Thorncroft *et al.* (2008)). As the AEWs develop in the following days, the peak convection is located ahead of the AEW trough, a feature seen in many earlier studies. Interestingly, as the AEWs move westward the peak in convection shifts into the trough and eventually shifts into the southerlies behind the AEW trough when they are over the ocean.

Figure 2.4 shows the vertical structure of the meridional wind and corresponding OLR for an easterly wave passage over Bamako (continental), and then Dakar (west coast).

While both patterns are tilted eastward with height up to the AEJ level (~700 hPa), at Dakar there is a westward tilt above 500 hPa as expected on a shear flow, while Bamako still has an eastward tilt. Radiosonde data have shown that at Bamako (12.5°N, 8.0°W) most AEWs had maximum amplitudes at the level of the AEJ, while at Dakar (14.7°N, 17.5°W) the waves had maximum amplitude between 850 and 950 hPa (Pytharoulis and Thorncroft, 1999). Although AEWs occur as waves with maximum amplitude at low levels north of the AEJ and waves with maximum amplitude close to the AEJ level further south,

both represent a single dynamic mode and propagate simultaneously across Africa (Pytharoulis and Thorncroft, 1999; Cornforth *et al.*, 2009).

Figure 2.5 displays the composite horizontal wind field and relative vorticity on several pressure levels associated with AEWs from the European Centre for Medium-Range Weather Forecasts (ECMWF) ERA-Interim reanalysis dataset, which shows the prominent structures also noted by observation-based studies. Below the level of the AEJ (1000 hPa and 850 hPa), twin vortices are noted either side of the AEJ axis (near 15°N, denoted by the highest

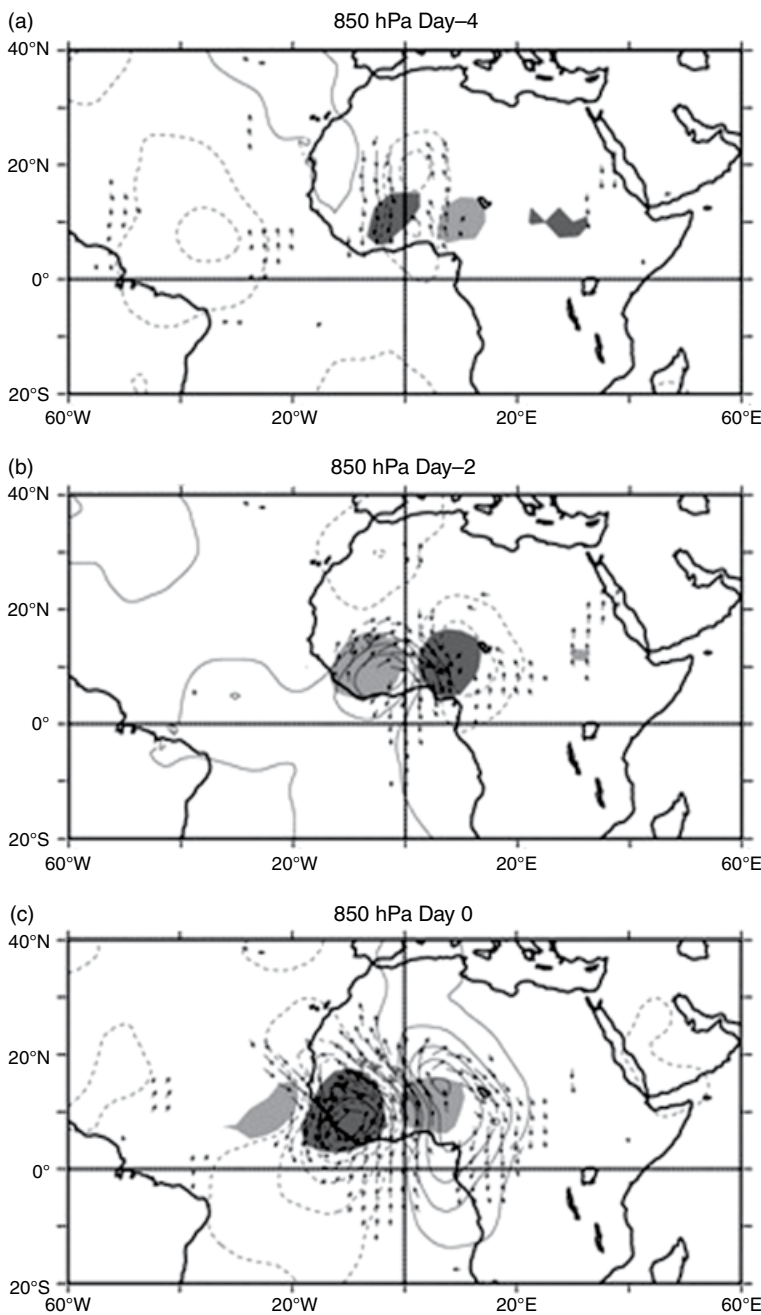
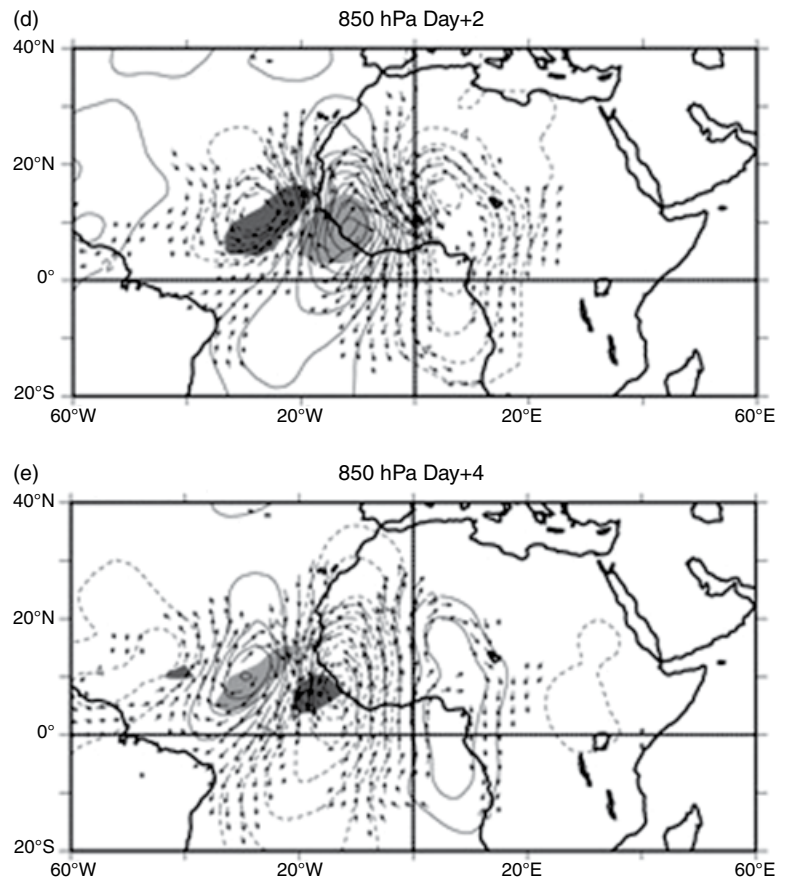


Figure 2.3 Composite AEW structure of 850 hPa streamfunction with anomalous convection. The plots are derived from a regression based on a space-time filtered time series of OLR at 10°N, 10°W in the so-called 'tropical depression' band. Dark shading denotes OLR anomalies less than -10 W m^{-2} (active convection), while light shading denotes OLR anomalies greater than $+10 \text{ W m}^{-2}$ (suppressed convection). *Source:* Figure 3 from Kiladis *et al.* (2006). ©American Meteorological Society. Used with permission.

Figure 2.3 (Cont'd)



wind speeds at the 700 hPa level). The northernmost of these vortices is collocated with the maximum surface temperature gradient (i.e. along the ITD), and the southern vortex is located near the peak rainfall. Peak relative vorticity amplitudes are observed at the 700 hPa level, where only a single maximum is seen close to, and equatorward of, the AEJ axis. Consistent with AEWs being a structure of the lower troposphere, at the 200 hPa level there is little discernible AEW structure, with the wind field being dominated by the upper-level tropical easterly jet (TEJ).

While most climatological studies of AEWs have stressed their dynamical structure, focusing on the dynamical trough at the AEJ level, Poan *et al.* (2013) have highlighted a moist-thermodynamic perspective of AEW structures, by basing their statistical composite AEW on the precipitable water (PW) anomaly (PW*). Although both perspectives are really analysing the same atmospheric structures, the choice of compositing field gives a different perspective on the same systems. In particular, using PW* to identify the AEWs emphasises structures in the northern Sahel, to the north of the AEJ, where the background PW gradient is particularly strong. From the PW* perspective, the mean period is 5–6 days, slightly

longer than found with dynamical criteria. Also, the wavelength is longer, at about 3800 km. AEW structures detected with PW* are emphasised on the northern flank of the AEJ where the meridional gradient of PW is maximum, and are consistent with earlier studies for this northern zone (Reed *et al.*, 1977; Kiladis *et al.*, 2006). Using the PW* perspective, some relationships between the thermodynamic structure and the winds are better identified, and the spatial and temporal footprint is larger so that AEWs can be detected earlier and further to the east. However, this approach to analysing AEWs remains an open area of research; for example, how the gradient in the PW* might influence AEW development remains unclear.

AEWs are very effectively analysed using 'Hovmöller' diagrams, contouring a signature field of AEW structure such as meridional wind, vorticity, OLR or PW*, on axes of longitude against time; these diagrams can even be a useful forecasting tool in real time. Figure 2.6 shows such Hovmöller diagrams for the 2011 monsoon season, comparing PW* and relative vorticity patterns. In Figure 2.6, the westward-moving AEW structures can be seen in both fields, and the speed of each AEW can be computed by the gradient of a linear feature in

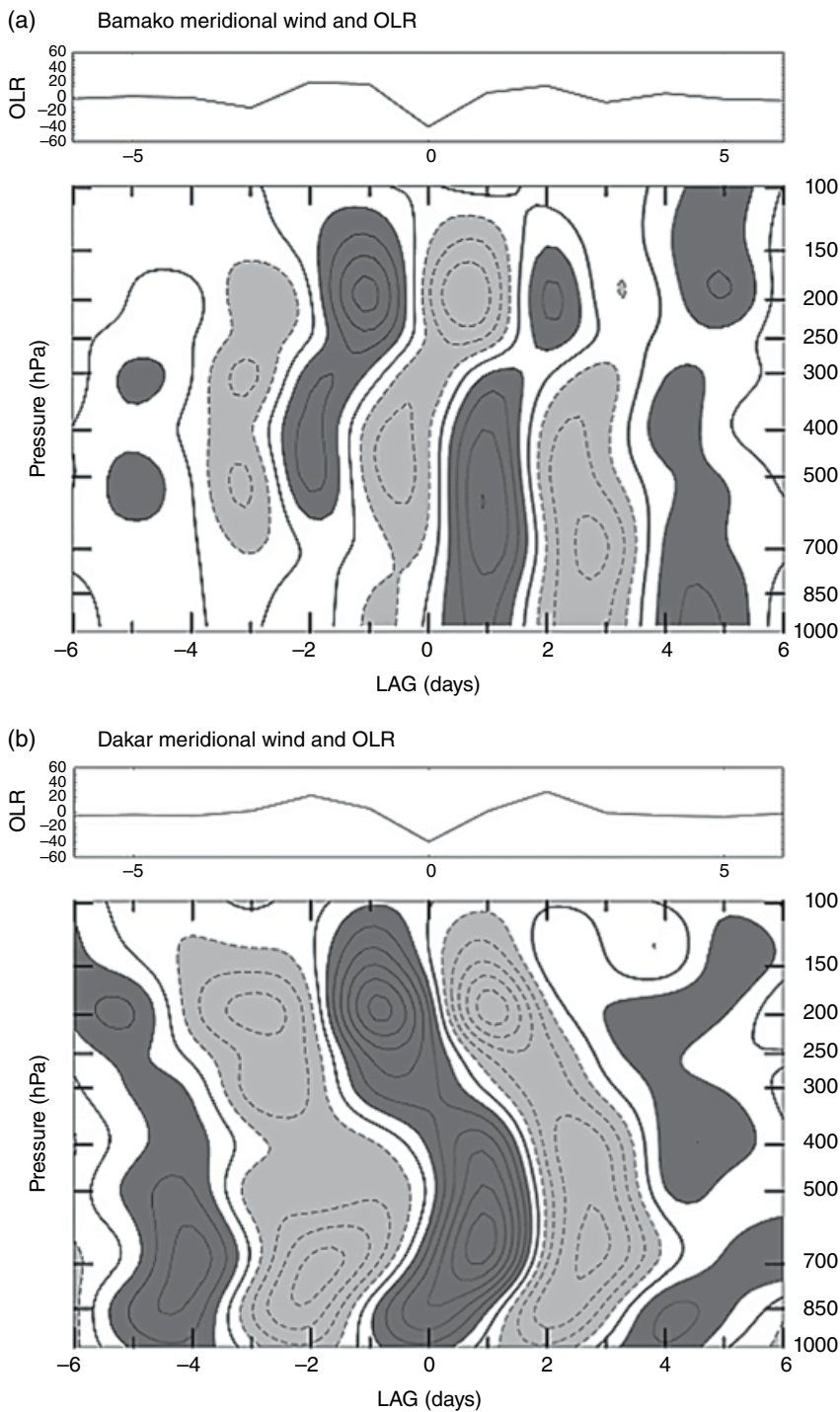


Figure 2.4 Time–height cross-section of the meridional wind anomaly at (a) Bamako and (b) Dakar, scaled to a -40 W m^{-2} perturbation in tropical depression-filtered OLR at the nearest grid point to each station. Contour interval is 0.5 m s^{-1} , negative contours dashed. Dark (light) shading denotes anomalies greater than (less than) 0.5 m s^{-1} . The associated OLR anomaly (W m^{-2}) is shown at the top. Source: Figure 10 from Kiladis *et al.* (2006) ©American Meteorological Society. Used with permission.

this diagram. Typically, the mean PW^* lies to the east of the wave trough, coincident with, and to the east of, the low-level southerly winds. These southerly winds cause an increase in PW^* over time, and therefore the PW^* builds on its western side, while decaying to its east where there are relatively dry northerlies. Figure 2.14 is another example of the use of a Hovmöller to analyse AEWs.

Figure 2.7 shows the horizontal structure of AEWs composited on PW^* by Poan *et al.* (2013). Maximum PW^* is located to the east of the wave trough, while maximum low-level southerly winds are in and to the east of the trough. This combination of winds and PW^* leads to an amplification and easterly propagation of the AEW (with southerly advection of moist air maximised in and to the west of the PW^*). Note that, as in Figure 2.3, the

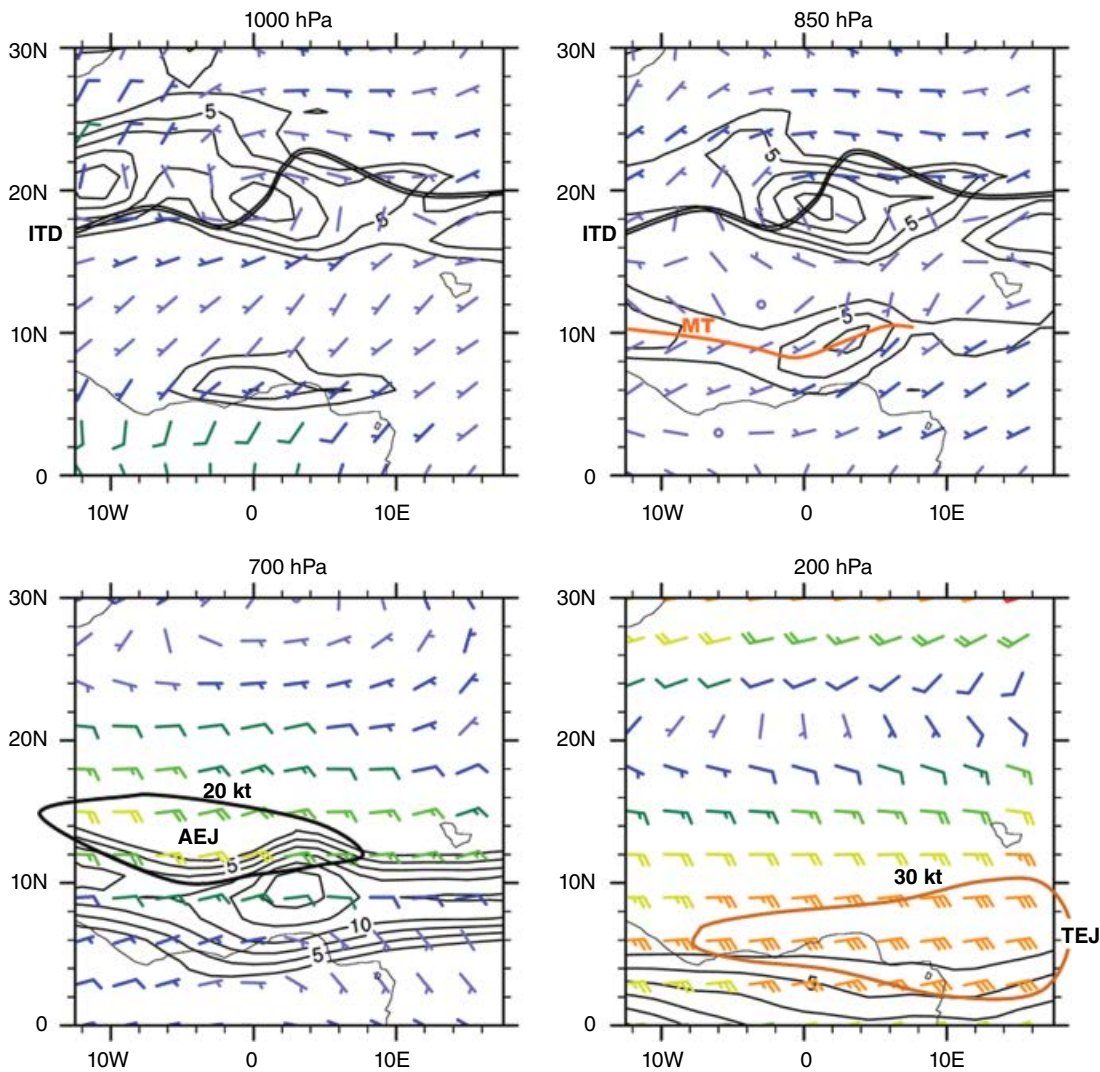


Figure 2.5 Vertical structure of AEW vorticity and winds, from a composite of AEW cases, based upon the 700 hPa trough axis passing the longitude of Niamey (2.5°E), and comprising 803 cases between 1989 and 2008, identified by the objective identification method of Berry *et al.* (2007). Composite winds (barbs, coloured in knots) and relative vorticity (positive values greater than $5 \times 10^{-6} \text{ s}^{-1}$ contoured every $5 \times 10^{-6} \text{ s}^{-1}$) are shown on different pressure levels from the ERA-Interim reanalysis dataset. The ITD, AEJ and TEJ have been overplotted consistently with the methods of Chapter 11.

trough in Figure 2.7 is tilted ‘upshear’ in a configuration that is consistent with barotropic growth of the AEWs (feeding on the kinetic energy of the AEJ). However, considerable variability in the trough orientation is seen from case to case.

The OLR patterns of Figure 2.7 indicate the peak in deep convection within and just ahead of the PW*, which means a peak in rainfall within and slightly to the east of the trough. However, this OLR pattern must be treated with considerable caution: these composites are based on the PW* and, therefore, will not emphasise the important and intense squall lines that develop and propagate into the areas of lower PW* to the west of the AEW trough. Figure 2.3 is an example of the link of observed OLR with the dynamical trough.

Figure 2.8 confirms the upshear tilt of the wave trough with height (for instance, the zero-line of v^* in Figure 2.8a tilts to the east with height at low levels); comparable patterns have been derived in other composite studies. The humidity and temperature fields, in contrast, are almost vertically aligned, and therefore the relationship between the trough and the thermodynamic (temperature and humidity) fields changes with height. Near the ground, the cool, moist air is mainly within the ridge (anticyclonic circulation), and in the southerly flow to the west of that.¹ At the AEJ level of 600–700 hPa the cool, moist air lies to the west of the southerly winds and to the east of the AEW trough. This eastward tilt is consistent with the composite waves gaining energy from baroclinic instability mechanisms (Section 2.1.3.5).

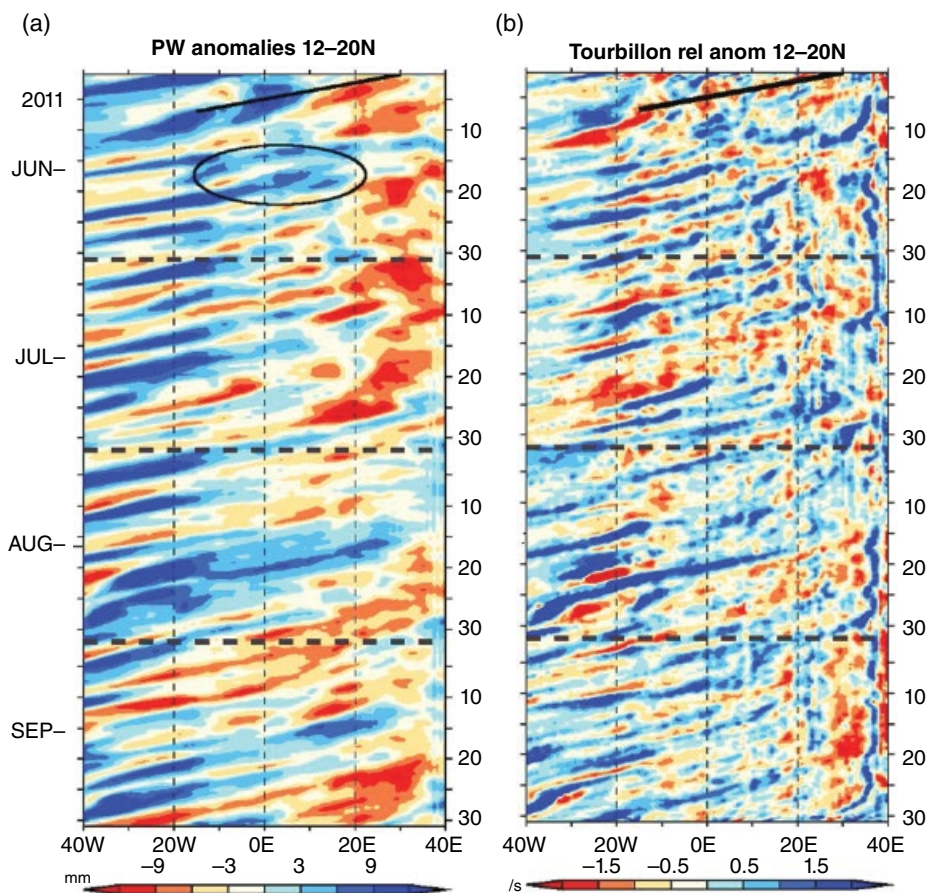


Figure 2.6 Time–longitude diagram of the 2011 June to September intraseasonal anomalies averaged over the 12–20°N band: (a) PW (mm) and (b) 850hPa relative vorticity ($\times 10^{-5} \text{ s}^{-1}$). The black solid lines materialise a slope of a -9 m s^{-1} velocity. Source: from Poan (2013).

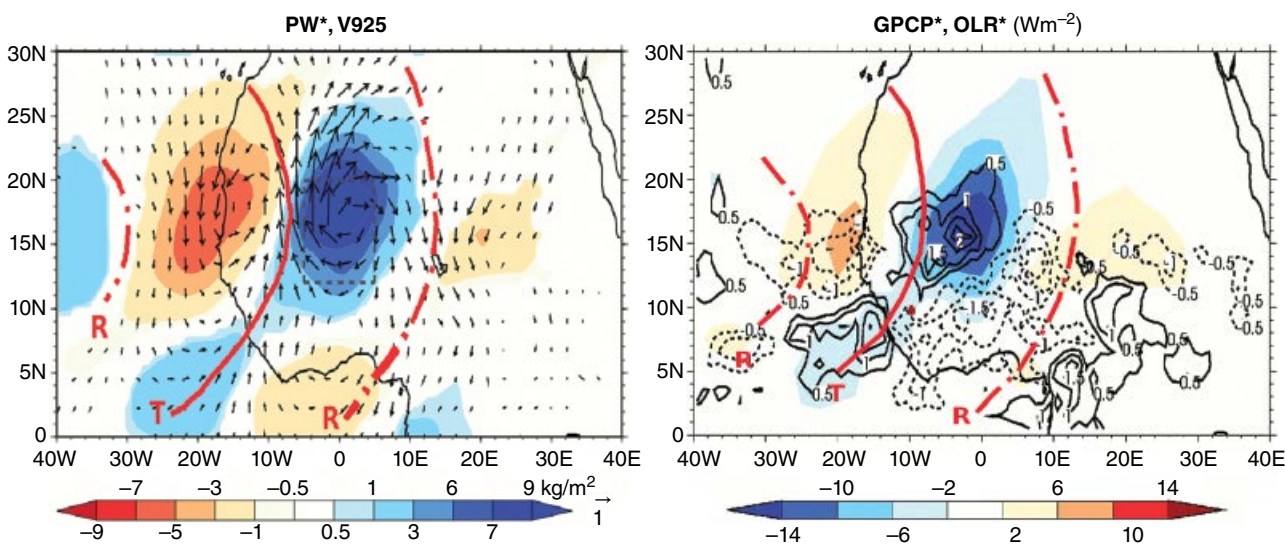


Figure 2.7 PW*, 925 hPa winds (left) and GPCP and OLR anomaly fields (right), based on a composite on the PW* field of AEWs (Poan *et al.*, 2013). The (red) trough and ridge lines are based on the wind fields at 600 hPa. Note that the relationship of OLR with the wave structure must be treated with caution because these structures do not effectively capture the very intense squall lines that propagate to the west of the AEW trough into areas of lower PW*. Source: ©American Meteorological Society. Used with permission.

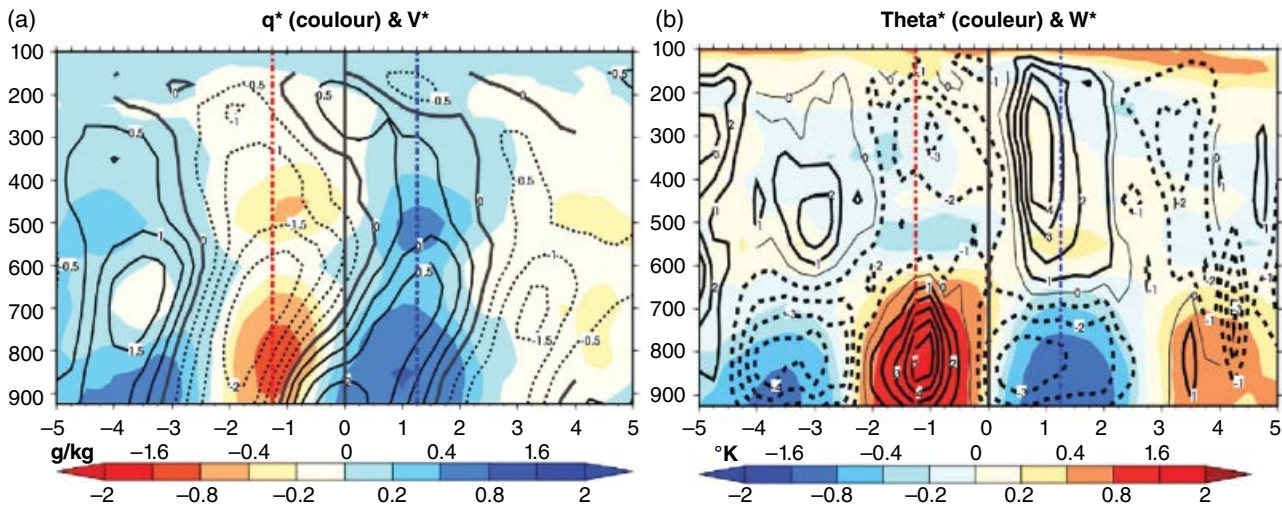


Figure 2.8 Vertical-lag composite of (a) specific humidity (g kg^{-1} , shaded) and meridional wind (m s^{-1} , contours) anomalies, (b) potential temperature (K, shaded) and vertical wind (mm s^{-1} , contours) anomalies, based on a composite on the PW^* field of AEWs. The vertical black line corresponds to the trough location at t_0 , whereas vertical dashed red and blue lines correspond to the passage of the dry/warm and moist/cold stages respectively (at $t_0 - 1.25$ and $t_0 + 1.25$). *Source:* from Poan (2013).

Although AEWs occur at low latitudes, there is some degree of thermal wind balance apparent in these composite plots. For instance, at zero longitude in Figure 2.8a there is northerly shear of the wind with height, with the cooler air to the east, consistent with thermal wind balance.

The composite maps of streamlines at low, medium and high levels, from the PW^* perspective (Figure 2.9), confirm these relationships. 850 hPa is close to the steering level of the AEWs, and therefore this is a level where strong, closed vortices exist. The winds at low levels act both to reinforce the high PW^* through cool, moist advection, and to cause it to propagate to the west.

The statistical and climatological perspectives on AEWs can hide the fact that there appears to be very great variability in AEW structure from case to case. Furthermore, the strong diurnal cycle of the boundary layer and of deep convection over West Africa means that there is a diurnal cycle of AEW structure, which is still not very well understood or documented. Bain *et al.* (2011), analysing an AEW case from 27 July 2006, showed how nocturnal acceleration of the low-level winds led to a surge of moisture northward into the wave trough, while daytime dry convective mixing in the north of the AEW led to a deceleration of the AEJ in that region.

2.1.3.3 African Easterly Wave Structure

In Section 2.1.3.2 we introduced evidence of the basic structure of AEWs, as it has been defined in various research studies. However, given that there is considerable variability in AEW structure from case to case, according to the maturity of an AEW, its geographic location and the time of day, it is difficult to generate a

single consensus for a single AEW structure. Furthermore, the scientific literature does not always accord with forecasters' experiences of daily synoptic analysis. The scientific papers have been dominated by description of composite structures, while synoptic case studies of AEWs are surprisingly rare. For instance, there appears to be a difference between the synoptic analysis of AEWs, very often showing 'downshear' tilt of the trough (e.g. Figure 2.16), and statistical composites showing 'upshear' tilt.²

For these reasons, presenting an AEW as a single structure would likely be misleading, because it would not reflect the wide range of observed structures. Instead, in describing AEW structures here, we emphasise their diversity. After lengthy discussion between researchers and forecasters, a modular approach is used here to describe AEW structures. This takes into account the key features, or elements of an AEW. The composite AEW structures, as well as any individual case study, may then be explained and discussed in terms of these elements. In listing the elements, we follow common forecasting practice and begin with the surface features.

- 1) *Surface or low-level structure.* The very first analyses of AEWs in the 1930s were based on the study of surface pressure tendencies. Forecasters still use these changes to infer the wave passage and its influence on weather conditions. Owing to the strong diurnal cycle of the surface pressure, the tendencies must be looked over 24 h or after removing the climatological diurnal cycle.

The wave structure has a very strong control on the boundary-layer structure, and the associated

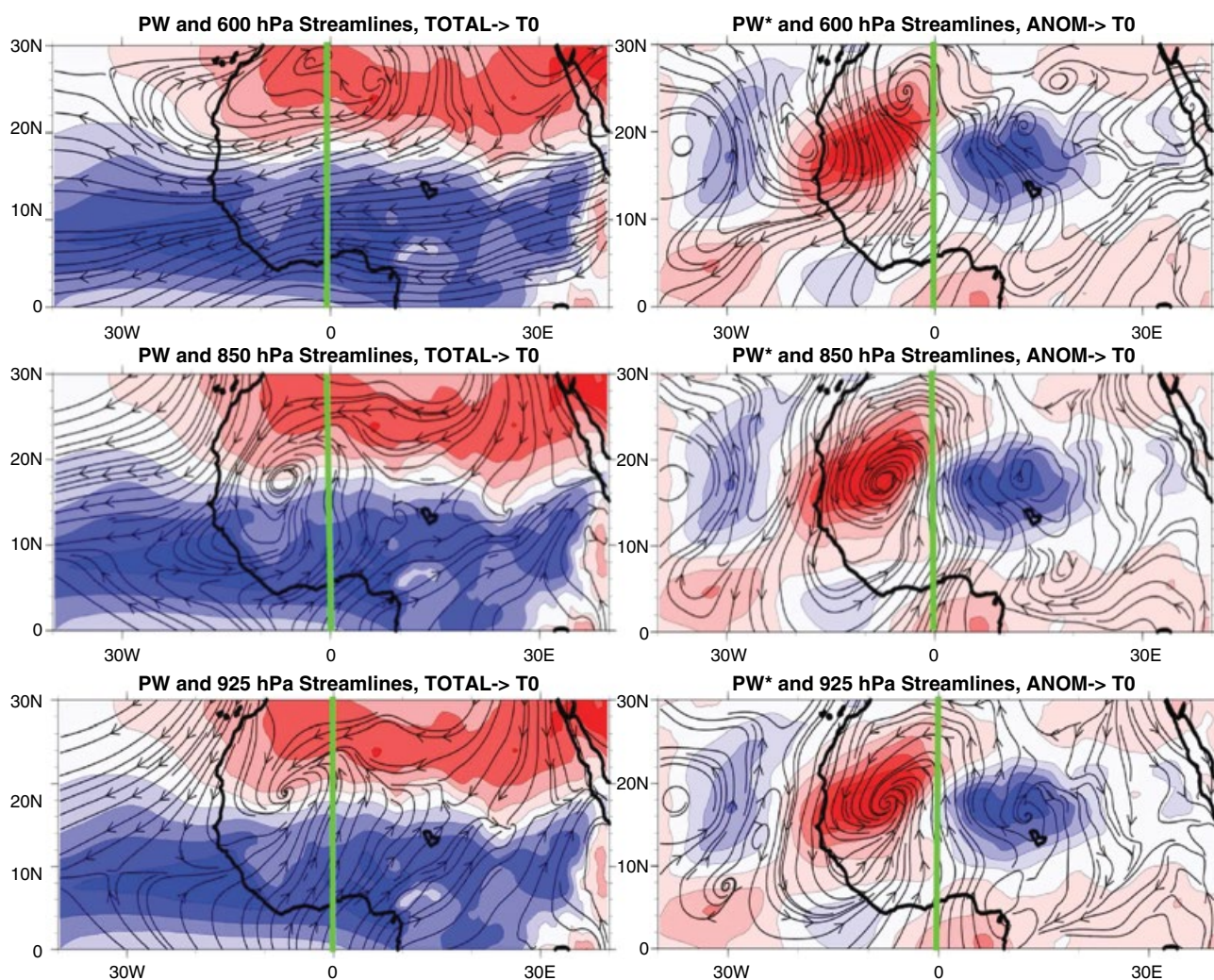


Figure 2.9 Composites of streamlines and PW (mm, shaded) fields at 925, 850 and 600 hPa at the passage (t_0) of the AEW at 0°E . The left and right columns correspond to the full and anomaly fields respectively. Source: from Poan (2013).

cloud fields. Air that is displaced northward typically has a cooler, shallower and more humid boundary layer, with more extensive shallow cumulus (collectively, a deeper monsoon layer) than air that has been displaced southward.

- 2) *ITD displacement.* The ITD typically has a strong northward incursion in association with the AEW, normally in and to the east of the AEW trough. The ITD has a very strong diurnal cycle, which tends to mask its synoptic evolution during the day, as the low-level air in zone B is mixed strongly with Saharan air above it. At night, the ITD regenerates strongly, pushing the ridge of cold air at low levels northward (Bain *et al.*, 2011).
- 3) *The AEW trough at AEJ level (e.g. 600 or 700 hPa).* The AEW trough is generally strongest at the AEJ level, and corresponds to the region of cyclonic curvature of the winds. In composite studies, the axis of the trough tilts upshear; that is, westward to the north

and to the south of the AEJ axis (e.g. Figures 2.3 and 2.7). In some synoptic events, the opposite shear is observed, with the trough tilting eastward to the north and south of the AEJ (e.g. Figure 2.16b).

- 4) *Waves and vortices on the monsoon trough (at 850 hPa).* AEWs propagate slower than the AEJ ($\sim 7\text{ m s}^{-1}$ as opposed to $12\text{--}15\text{ m s}^{-1}$), and therefore the wave steering level lies below the jet, often close to 850 hPa. The vorticity associated with the wave trough extends vertically below the AEJ level, and the vorticity at 850 hPa very often represents closed circulations, or vortices, which can be diagnosed from 850 hPa wind vectors or streamline maps for instance. These vortices may be enhanced by convective systems and are very important in the regeneration of convection on a subsequent day. Vortices may also on some occasions extend to higher and lower altitudes, reflecting a greater depth of the system.

5) *Precipitable water.* The PW is an integrated measure of the northward penetration of the monsoon system, and it shows a strong variability associated with AEW structure. AEW patterns are strongly highlighted in the PW* field (Poan *et al.*, 2013), and in some cases³ PW* may present a more robust diagnosis of AEW structure, and its precipitation patterns in particular, than the wind fields, since it integrates the greater variability of the winds and advection. In composite analyses, the peak PW* lies to the east of the AEW trough, where there are southerly winds at the AEJ level.

The patterns of deep convective stability (CAPE and CIN) are more complex, because the low-level equivalent potential temperature θ_e , which controls CAPE, has a maximum just to the south of the AEJ (e.g. see Figure 2.2 and Thorncroft *et al.* (2003)), while CIN is also controlled by the temperatures above the boundary layer. Typically, this leads to a southwest-to-northeast tilt in the pattern of high CAPE associated with an AEW, because low-level θ_e is high in the northward surge of moist air to the northeast of the trough (Figure 2.7), but is also high where warm (and humid) air is carried in the northerlies to the southwest of the trough (see Figure 2.7 and Figure 11.17b).

6) *Monsoon depth.* Various measures of the monsoon depth have been proposed, based on changes in the wind direction or on depth of the thermodynamic monsoon layer (see Section 11.10). Where the monsoon layer is deep, there tends to be a deep layer of cool, humid air with a general southerly advection. This intrusion of cool monsoon air is essentially collocated with the high PW*. The coolness of the air, through the thermal wind relation, tends to lead to relative anticyclonic flow at low levels (or a weakening of the cyclonic flow). For instance, in composite wave structures (Reed *et al.*, 1977) the waves are cold-core, with the deep, cool monsoon layer close to the AEW trough axis, and the vorticity weakening with height below the trough.

Analysis and drawing rules for each of these elements are provided in Chapter 11.

We can discuss the typical AEW structures in terms of these features (e.g. the downstream changes in the vertical structure). A schematic interpretation of the composite AEW structures in these terms is now shown in Figure 2.10.

Figure 2.10 has been drafted for this book as a result of meetings and discussions among operational forecasters, academics and modellers, and represents a new consensus on AEW structure. A number of important points must be made in relation to the fields and their relationships.

1) *Panels 1 and 2 at 600–700 hPa represent the most common levels for diagnosing the presence of AEWs*, close to the AEJ level, with trough and ridge lines related to the curvature of the streamlines (here defined where $v = 0$). The typical wavelength is 3000 km or 30° of longitude from trough to trough. Open waves are more typical at this level than strong, closed circulation centres. However, closed circulation centres are possible in some cases, especially in the south (as shown in panel 1).

The horizontal tilt of the troughs, as diagnosed in composites from model analyses, is as shown in panel 1; that is, upshear tilt (extending to the west, both north and south of the AEJ core). However, individual cases show variations in this tilt, or the tilt evolving as a wave moves toward the west.

A westward tilt of the wave trough leads to faster AEJ winds to the east of the trough, as shown in panel 2 (because in this region the streamlines are closer together). Eastward tilt is also possible, as in the example in Figure 2.16. Breaks in the jet core are commonly possible, when an AEW is intense (see online case study CS01⁴, 1–10 August 2012, or the extreme flood case CS04 of Ouagadougou 1 September 2009).

2) *Initiation of deep convection has a wide spread of possible locations, but a consensus for the peak and distribution are shown here.* Fast-moving mesoscale convective systems (MCSs) typically occur along the location of the AEJ core ahead of the trough and are favoured by mid-level dry air and strong shear (Sections 3.1.2.2 and 3.1.2.3). Slower-moving convective systems are found to the south, where wind shear is weaker and the monsoon depth is deeper.

3) *Panels 3 and 4 show the winds, vortices and PW* at 850 hPa*, close to the steering level of typical AEWs. The thermodynamic signal of the AEWs is generally maximised in these levels below the AEJ. The PW* are approximately collocated with thermal anomalies, as cool, moist air is advancing northward to the east of the trough and warm, dry air moves southward to the west of the AEJ-level trough.

4) *A closed vortex is commonly observed at 850 hPa, and usually (though not always) to the west of the AEJ-level trough.* This is a typical signature of a baroclinic wave tilt. The 850 hPa vortices are connected with the line of maximum 850 hPa vorticity, to the south of the AEJ, to delineate the ‘monsoon trough’ (see Section 11.10).

It is important to note that forecasters associate this 850 hPa vortex with a likely area for the development of thunderstorms.

It should be recognised that, in general, the monsoon trough may not be a continuous line. The example of Figure 11.14 shows a rather continuous configuration of the monsoon trough, but on other occasions the

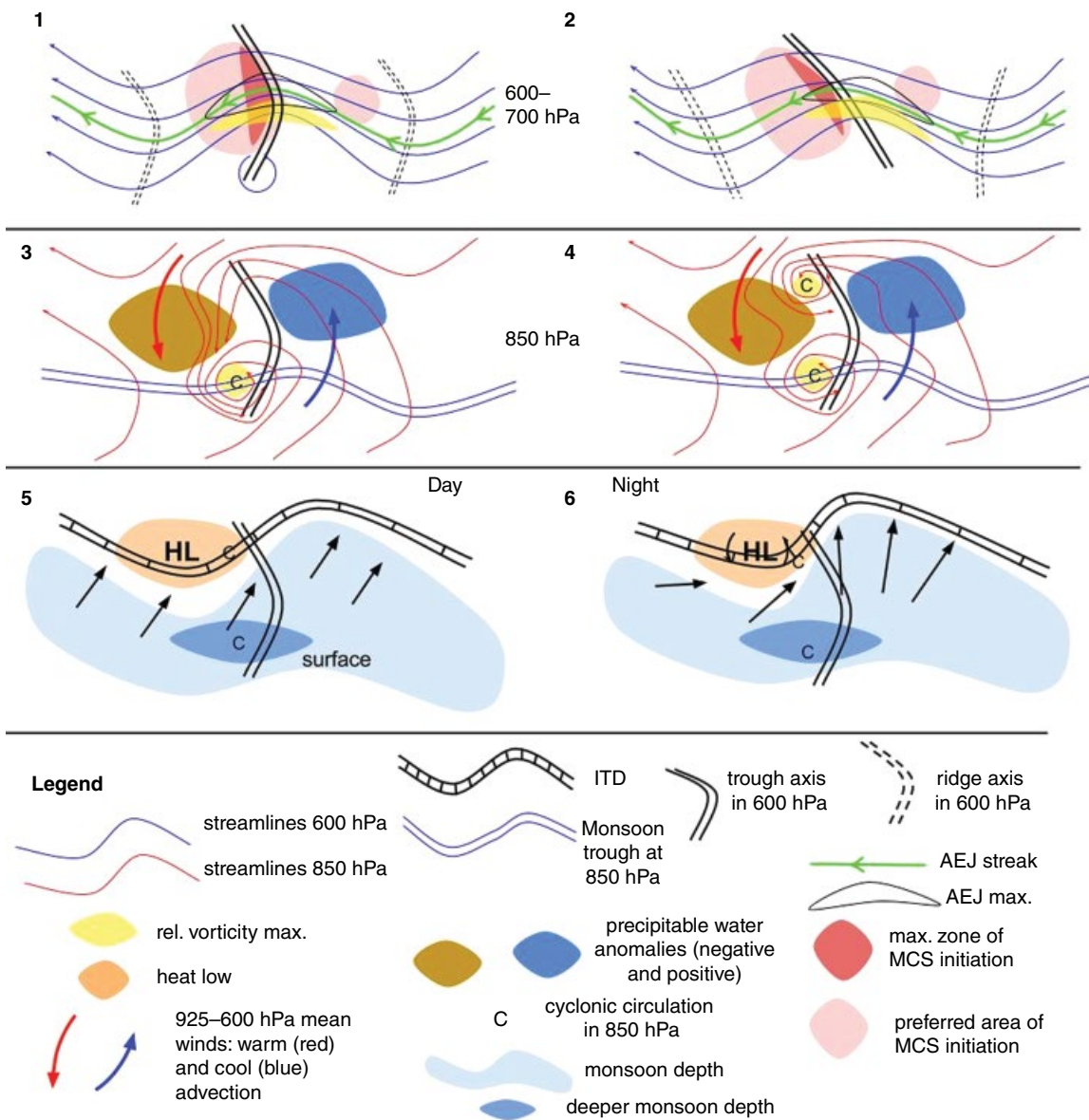


Figure 2.10 Schematic of the various observable elements of an AEW, and likely relationships between these. Left-hand panels show a 'normal' situation, as far as this exists, while right-hand panels show common alternatives. For example, the structure in panel 2 would be expected in an environment with additional barotropic shear, with a stronger easterly wind to the north (i.e. $U_y < 0$).

monsoon flow may be so deep and strong that the monsoon trough disappears in the southerly flow at the rear of the trough (in which case the monsoon trough may effectively exist at a lower pressure level).

On many occasions, a northern vortex is also seen on the ITD at the 850 hPa level (panel 4). If it is absent, the vortex may simply be shallower, and seen on the 925 hPa level instead. When plotting the monsoon trough, it is important not to connect the ITD vortices with the monsoon trough.

5) Panels 5 and 6 show the surface signature of the AEW. A significant north-south deviation in the ITD follows the AEW (also seen at 925 hPa). Monsoon depth

follows the wave of ITD extensions to the north (e.g. Figure 11.16), and is commonly observed to be deepest in the area of the cyclonic circulation south of the AEJ, as marked here. Forecasters use the northward extension of the ITD to describe associated shifts in zones B-D (Figure 1.1) of the monsoon system; for instance, where the ITD is pushed to the north, we expect zones B, C and D similarly to be pushed northward.

Increased monsoon depth generally increases cloudiness in the northern region. Associated with the movement of the ITD, there is a southward extension of the SHL to the west of the trough with lower cloud cover and high insolation.

6) *Surface fields have a substantial diurnal cycle, especially in the north (zone B).* A surge of low-level winds northward into the heat low, plus a cyclonic circulation around the heat low, which both intensify overnight, push the ITD northward by some 300–500 km, especially to the east of the heat low anomaly and AEW trough (panel 6).

Figure 2.10 relates to the structure of AEWs over the continent. As AEWs move westward over the coast and the Atlantic Ocean, three other elements play a role in the AEW structure:

- *A semi-permanent vorticity maximum over the Guinea Highlands, or Guinea/Sénégal coast.* This feature appears to be sustained by the regular deep convection occurring over and downstream of the Highlands.
- *Equatorward cold advection off the west coast of the continent.* As the wave trough moves over the coast, the northerly winds ahead of the trough no longer advect warm air, but instead advect cooler air at low levels, triggering baroclinic decay immediately. This explains why ‘marine AEWs’ are more barotropic in nature and have a weaker vertical tilt.
- *The intertropical convergence zone (ITCZ) over the Atlantic Ocean.* The reduced low-level thermal contrasts and lack of heat low over the ocean mean that the maximum rainy zone reverts to a more classical ITCZ structure, with low-level convergence roughly collocated with the maximum deep convection and rainfall. Effectively the ITD and monsoon trough merge as the wave moves over the ocean, to form a more vertically aligned trough.

It has repeatedly been emphasised here that there is considerable variation in AEW structure from case to case. Section 2.2 describes typical combinations of the dynamical elements that make up typical AEW patterns in different contexts.

2.1.3.4 African Easterly Wave Genesis

2.1.3.4.1 Upstream Triggers

Observational studies have consistently demonstrated that AEWs are predominantly generated over the African continent to the east of 10°E. Commonly, upstream convection, in an East African region including the Darfur Mountains (15°N, 23°E) and the Ethiopian Highlands (10°N, 35°E), initiates AEWs near the entrance of the AEJ (Hall *et al.*, 2006; Kiladis *et al.*, 2006; Mekonnen *et al.*, 2006; Thorncroft *et al.*, 2008; Leroux and Hall, 2009). Hall *et al.* (2006) showed in idealised modelling studies that intense localised heating (a proxy for mesoscale convective systems) in the entrance region of the AEJ could excite synoptic structures resembling AEWs downstream. The hypothesis that finite-amplitude impulses of heating result in the genesis of AEWs is

supported by case studies (e.g. Berry and Thorncroft, 2005), showing AEWs generated following a large burst of deep convection over central Africa. Thorncroft *et al.* (2008) demonstrated that the genesis of AEWs is sensitive to the location of the initial convective perturbation; they are more efficiently triggered by heating close to the entrance of the AEJ. The implication is that the intermittency of observed easterly waves may be in part explained by the variability of convective activity toward the east, instead of purely by considerations of the jet structure. More generally, Leroux *et al.* (2010) found that subseasonal variability of AEWs tends to be preceded by anomalous convection in the Darfur region. Leroux and Hall (2009) suggested that the AEW response also depends on the AEJ structure, with wider and stronger AEJ (strong shear and PV reversals over an extended region near the AEJ) producing more intense AEWs – entirely consistent with baroclinic growth (see also Hsieh and Cook (2005)). In idealised simulations with moist processes, Cornforth *et al.* (2009) showed that moist AEWs were characterised by intermittent periods of growth and decay that were correlated with increases and decreases in the mean rainfall respectively but anticorrelated with jet strength. The strong interdependence between the AEJ, the AEWs, the moist convection and the upper levels establishes an *internal variability* on a timescale of 8–10 days in the idealised model consistent with the observed average 9-day cycle of wet (dry) sequences (e.g. Sultan *et al.*, 2003).

Influences from mid-latitudes (e.g. Leroux *et al.*, 2011) may also help modulate the amplitude of AEW activity on intraseasonal timescales. A long integration of a simple GCM in an artificially dry context simulating the northern summertime global circulation produces a summertime climatology that includes a realistic AEJ and westward-propagating 3–5-day disturbances over West Africa. These simulated waves display intraseasonal intermittency, as do the observed AEWs. Further experiments designed to discern the source of this intermittency in the model show that the simulated waves were mainly triggered by dynamical precursors coming from the North Atlantic storm track.

2.1.3.4.2 Large-scale Dynamics

In order to explain the full structure of the AEWs, it is essential to consider not only the role of convection but also the large-scale dynamical ‘mode’ of wave dynamics. The vertical and horizontal shears associated with the mean AEJ satisfy the Charney and Stern (1962) criteria for baroclinic and barotropic instability (e.g. Burpee, 1974). Idealised modelling studies (e.g. Thorncroft and Hoskins, 1994; Cornforth *et al.*, 2009) have shown that the most unstable dynamic mode growing on the AEJ has similar spatial structures to observed AEWs and also demonstrated that AEWs can amplify by barotropic and baroclinic energy exchanges. In light of these results it

has been contended that the genesis of AEWs is associated with initially small perturbations to the flow over central and eastern Africa that increase in amplitude owing to the unstable nature of the background flow. However, analogous to the genesis of baroclinic waves in the mid-latitudes, it is recognised that the dynamic instability of the background flow is too slow (relative to observed wave lifecycles and observed wave precursors) to explain the genesis of AEWs, although such dynamical instability does appear to influence the growth and structure of waves once they have been initiated. Although a coherent instability mode may not be essential to wave initiation, nevertheless a 'growing configuration' of wave modes on the basic state AEJ will emerge. Recent work has also highlighted an alternative mechanism for AEW genesis over Africa that, instead of downstream development from upstream

triggers, involves upstream energy dispersion from the west (Diaz and Aiyyer, 2013).

2.1.3.5 African Easterly Wave Dynamics and Evolution

The AEJ satisfies the Charney and Stern (1962) barotropic and baroclinic instability criterion, meaning that the sign reversal of the meridional PV gradient (Figure 2.11) satisfies a necessary condition for instability of the mean flow (Burpee, 1972; Thorncroft and Blackburn, 1999; Dickinson and Molinari, 2000). The sign reversal of PV at the AEJ level is consistent with the presence of a strip of high PV on the southern flank of the AEJ, which is in turn augmented by deep convection during the active monsoon.

The genesis of AEWs through small-amplitude barotropic or baroclinic instability is highly relevant to the structure of AEWs over West Africa even if time dependence

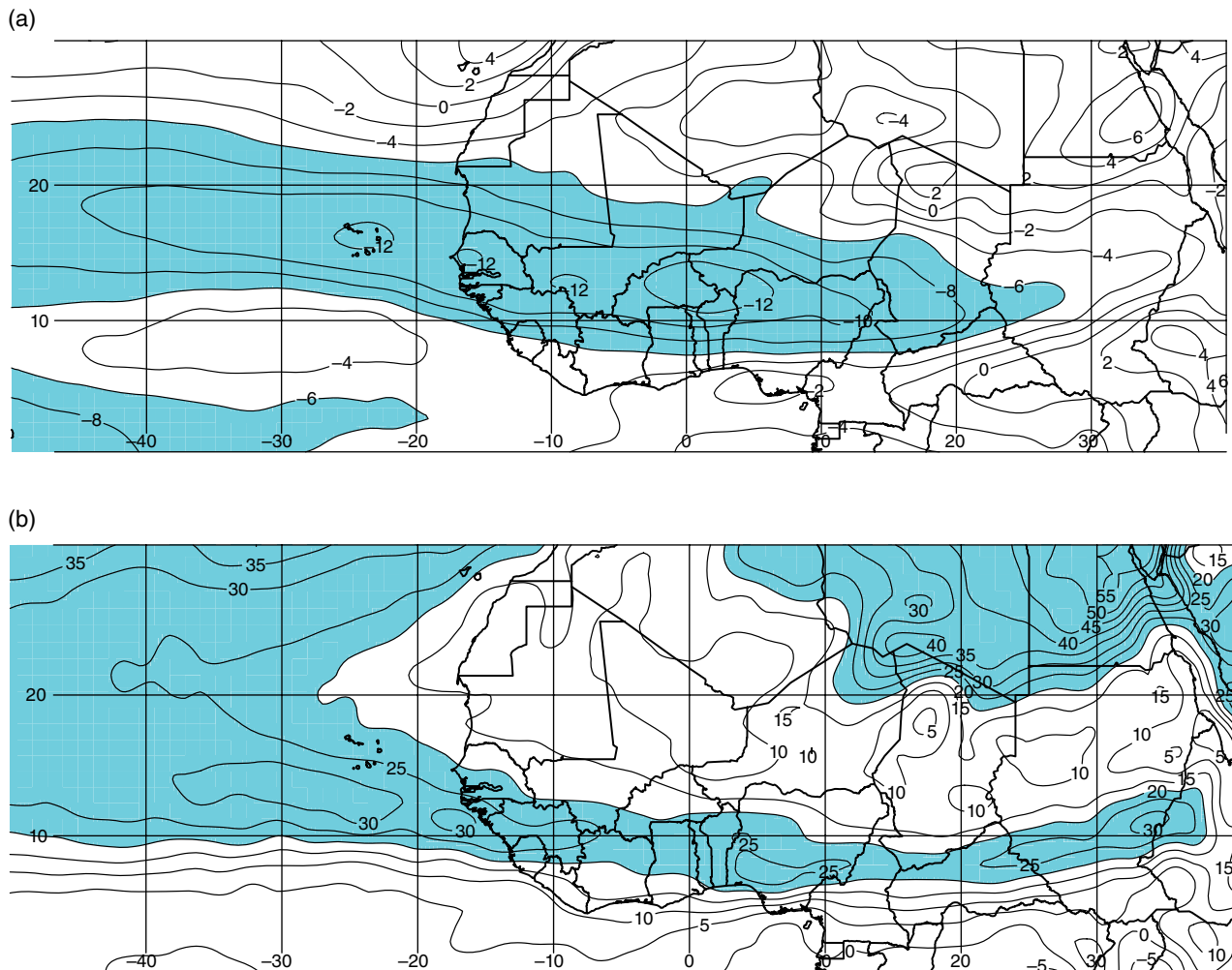


Figure 2.11 Illustration of the meridional PV reversal. Panels (a) and (b) (based on operational ECMWF analyses and adapted from Figure 1 in Thorncroft *et al.* (2003)) show (a) zonal wind and (b) PV, on the 600 hPa surface. The maximum PV on this level is to the south of the AEJ maximum (each shaded blue), with low PV to the north of the AEJ. Source: ©American Meteorological Society. Used with permission.

differs in the initial-value problem with finite-value precursors (Section 2.1.3.4). AEWs are large-amplitude waves whose evolution is strongly influenced by these barotropic and baroclinic processes, and Rossby wave dynamics in particular. For example, the typically slow growth of an AEW once its structure has emerged and it then continues to propagate westward through the WAM system is entirely consistent with a slow baroclinic growth rate. As such, understanding the behaviour of these waves and instabilities can help us to understand the evolution of the mature AEWs.

Basic theory of synoptic-scale instabilities shows that the waves can gain energy from barotropic processes if the trough tilts 'upshear' in the horizontal – that is, if the trough extends westward with latitude, both north and south of the AEJ core latitude (as in Figure 2.10, panel 1). In this case, the wave will gain energy from the basic kinetic energy of the AEJ itself. The composite AEW patterns seen in Figures 2.3 and 2.7 confirm that, on average, AEWs have a significant element of barotropic instability (although individual cases may differ from this structure). Similarly, waves can gain energy through baroclinic mechanisms if the wave trough tilts upshear (eastward; see Figures 2.8 and 2.12) with height, below the AEJ core, in which case the wave gains energy through thermal advection, with warm northerlies intensifying the warm sector of the AEW. Again, the structures seen in Figure 2.8 agree with the baroclinic instability model, where there is cool, moist southerly advection at low levels within and to the west of the low-level cool anomaly; this pattern acts both to strengthen the cool anomaly and to cause it to propagate to the west (as a surface Rossby wave – see Parker (2008)). In turn, the westward propagation at low levels enables the low-

level structure of the wave to keep up with the easterly motion of the wave at the AEJ level. The whole system has a steering level some way between the surface and the AEJ level, typically around 850 hPa.

The relationships between the trough, the winds and the vorticity structures at different levels are demonstrated using fields taken from an AEW case during August 2000. In Figure 2.13a on the large scale, equatorward of the 700 hPa AEJ axis (denoted by the thick red line), there is a zonally orientated (east–west) strip of positive relative vorticity. Similarly, at 925 hPa the temperature field exhibits a well-defined, zonally orientated zone of temperature gradient, reflecting the zonal nature of the AEJ and the monsoon. The AEW structure in this case is evident as a wavelike disturbance to this zonally orientated background; the middle of the relative vorticity perturbation is marked by the trough axis (black line), and the warm temperature perturbation is located slightly ahead (west) of the trough. Baroclinic growth will result if the flows due to the vorticity (and PV) at the different levels interact, as their configuration means that the flow around each would increase the amplitude of the other. It is also expected that barotropic growth would result from the flow around the 700 hPa vorticity maximum distorting the large-scale background 'strip' of vorticity. These dynamic growth concepts are identical to those applied in mid-latitude systems and consistent with the observed structures.

Although the AEW structures observed have a configuration that is consistent with growth via dry dynamics, calculations from idealised simulations of AEWs have shown that the dry dynamics act too slowly to fully describe the observed growth rate. Based upon a case study of the event shown in Figure 2.13, Berry and

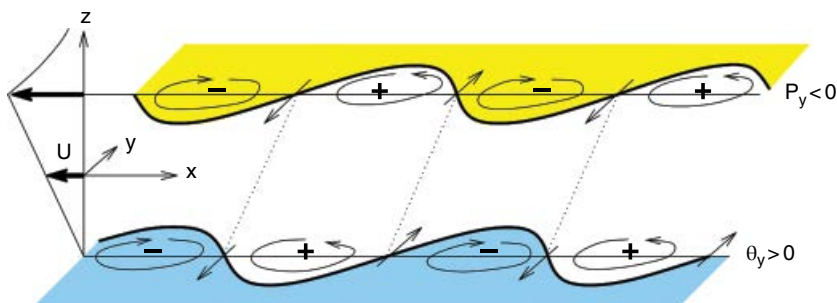


Figure 2.12 A schematic depicting the meridional displacements of air and associated circulations within an AEW that are predicted for a 'baroclinic' growth configuration. An 'upper Rossby wave component' propagates along the African easterly jet and interacts with a 'lower wave' propagating westward. The upper wave exists in the jet core where the meridional PV gradient (P_y) is negative. At this level, *southward displacement* of air from above the Sahara (shaded yellow) must create a negative PV anomaly and anticyclonic circulation, enabling westward *propagation* relative to the surface flow. The lower wave exists on the meridional potential temperature gradient, which is positive, so that *northward displacement* brings cooler, moist air (shaded blue) from the south which is associated with anticyclonic circulation, enabling westward *propagation* relative to the surface flow. When the circulations induced by the upper wave are positioned east of the circulations induced by the lower wave (velocity components tilt eastward as indicated by dotted lines), their interaction by meridional advection results in mutual growth.

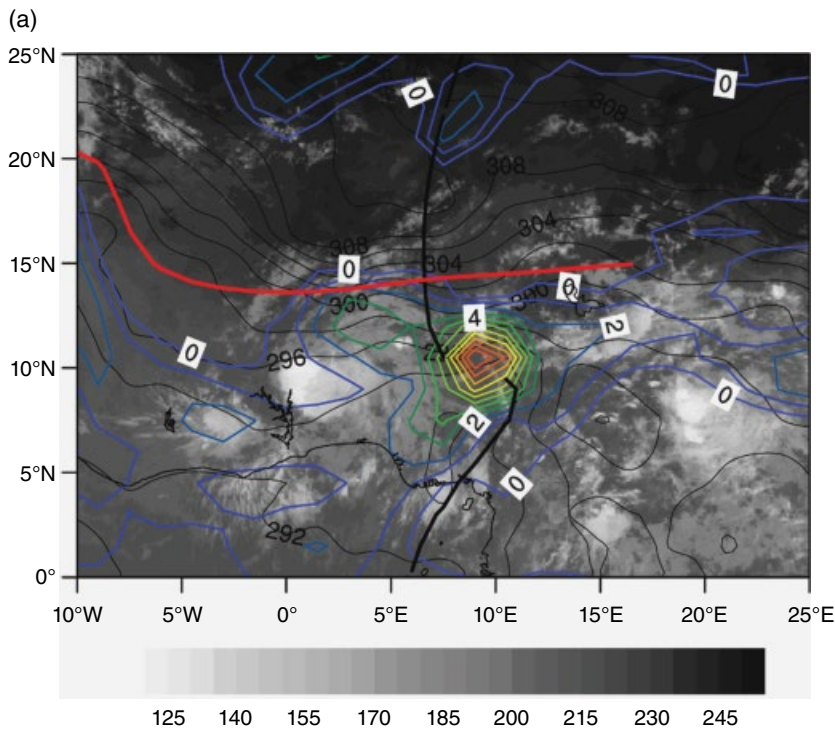
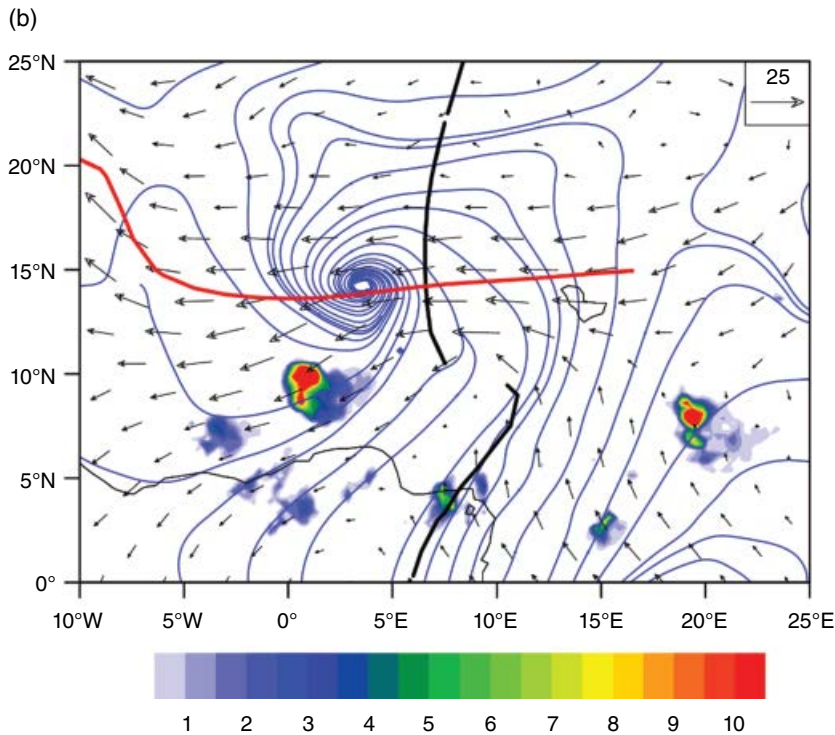


Figure 2.13 Synoptic maps of ECMWF ERA-Interim reanalysis fields on 1 August 2000, 1200 UTC: (a) 700 hPa relative vorticity (coloured lines), 925 hPa temperature (thin black lines), 700 hPa objective trough (thick black line) and objective jet axes (thick red line, see Berry *et al.* (2007) for definition). (b) Mean TRMM 3B42 estimated precipitation rate (mm h^{-1} , shaded according to legend), Streamlines at 925 hPa (blue streamlines) and wind vectors at 700 hPa. The same objective trough and jet axes as in (a) are overlaid.



Thorncroft (2005) suggested that the presence of organised convective systems increases the growth rate of the synoptic AEW (Cornforth *et al.*, 2009). It was hypothesised that the very intense mesoscale vorticity centres generated by the convection within the AEW are a key catalyst to AEW growth. These authors suggested that, as convection is preferred near to and ahead of the trough axis, the summation of the flow associated with

the small-scale vorticity centres will project upscale and enhance the mid-level flow around the AEW, increasing both the AEW amplitude and its growth rate via dry dynamics. In a numerical modelling study, Berry and Thorncroft (2012) revealed that an AEW will weaken on a timescale of a few days if convective systems are removed, underlining the importance of convection and its coupling to AEWs.

2.1.3.6 Relationship with Deep Convection

In the WAM, AEWs have a modulating effect on rainfall, with some estimates suggesting that in excess of 60% of organised squall lines during summer are associated with AEWs (e.g. Fink and Reiner, 2003).⁵ Composite analyses (e.g. Reed *et al.*, 1977) indicate that rainfall and cloudiness are primarily peaked ahead (west) of the mid-level trough axis and south of the AEJ core. Some studies have also noted a secondary peak of convective rainfall behind (east of) the mid-level trough axis, poleward of the AEJ axis (as illustrated by Poan's composite of Figure 2.7b).

More detailed analysis of individual convective systems associated with AEWs (e.g. Payne and McGarry, 1977) have shown that MCSs tend to propagate twice as fast as AEWs, consistent with being driven by downdrafts originating near the mid-level AEJ (e.g. see Rowell and Milford (1993), Chong and Hauser (1989) and Lafore and Moncrieff (1989)). This suggests that the preferred regions of rainfall consist of many convective systems travelling through a particular phase of the AEW, rather than having a single persistent area of rainfall moving at the same speed as the AEW. In this sense, the genesis, maturity and decay locations for MCSs within AEWs may be distinct. The movement of convective systems through AEWs, the variety of possible AEW configurations and the distinct diurnal cycle of the convection all add complexity to the question of how rainfall is related to mean AEW structure.

The observed relationship between AEWs and rainfall is illustrated by Figure 2.14, which shows a Hovmöller space–time diagram of 700 hPa curvature vorticity from the National Centers for Environmental Prediction (NCEP) Global Forecast System (GFS) operational analysis (a diagnostic of AEW trough location used by Berry *et al.* (2007)) overlaid with rainfall rate estimates from the CMORPH dataset (Joyce *et al.*, 2004); both fields are averaged over 5–15°N for the month of August 2004. In this figure the passage of AEW troughs can be distinguished by the westward-moving curvature vorticity maxima, while convective systems can be noted by the smaller scale bands of rainfall that also propagate westward. Note that the rainfall does not show individual convective systems, as a consequence of the averaging in latitude; instead, it signifies groups or 'envelopes' of convective systems.

To show more details of a particular case, Figure 2.15 shows MCSs associated with easterly waves during August 2006, including the precursors to Hurricane Helene. In the figure, the trough of the westernmost AEW and the inverted 'V' cloud pattern are marked by dashed lines at 1800 UTC on 6 September (upper left panel). At that time MCSs are on both sides, but on subsequent days convection is enhanced ahead of the trough.

There have been many observational studies explaining the location and type of convective clouds relative to the

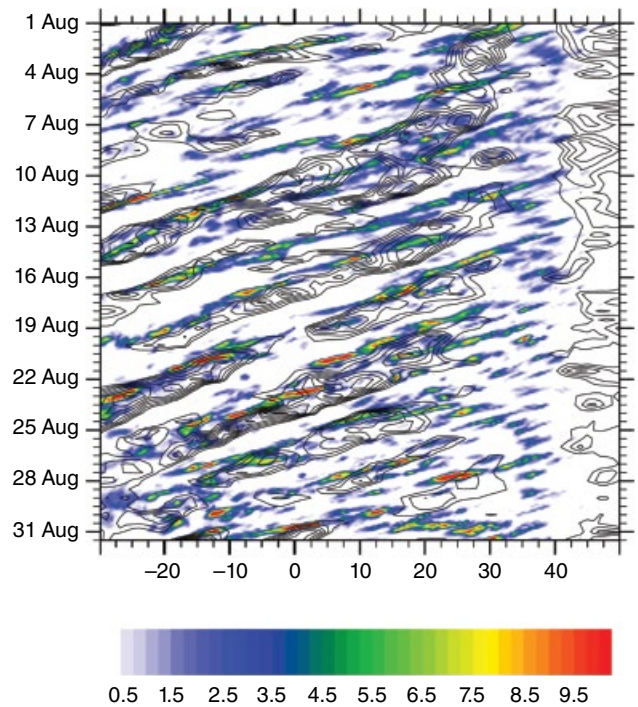


Figure 2.14 Hovmöller space–time diagram of 700 hPa curvature vorticity (positive values greater than $2 \times 10^{-6} \text{ s}^{-1}$ contoured every $2 \times 10^{-6} \text{ s}^{-1}$) from GFS operational analyses and CMORPH precipitation estimate (shaded in mm h^{-1} , according to colour bar), both averaged 5–15°N for the month of August 2004.

AEW trough. Several studies have concluded that deep convective clouds tend to occur at or ahead of the AEW trough (Carlson 1969a,b; Reed *et al.*, 1977; Payne and McGarry, 1977; Diedhiou *et al.*, 1999; Kiladis *et al.*, 2006). Some of these studies included waves over the Atlantic and along the West African coast and focused on synoptic-scale convection. Other studies of mesoscale convection over West Africa found that organised convective systems are also initiated east of the AEW cyclonic centres, particularly to the north of the AEJ (Fink *et al.*, 2006; Laing *et al.*, 2008; Cifelli *et al.*, 2010). Those studies also observed MCSs that developed behind the AEW trough and propagated into the region ahead of the AEW trough (e.g. Figure 2.16).

Earlier studies by Burpee (1974), Duvel (1990), Mathon *et al.* (2002) and Fink and Reiner (2003) observed enhanced convective precipitation ahead of the AEW ridge for systems north of 12.5°N (e.g. Figure 2.17). The enhancement of convection and precipitation at or behind the AEW trough, observed mainly in the northern Sahel, is primarily influenced by moisture availability – the northward transport of moisture from the ocean and equatorial forests – and therefore matches the location of high PW* seen in Figure 2.7, relative to the wave trough. Note also in Figure 2.17 the large spatial spread in initiation locations relative to the wave trough. In contrast with mid-latitude

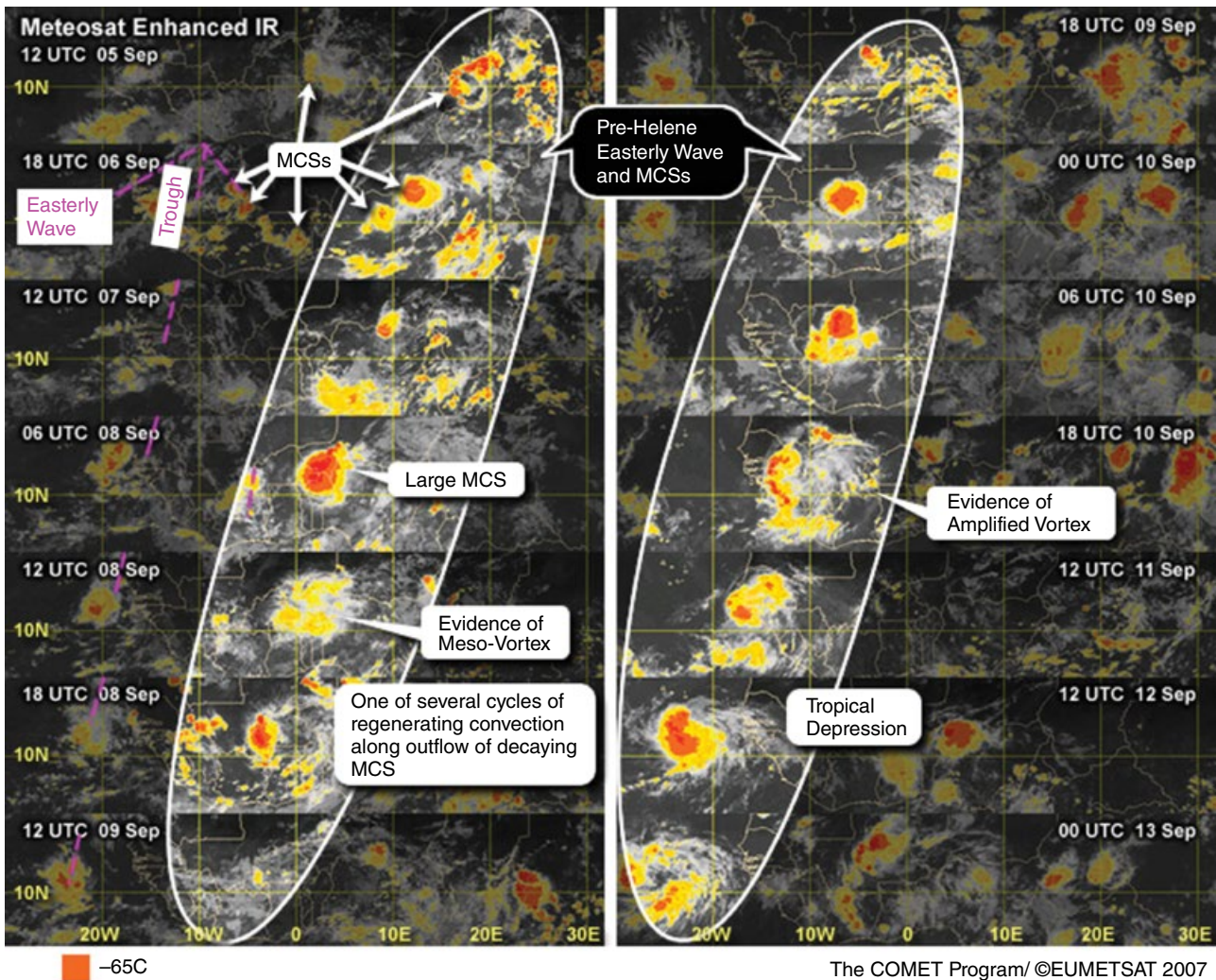


Figure 2.15 Enhanced infrared images of AEWs and MCSs between 1200 UTC 5 September and 0000 UTC 13 September 2006, precursors to Helene (2006). Source: from Laing and Evans (2011).

weather systems, the convective initiation is only relatively loosely dictated by the AEW structure, and other factors such as topographic patterns have an important role also in determining the location of convective initiation.

Note that the tilt of the trough axis to the north and south of the AEJ core means that the location of convection ahead of and behind the trough can have some ambiguity: convection to the south of the AEJ, which is collocated with the trough at this latitude, may be significantly to the west of the trough at the AEJ latitude, as in Figure 2.7.

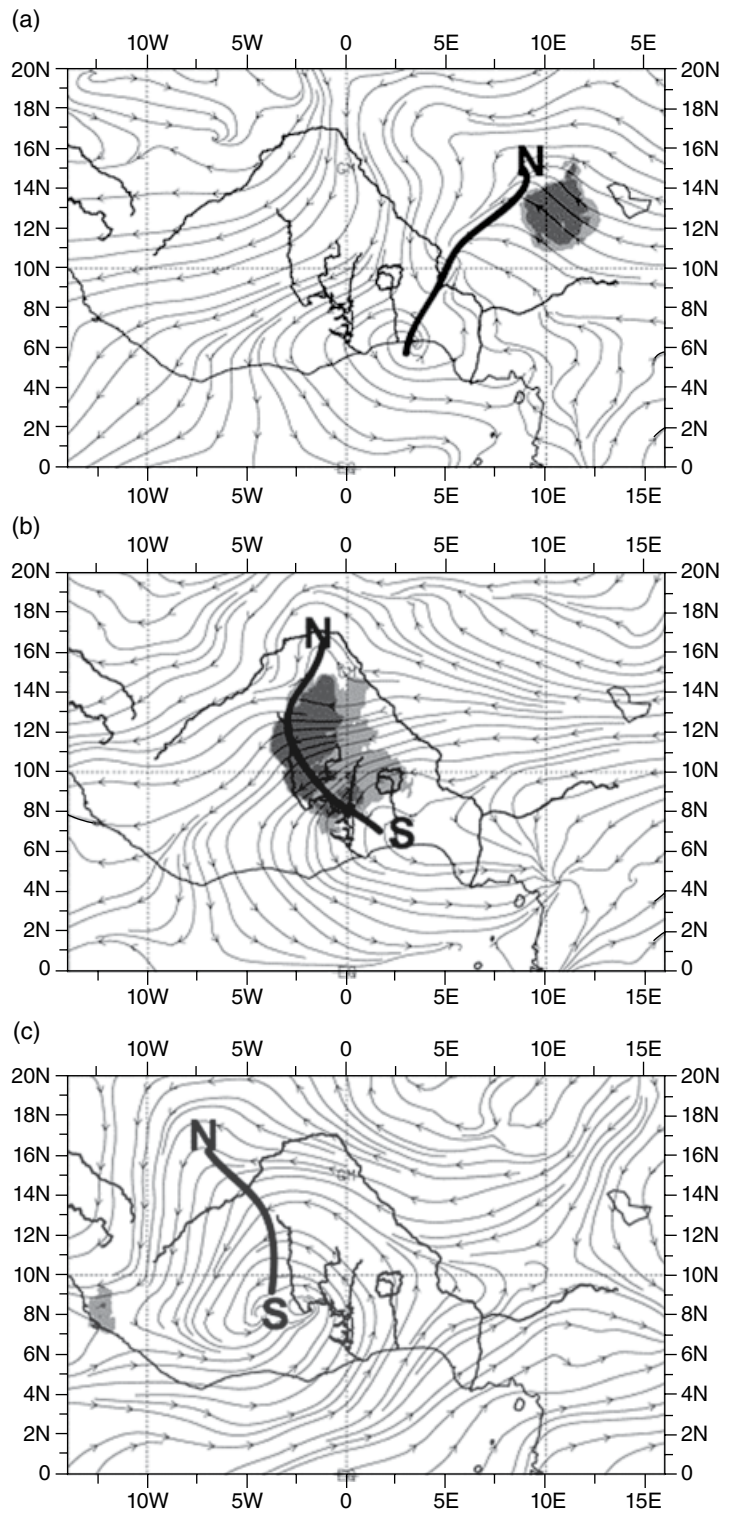
The interaction of the vorticity associated with AEWs and the mesoscale vorticity associated with MCSs is an area of active research. Some tropical cyclones, such as Alberto (in 2000), begin as AEW–MCS systems that initiate near the mountains of East Africa (the Darfur Mountains and Ethiopian Highlands) and undergo cycles of decay and regeneration while moving westward. The swirling cloud pattern at 1200 UTC 8 September

and 1800 UTC 10 September (Figure 2.15) indicates the presence of an MCV, a feature that sometimes forms in the stratiform region of decaying MCSs. The pre-Helene vortices appear to amplify over the continent within the AEW structure, a strong vortex emerges from the continent and tropical cyclogenesis occurs soon after. These observations support the notion that mesoscale convection gives rise to positive PV anomalies in the lower troposphere for tropical cyclogenesis.

2.1.3.7 Downstream Transformation

AEWs are frequently observed to traverse the Atlantic Ocean and move into the Caribbean region. During their transition across the ocean they tend to retain regions of deep convection (that can be tracked using satellite imagery) and thus remain a hazard to shipping and aviation. In the Caribbean region, AEWs can bring disturbed weather to the islands and remain an important feature

Figure 2.16 (a) Streamlines on the 850 hPa surface at 0600 UTC 3 September, (b) 0000 UTC 4 September and (c) 1800 UTC 4 September 2002. Also shown are the location of the Upper Ouémé Valley and the areas enclosed by the 233 K (light grey) and 213 K (dark grey) brightness temperatures used to track this and all other subtype Ia (advective organised convective systems) cloud systems. The analysed cyclonic centres of northerly and southerly AEWs are labelled 'N' and 'S' respectively. The bold AEW trough lines delineate the subjectively analysed maximum cyclonic curvature between the two AEW vortices. *Source:* Figure 11 from Fink *et al.* (2006). ©American Meteorological Society. Used with permission.



for weather forecasters to consider. In addition to the rainfall component, synoptic ridges associated with AEWs can transport large amounts of Saharan dust across the Atlantic Ocean (e.g. see Zipser *et al.* (2009) and Dunion and Velden (2004)). On some occasions, AEWs have been observed to interact with mid-latitude

disturbances and act as the moisture source for rainfall in northwestern Africa (Knippertz *et al.*, 2003).

AEWs are an important precursor to Atlantic and eastern Pacific tropical cyclones. Although the tropical cyclones occur outside the domain served by West African forecasters, it remains important for forecasters

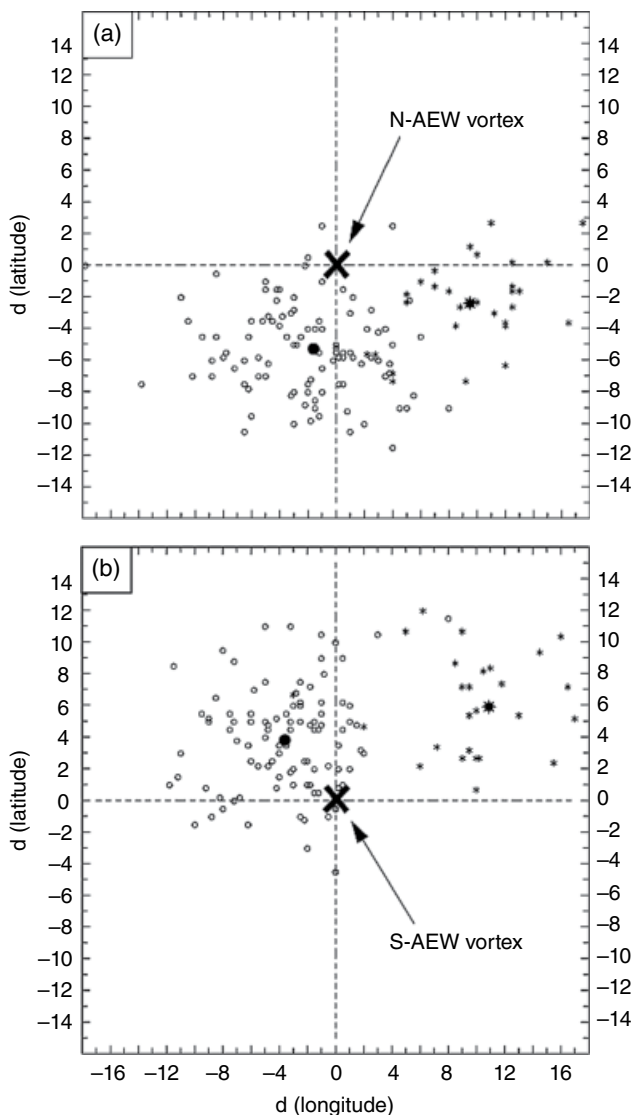


Figure 2.17 Scatterplots of the positions of origin points of squall lines relative to the simultaneous locations of the accompanying (a) northerly and (b) southerly AEW vortices. The abscissa (ordinate) denotes the longitudinal (latitudinal) distance, with negative values indicating that the squall line origin is west (south) of the respective vortices. The open circles represent squall lines that formed west of the AEW trough, while the stars denote squall lines assigned to AEW phase intervals in the southerly flow east of the trough, north of 12.5°N . The mean positions of either class of squall lines are indicated by the large bold circles and stars respectively. In both diagrams, d is difference, and both cover the periods May–October 1998 and 1999. *Source:* Figure 11 from Fink and Reiner (2003). Copyright John Wiley and Sons. Reproduced with permission.

to have some understanding of the process of transformation from an AEW into a tropical cyclone. While the locations at which the cyclone forms vary from case to case depending on the environment and the nature of the AEW, there are well-documented cases of tropical cyclogenesis occurring close to the West African coastline – for example, Hurricane Alberto in 2000 (e.g. Lin *et al.*, 2005)

and Tropical Storm Debby in 2006 (e.g. Jenkins *et al.*, 2008; Ventrice *et al.*, 2012; Lin *et al.*, 2013). In such cases, intensification of convection within the AEW toward a tropical cyclone may begin partially over land, posing a potential flooding risk (e.g. Jenkins *et al.*, 2010). Furthermore, tropical cyclones forming close to the coastline can have a negative impact on shipping, fishing, and so on in the countries of West Africa.

A high fraction of North Atlantic hurricanes have AEWs as their trigger. For example, 2005 was a particularly active hurricane season, with 23 out of 31 named storms originating from AEWs. In comparison, 2006 was a quiet season, with 7 out of only 10 named storms originating from AEWs (National Hurricane Center, 2015). Over Africa, AEWs are often characterised by a low-level vortex north of the AEJ and an AEJ-level vortex south of the AEJ (see Section 2.1.3.2). However, as the AEWs move westward across the West African coast and into the East Atlantic the southern vortex tends to develop a low-level circulation consistent with increased frequency of deep convection in the coastal region (Janiga and Thorncroft, 2013). Hopsch *et al.* (2007) compared the mean structure of AEWs that were associated with East Atlantic tropical cyclogenesis and those that were not. They noted that the mean structure of AEWs that developed tended to have stronger low-level vorticity, stronger vertical motion and higher humidities throughout the troposphere in the trough. Several recent studies have extended this work (e.g. Agudelo *et al.*, 2011; Leppert *et al.*, 2013a,b; Cecelski and Zhang, 2013). Rowell *et al.* (2016) indicate that developing AEWs usually have a stronger AEJ on the poleward side of the relative vorticity maximum. Consistent with the AEJ strength, developing AEWs generally have a stronger relative vorticity maximum over the lifetime of the AEW and developers tend to develop faster, with a statistically significant increase over non-developers in the first 48 h once west of 20°W . Developing AEWs tend to have a mean SST greater than 27°C , and this is particularly significant over the first 48 h, where the great majority of developers have an SST greater than 27°C . Also, the developing AEWs pass through a more humid troposphere, particularly at the AEJ level and above. The consensus from these studies is that AEWs that have stronger low-level circulations, moister columns and have more ubiquitous convection as they track into the East Atlantic are more likely to be associated with tropical cyclogenesis.

2.1.4 Mid-latitude Troughs and Upper-level Troughs

Upper-level troughs from the mid-latitudes significantly affect tropical West Africa during the boreal winter half year (Knippertz, 2007). A widely used method for identifying such systems is to detect significant anomalies in

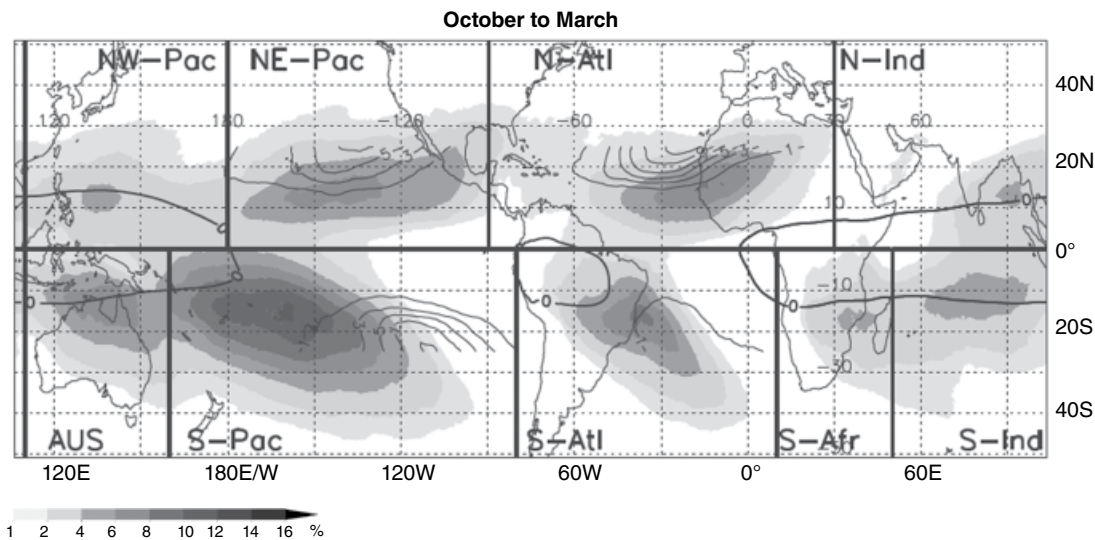


Figure 2.18 Mean tropical plume frequency (%; shaded) for October–March between 1983/84 and 2005/06. The contours display the mean frequency of troughs at low latitudes (%) detected by Fröhlich and Knippertz (2008) in the ERA-40 data between 1980 and 2001. The bold grey contour presents the zero line of the mean zonal wind at 200 hPa indicating equatorial easterlies from the western Pacific to the eastern Atlantic and over South America, with westerlies elsewhere. *Source:* Figure 4a from Fröhlich *et al.* (2013). ©American Meteorological Society. Used with permission.

PV, either on an isentropic surface that intersects the subtropical tropopause, or averaged over the upper troposphere/lower stratosphere. Climatologies of these so-called PV intrusions or cut-offs show a frequency maximum over the Atlantic Ocean near northwestern Africa (Figure 2.18). For lower isentropic levels, the maximum shifts northeastward into the Mediterranean Sea – see Wernli and Sprenger (2007: figure 4). The frequency of PV intrusions is largely reduced during the summer half year (Fröhlich and Knippertz, 2008).

Linear Rossby wave theory provides a first-order explanation for the geographical, vertical, seasonal and even interannual behaviour of mid-latitude trough penetration to low latitudes. Mean zonal winds near the tropopause are strongly westerly over the tropical East Pacific and Atlantic Oceans (see Figure 2.18). This allows a propagation of Rossby wave energy into these regions, which have been referred to as ‘westerly ducts’ for this reason (Webster and Holton, 1982; Hoskins and Ambrizzi, 1993; Kiladis and Weickmann, 1997). The westerly winds weaken during the summer half of the year and toward lower levels, associated with a reduction in trough occurrence (Tomas and Webster, 1994; Fröhlich and Knippertz 2008). The El Niño/Southern Oscillation modifies the equatorial winds on interannual timescales, causing a tendency of reduced PV intrusion activity over the Pacific Ocean and enhanced PV intrusion activity over the Atlantic (Waugh and Polvani, 2000).

A clear indicator of the penetration of an upper-level trough into low latitudes in satellite imagery is the occurrence of a tropical plume on its eastern flank (Iskenderian, 1995; Knippertz, 2005). Tropical plumes are elongated

continuous bands of mainly upper- and middle-level clouds that stretch for thousands of kilometres poleward and eastward from the ITCZ into the subtropics (Figure 2.19). Usually, an anomalously strong subtropical jet (STJ) streak is aligned along the often-sharp poleward edge of the tropical plume (Figure 2.19). Climatological studies show a tropical plume frequency maximum over the eastern Atlantic/western West Africa, consistent with the PV intrusion climatology (Figure 2.18). Amounts of precipitation associated with tropical plumes differ largely between systems and along the axis of the tropical plume. Knippertz (2005), for example, describes a tropical plume that is rooted in ITCZ convection over South America, stretches across the Atlantic as an upper-tropospheric cloud band and is finally associated with heavy precipitation over northwestern Africa.

The precipitation events associated with upper-level troughs over tropical West Africa during the dry season November to March are sometimes referred to as ‘Heug’ or ‘Mango’ rains. They are irregular in time, space and magnitude. Their climatological contribution to annual rainfalls is estimated to be on the order of a few per cent only, which is hardly relevant for agriculture (Seck, 1962; Gaye *et al.*, 1994). There are, however, examples of much more significant dry-season rainfalls associated with upper-level troughs. Such events can have substantial impacts on local hydrology and human activities, from the greening of pastures to the flooding and rotting of harvests (Knippertz and Martin, 2005; Fall *et al.*, 2007; Knippertz and Fink, 2008).

The climatology and past case studies suggest a distinction of two different stereotypical cases and

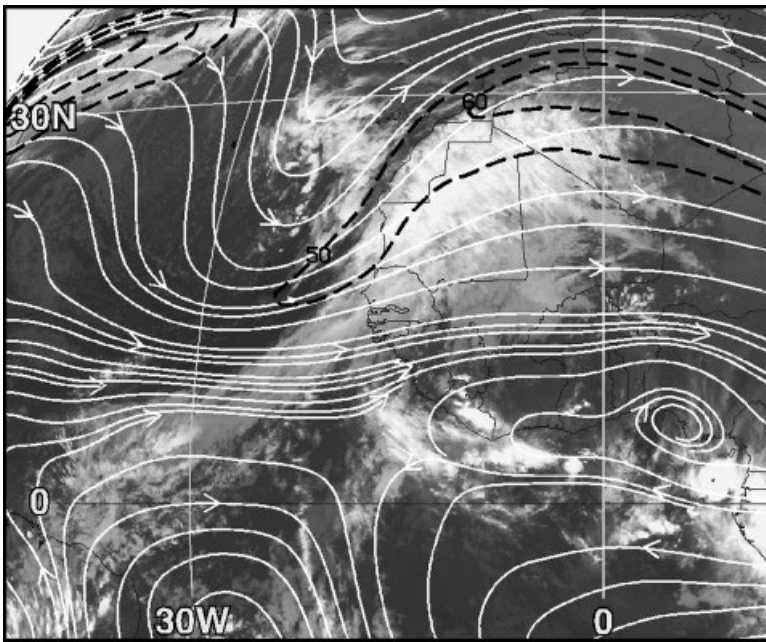


Figure 2.19 Meteosat infrared satellite image for 0000 UTC 10 January 2002 with superimposed isotachs (dashed black in m s^{-1}) and streamlines (in white), both at the 345 K isentropic level. Source: slightly modified version of Figure 2c from Knippertz and Martin (2005). Used with the permission of the Royal Meteorological Society.

mechanisms. Although in each of these mechanisms the flow pumps the ITD northward together with deep moisture, the trough and STJ positions differ.

1) Sahelian/Saharan countries close to the west coast of West Africa, such as Sénégal, Gambia, Mauritania and Mali, can be directly affected by upper-level troughs penetrating southward over the eastern Atlantic Ocean, as the ones shown in the climatology and case example in Figures 2.18 and 2.19. Significant events have been described by a number of authors, including Seck (1962), Borgne (1979), Gaye *et al.* (1994) and Knippertz and Martin (2005). An interesting case worth mentioning is the record-breaking, high-impact case during 9–11 January 2002 (Figure 2.19). Storm totals of more than 50 mm fell over a widespread area covering northwestern Sénégal and southwestern Mauritania. New January precipitation records were broken at several observing stations, led by Podor in northern Sénégal with 115.8 mm. Several people were killed in collapsing houses or through hypothermia, buildings were damaged or destroyed by flooding, and the loss of crop and livestock was substantial (Fall *et al.*, 2007). Several dynamical ingredients are necessary to create such an extreme event (Knippertz and Martin, 2005), as depicted in Figure 2.20a: (a) A previous low-latitude upper-trough instigates a transport of moist air from the Atlantic and the inner tropics toward the western Sahel without generating any significant precipitation; (b) the moistening of lower levels causes a significant destabilisation in the region of interest; (c) a subsequent trough releases the convective instability

through weak forcing for mid-level ascent; (d) there are indications that inertial instability in the right entrance region of the STJ streak might further enhance uplift. Knippertz and Martin (2005) show that a succession of two troughs is not necessary toward the end of the rainy season, when the spatial distance to the main moisture reservoir is smaller, so that sufficient transport can be achieved by one persistent system.

2) The entire Guineo-Soudanian zone ($\sim 7\text{--}12^\circ\text{N}$) can be affected by occasional northward shifts of the main rain zone, which usually end just north of the Guinea Coast during the dry season. Knippertz and Fink (2008) document that these shifts can be triggered by the penetration of an upper-level disturbance into northern Africa (Figure 2.20b). This is more indirectly communicated through falling pressures over the Sahara and Sahel in the right entrance region of the anomalous STJ streak to the southeast of the positively tilted trough, where warm advection prevails at upper levels (this corresponds to ascending poleward flow ahead of the trough). The associated northward shift and intensification of the usually weak continental heat low allows moist southerlies to penetrate further than normal into the continent. Daytime heating of the (at this time of the year) rather dry land surface can then trigger deep moist convection and dry-season precipitation. As for the western Sahel cases, dry-season precipitation events are often preceded by very persistent or repeated troughing over northern Africa, which allows the slowly responding tropical circulation to attune to the forcing (Knippertz and Fink, 2009).

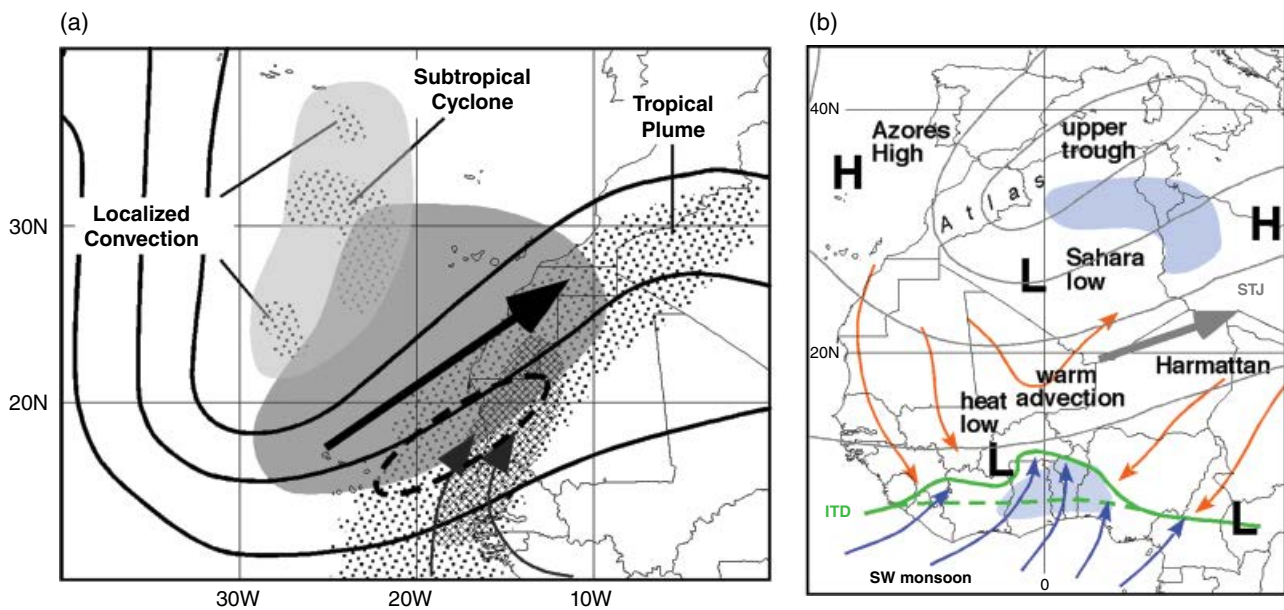


Figure 2.20 Schematic depictions of the large-scale circulation associated with dry-season precipitation over West Africa associated with low-latitude upper-level disturbances from the extratropics. (a) Cases with a direct influence from the upper trough, mostly affecting the western Sahel. Thick black lines delineate the low-latitude upper trough and the thick arrow indicates the associated STJ streak. Thin grey arrows show mid-level moisture transports from the deep tropics. Stippled regions indicate high clouds, and hatching delineates the major precipitation zone. Light (dark) grey shading depicts the region of convective instability under the coldest air at upper levels (positive quasi-geostrophic forcing for mid-level ascent). The dashed lines bound a region of upper-level inertial instability along the anticyclonic shear side of the jet. *Source:* Figure 11 from Knippertz (2007). Used with permission. (b) Cases with an indirect influence from the upper trough, mostly affecting the Soudano-Sahelian zone. Grey lines depict upper-level geopotential height. The green dashed and solid lines show the climatological and the actual position of the intertropical front that separates dry continental air and northerly flow from moister air and southerly flow. Regions with precipitation are shaded in blue. For more details, see text. *Source:* modified version of Figure 14 from Knippertz and Fink (2008). ©American Meteorological Society. Used with permission.

A scientific result with great relevance for operational weather forecasting in tropical West Africa during the dry season is the enhanced predictability of rainfall directly or indirectly associated with extratropical troughs. The detailed modelling case study by Meier and Knippertz (2009) shows fairly robust predictions of the extraordinary January 2002 case over Sénégal and Mauritania up to lead times of 7 days, consistent with the successful reproduction of the case with regional models by Knippertz and Martin (2005) and Fall *et al.* (2007). Statistical evaluations of 5-day forecasts of unusual dry-season rainfall events in the Guineo-Soudanian zone with the model of the ECMWF indicate that extratropical influence enhances predictive skill (Knippertz and Fink, 2009). These results should encourage forecasters to take advantage of available dry-season precipitation forecasts in terms of the dissemination of early warnings.

2.1.5 Extratropical Dry Air Intrusions

Layers of very dry air (relative humidity (RH) <10%) are observed over many tropical regions in the free troposphere. In a generally rather moist immediate environment, such dryness can only be fed by air originating

from the upper level of the extratropics, where similar potential temperatures and water vapour mixing ratios exist. As a result, these dry layers are known as dry ‘intrusions’ to highlight their non-tropical origins. These layers have been shown to modulate convective activity strongly over the tropical oceans at various scales (Brown and Zhang, 1997; Redelsperger *et al.*, 2002).

Such extratropical dry air intrusions have also been identified in the WAM mid-troposphere (Roca *et al.*, 2005). The analysis revealed that, at 500 hPa over the Sahel, dry air originating in the upper levels (200–250 hPa) on the anticyclonic side of the polar jet stream around 50°N is frequently observed at various scales. The dry intrusions start subsiding over Europe and travel south on the 330 K isentropic level reaching, a few days later, the Sahelian mid-troposphere (Figure 2.21).

Mid-tropospheric dry air influences convective activity and rainfall variability in various ways. Dry air generally has an inhibiting effect on the first initiation of convection, as a result of the temperature inversion induced by long-wave radiation at the bottom of the dry layer (Mapes and Zuidema, 1996) or by entrainment of dry air into ascending parcels that decreases their buoyancy and limits the vertical development of the convective clouds (e.g. Parsons *et al.*, 2000). In contrast, mid-level dry air favours the organisation

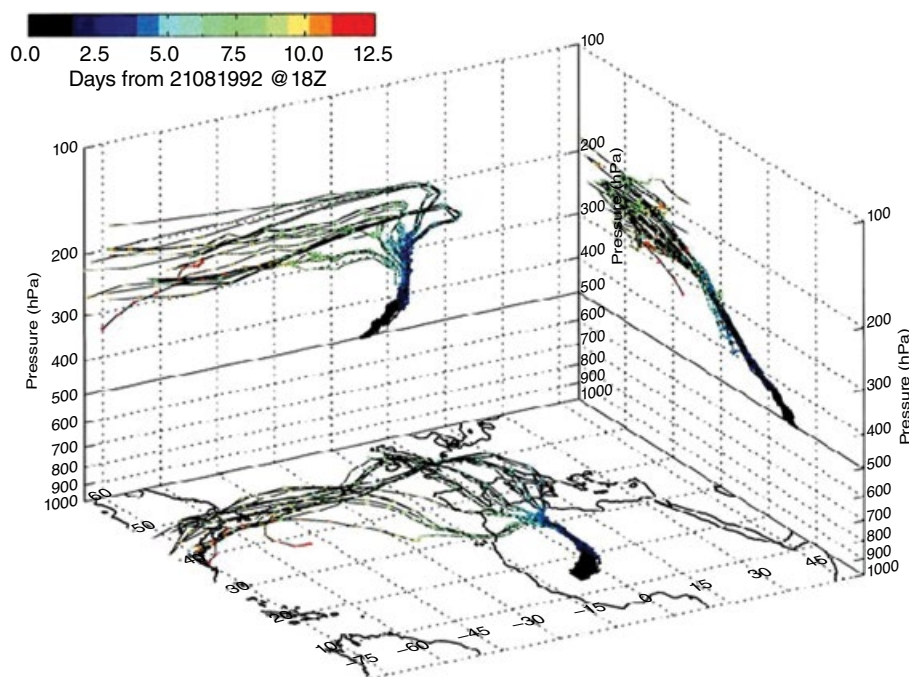


Figure 2.21 Three-dimensional view of an ensemble of back trajectories initially located at 500 hPa centred at (a) 15°N, 6°W. The colour scale indicates the duration of the air mass along the trajectory in days since 1800 UTC 21 August 1992. Source: Figure 9(a) from Roca *et al.* (2005). ©American Meteorological Society. Used with permission.

of convection into squall lines, by feeding downdraughts and mid-level rear-inflow currents, known to be key elements of organised convective systems (Section 3.1.3).

Figure 2.22 shows the Hovmöller diagram of the RH at 500 hPa averaged over the 12.5°N–17.5°N latitude belt for the 2006 season, along with the latitude of last saturation of the air masses, and reveals some features of dry intrusion events. Three substantial events, labelled 1 to 3, correspond to pan-West African dry intrusions. These plumes are composed of very dry air with RH below 10% and even below 5% at some points, and last from 3 to 5 days. These dry structures travel from around 25°E to the Atlantic coast. The three events are separated by around 40–50 days and are thought to be associated with Madden–Julian oscillation (MJO) events that were clearly depicted in the equatorial wind anomaly during the season (Janicot *et al.*, 2008), although the link between the pan-African dry events and the MJO is not direct.

A second type of event with smaller-scale dry structures with RH below 10% is also observed. This latter mode is more restricted to the Sahel region and exhibits synoptic timescales (see also Roca *et al.* (2005)).

The three dry intrusions highlighted in Figure 2.22 each led to a substantial reduction in West African rainfall. South of the ITD, down to the coastal regions, the average rainfall anomaly associated with these three events was negative, around 5 mm day⁻¹; a significant portion of the

seasonal rain. The cloudiness and MCS anomalies concur with the rainfall anomaly, leading to a large, well-spread, negative anomaly associated with the dry intrusions. Note that during the three events, AEWs were active over the region but did not yield significant rainfall or deep convective events (Deme and Roca, 2008).

2.1.6 Guinea Coast Systems

2.1.6.1 Guinea Coast Cloud and Rainfall

The Guinea Coast is defined here as the region between Cape Palmas and the Niger delta in the south and the ninth parallel in the north. Between 8°N and 9°N, the annual cycle of rainfall changes from bimodal in the south to unimodal in the Soudano-Sahelian zone. The Guinea Coast region has annual precipitation in excess of 1000 mm, with more than 2000 mm in some places (Section 1.2). Consequently, the natural vegetation ranges from rainforest to a semi-deciduous tree savannah.

The Guinea Coast experiences different types of rainfall. A categorisation into different types of rainfall has been made by, for example, Acheampong (1982), Omotosho (1985), Kamara (1986), and Fink *et al.* (2006, 2010). In principle, these authors distinguish between squally MCSs or disturbance lines (Section 3.1.3.2), monsoon or vortex rainfall, and isolated thunderstorms. Other types of rainfall are afternoon thunderstorms that

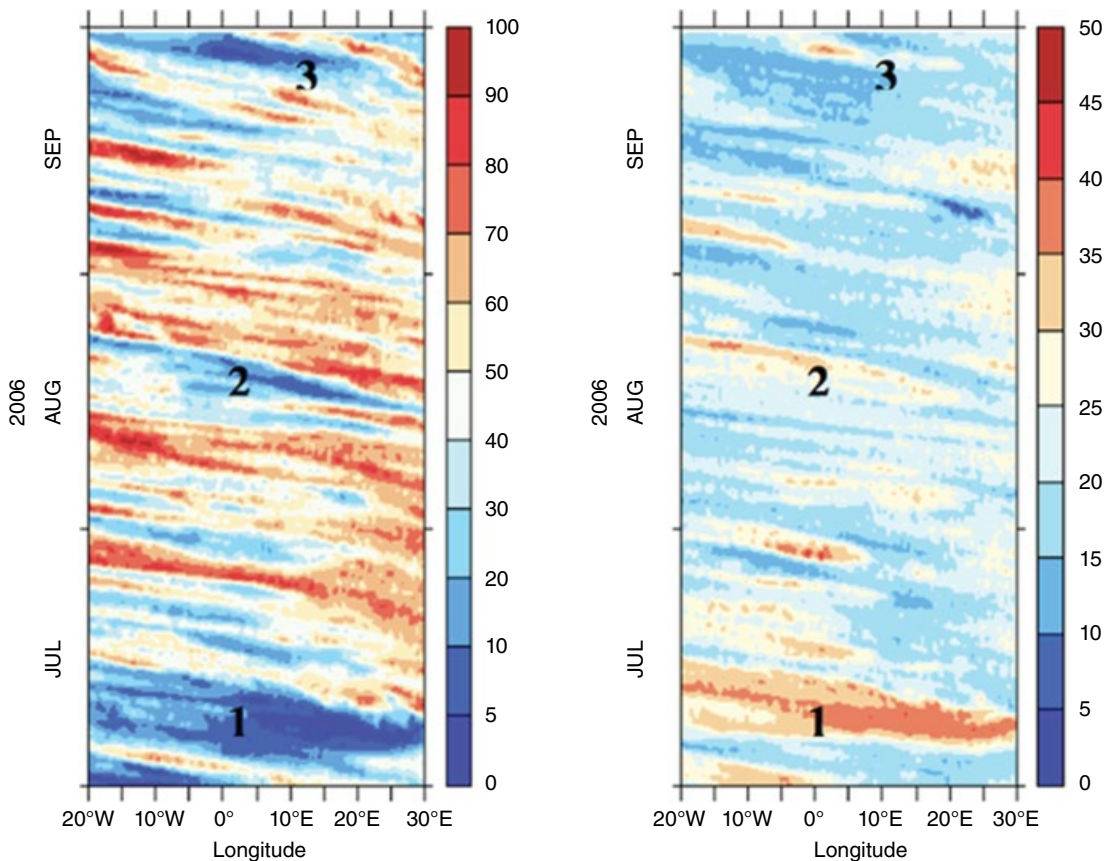


Figure 2.22 Time–longitude diagram averaged over the 12.5–17.5°N latitude belt for the 2006 season. Left: RH at 500 hPa. Right: latitude of last saturation (degrees north). The bold numbers correspond to the three identified large events. Both the humidity and the last saturation information come from a Lagrangian modelling effort (Pierrehumbert, 1998; Pierrehumbert and Roca, 1998) fed by NCEP/GFS analysis.

are aligned parallel to the coast and are associated with the land–sea breeze (Section 4.1.4.2), and dry-season rainfall events in relation to the tropical–extratropical interactions described in Section 2.1.4. In the following, the synoptic conditions associated with MCSs and vortex rainfall are briefly described.

MCSs at the Guinea Coast can occur throughout the year, but they are rare between December and February and confined to the immediate coastline. They are more frequent between March and November, and peak in April–May before the first rainy season, and October after the second rainy season (Acheampong, 1982; Omotosho, 1985). This is because, at this time of the year, a mid-level northeasterly wind component (Figure 1.25) provides the low-level vertical shear and mid-level dryness necessary for the organisation of the convection into MCSs (Section 3.1.3.2). Contrary to the conditions in the Sahel during its rainy season, the Guinea Coast zone is characterised by moister and less sheared vertical profiles throughout most of the year (Parker *et al.*, 2005a). Therefore, MCSs in the coastal zone tend to have a slower westward propagation speed and reveal warmer cloud-top temperatures in infrared

satellite imagery than systems that occur further north (Schrage and Fink, 2007). Owing to the moister troposphere and slower propagation speed, rainfall amounts are not necessarily lower than for Sahelian MCSs and can cause severe local flooding. However, peak gusts, temperature and specific humidity drops are less pronounced than in the Sahel even though hurricane-force winds have been reported along the Guinea Coast in association with the arrival of a convective cold pool (Section 3.1.2.2).

Another type of rainfall at the Guinea Coast has been termed ‘monsoonal rains’. These are prolonged periods (longer than 4–6 h) of steady or intermittent, light to moderate rains from convection with low electrical activity (Eldridge, 1957; Kamara, 1986; Buckle, 1996). Fink *et al.* (2006) speculated that some monsoon rainfall events might be dynamically linked to low- to mid-tropospheric vortices and used the term ‘vortex-type rainfall’⁶ for a weather pattern when deep westerlies were observed as a consequence of a nearly stationary mid-level vortex to the north of the Guinea Coast. This rainfall type was associated with a very moist troposphere with low CAPE, small CIN and low shear in the lower troposphere, but strong TEJ winds aloft. While this environment is not conducive

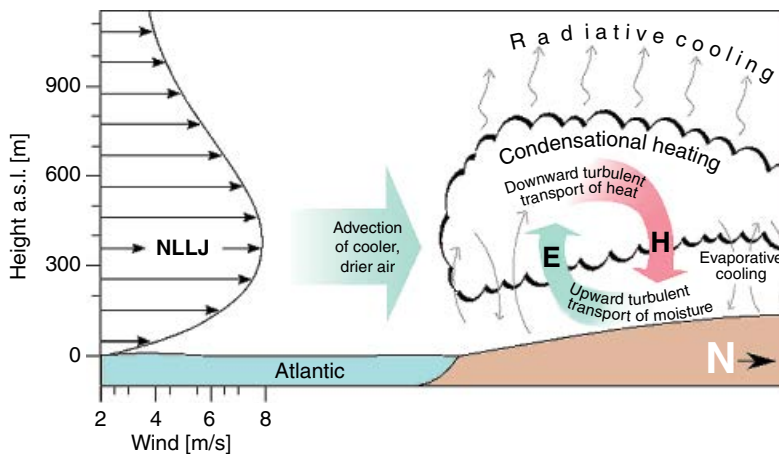


Figure 2.23 Meteorological processes associated with the formation of low-level stratiform cloud decks at the Guinea Coast. The NLLJ is driven by the onshore pressure gradient, enhanced by the sea breeze, and causes cold air advection from the Atlantic Ocean, the turbulent upward mixing of moisture (E) and downward mixing of warmer air (H). These processes dominate over detrimental effects like dry air advection by the NLLJ and early night near-surface inversions (not shown) during most nights of the wet season, and thus the night-time cloud formation is widespread. *Source:* Figure 12(a) from Schuster *et al.* (2013). ©American Meteorological Society. Used with permission.

to the formation of MCSs, the vortex in the lower troposphere may be associated with low-level synoptic-scale convergence that triggers the convection, especially at daytime. However, not much is known about the dynamics of this rainfall type, nor the origin of the vortices. Achaempong (1982) speculates the low-level vortices are related to orographic effects. It may not be excluded, however, that some of the slow-moving vortices are decelerated or stalling AEWs – an AEW behaviour that has been noted for the 1 September 2009 extreme rainfall event at Ouagadougou (see Section 2.2.2.2).

In 2002, a vortex-type event occurred at the end of the summer monsoon. The presence of a mid- and upper-level trough from the mid-latitudes blocked the usual easterly air current of the AEJ. As a result, deep westerly winds were present up to a level of about 500 hPa. This period was characterised by frequent rain events, indicating that the troposphere was supplied by sufficient water vapour from the Gulf of Guinea. Over various parts of Togo, Benin and Nigeria, deep convection was initiated during the morning hours of 1 October 2002. The cloud cells merged to one single MCS that moved toward the southwest. This cloud system finally collapsed east of Lake Volta during the night hours on 2 October 2002. The radiosonde observations from Parakou from 1 October 2010 at 1200 UTC show an unstable layering of the troposphere, up to about the 200 hPa level, leading to the widespread occurrence of deep convection. In Benin's synoptic stations this deep convection resulted in rainfall amounts of 21 mm, 13 mm, 2 mm and 0.5 mm at Savè, Bohicon, Natitingou and Cotonou respectively.

A rather recurrent weather feature at the Guinea Coast during the wet season is the southwesterly night-time low-level jet (NLLJ; see Section 4.1.3.2) and associated, extensive low-level stratiform cloudiness. Clearly, for aviation weather, the NLLJ and low-level clouds are important, especially for airports inland of the Guinea Coast. The cloud base is so low that it sometimes rests at

the surface and causes fog, especially over higher terrain (Section 4.1.3.3). The low-level cloudiness was first mentioned by Schrage and Fink (2007) and it is the typical situation for nights that lack deep convection, though some clear nights occur as well. Van der Linden *et al.* (2015) created a low-level cloud climatology and showed that, after sunset, the zone of abundant low-level stratiform clouds is confined to latitudes south of 6–7°N but starts to spread inland during early night hours. Its maximum northward extent is reached between 0900 and 1000 UTC when its northern edge is located between 10°N and 11°N. The area affected by a large fraction of nocturnal and morning low-level clouds between 10°W and 10°E is in the order of 800 000 km². Schuster *et al.* (2013) summarised the mechanisms that favour or disfavour the genesis of the low-level cloudiness (Figure 2.23). A strong night-time low-level jet promotes upward mixing of moisture and cooler air as well as cold air advection from the cool waters of the Gulf of Guinea. Detrimental to the formation of the low-level clouds is a strong surface inversion early in the night and dry air advection from the Atlantic Ocean. Once formed, the OLR at the top of the cloud layer seems to stabilise the cloud layer. It is important to note that the night-time inland spreading of the low-level clouds, as described in van der Linden *et al.* (2015), is not an advection feature, but a northward propagation of turbulence underneath the evolving NLLJ. Apparently, there are subtle balances during non-precipitative nights that determine whether clouds form or not. As a consequence, about one-third of the nights remained clear at Djougou (central Benin) during June–October 2006 (Schrage and Fink, 2012), and models struggle to have a realistic climatological representation or to forecast the cloud layer (Knippertz *et al.*, 2011; Schuster *et al.*, 2013).

2.1.6.2 The Little Dry Season

The areas southwest of Nigeria, and coastal parts of Benin, Togo, Ghana and Cote d'Ivoire, experience the

influence of the “little dry season” (which corresponds to ‘zone D’ of Figure 1.1). This phenomenon occurs between July and August when negative anomalies are observed in the rainfall pattern. A drop in static energy is associated with its occurrence. Cold winds, low surface temperatures, morning drizzle, sunny afternoons and partly cloudy conditions characterise this period.

The effect of a prolonged little dry season can be positive or negative. During this period, some crops that have suffered from excess water normally get some relief. Also, this period presents a favourable environment for cold-related diseases.

The mechanism of formation of the little dry season has been linked to some of the meteorological parameters – rainfall, pressure, equivalent potential temperature, surface temperature, surface wind and SST. Most simply, it is linked to the northward progression of the ITD and the whole monsoon system around the time of monsoon onset. Though the little dry season occurs annually, its onset, duration and cessation vary from year to year.

Over the years it has been observed that the peak surface pressures are, by July, linked to the little dry season. During this period, the high pressure builds in the Gulf of Guinea and the St. Helena high pressure cell exhibits significant anticyclogenesis. This effect spreads to the coastal areas of West Africa, where sinking motion is established and convection is reduced to a minimum. The classical flow over the Gulf of Guinea during this period is anticyclonic. Owing to upwelling off the Gulf of

Guinea, there is a cooling in the SST during this period. It shall be stressed, however, that the little dry season is most pronounced where coastal upwelling and cold SSTs are strongest; that is, along the coasts of Ghana east of the Cape of the Three Points as well as along the coasts of Togo and Benin. The little dry season is weak or absent where warm onshore waters persist and the coastline is perpendicular to the southwest monsoon winds; for example, the Niger delta in Nigeria and the Pepper Coast of Liberia (see Figures 1.5 and 1.25).

2.1.7 Synoptic-scale Land-surface Feedbacks

Moist convection is strongly modulated by synoptic variability, as discussed in Section 2.1, and the diabatic heating associated with convection is considered to play an important role in the growth of AEWs. Here, we consider an additional feedback between rainy systems and the synoptic dynamics, which operates via the impact of rainfall on soil moisture and the surface energy balance. Surface fluxes of sensible and latent heat in sparsely vegetated regions of Africa are very sensitive to rainfall in previous days. For 2–3 days after rainfall, the daytime turbulent fluxes are dominated by latent heat, with only weak exchange of sensible heat with the planetary boundary layer (PBL; Kohler *et al.*, 2010).

An example of synoptic-scale variability in surface fluxes is shown in Figure 2.24. Rain occurred across much of the southern part of the domain in the preceding 36 h,

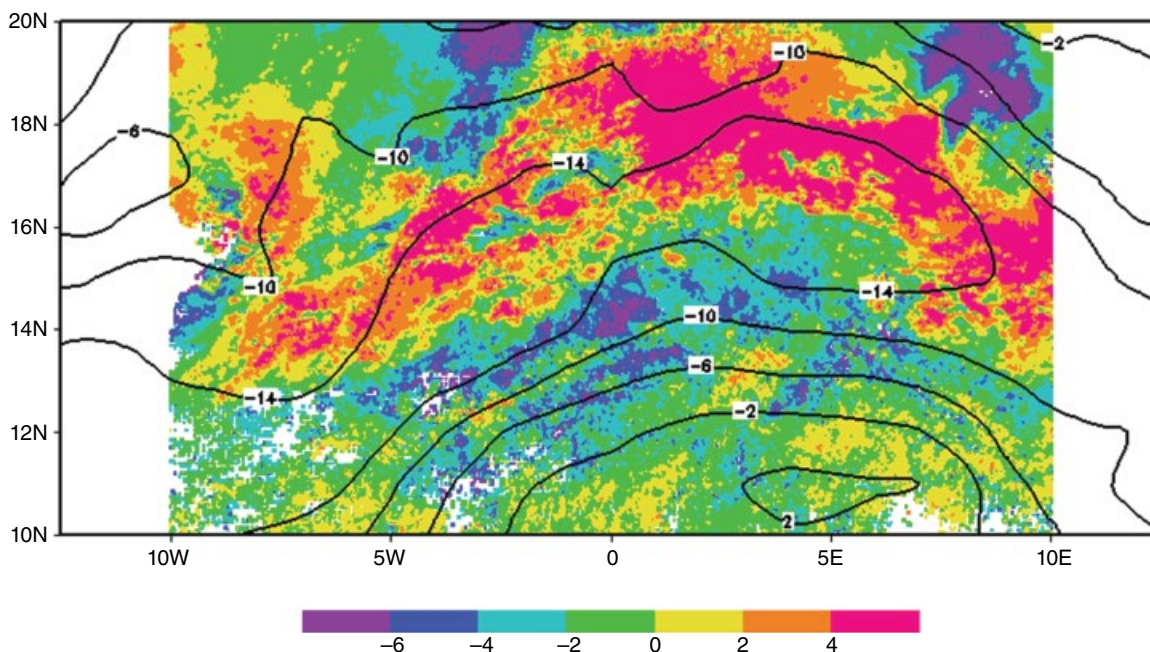


Figure 2.24 Daytime land surface temperatures (shading; K) on 26 July 2006 derived from Meteosat Second Generation (<http://landsaf.meteo.pt>) anomalies from the 30-week mean. The (pink) band of positive temperature anomalies denotes a dry region, whilst the relatively cool (blue) conditions to the south indicate high soil moisture from storms in the previous 36 h. The zonal wind (m s^{-1}) at 700 hPa from the ECMWF operational analysis for 1200 UTC on that day is overlain, indicating a significant kink in the AEJ.

extending as far north as 16°N in the central region. This rain occurred in association with a developing wave, depicted by the 700 hPa zonal wind (Bain *et al.*, 2010). In this case, the atmosphere induced a wave-like structure in soil moisture and surface fluxes. According to estimates from an ensemble of land models forced by observations as part of the AMMA Land Model Intercomparison Project (ALMIP; Boone *et al.*, 2009), the antecedent rainfall pattern resulted in very marked spatial variability of surface fluxes; 24 h mean values of sensible and latent heat fluxes were of the order of 70 W m⁻² and 20 W m⁻² respectively in the dry (pink) areas, compared with sensible and latent heat fluxes of 0 W m⁻² and 120 W m⁻² respectively in the recently wetted (blue/purple) region at 14–16°N. Such strong contrasts in surface fluxes have been shown to have a substantial impact on the lower atmosphere (Kohler *et al.*, 2010).

Figure 2.25 illustrates the geographical distribution of variability in surface fluxes on synoptic timescales. The data, again derived from the ALMIP dataset, depict a band of strong variability in sensible heat (and also latent heat, not shown) across the Sahel belt during the monsoon season. The location of this band is determined largely by day-to-day variability in near-surface soil moisture and its impact on evapotranspiration. South of the Sahel, the vegetation is dense, and latent heat flux is dominated by transpiration of soil water stored in the root zone. In the Sahel, evaporation direct from the soil becomes an important term in the energy balance, driven by rainfall typically every few days. Finally, in the north, though the land is sensitive to soil water, lack of rainfall restricts variations in surface fluxes. On top of this

hydrological driver one can also add radiative forcing, where cloud cover restricts the total surface energy flux.

There have been several modelling studies that have examined in detail how soil moisture feedbacks influence West Africa at the synoptic scale. In an early study, Walker and Rowntree (1977) found a strong sensitivity of a developing AEW to soil moisture in their simulations. Cook (1999) highlighted the importance of the meridional gradient in soil moisture for the maintenance of the AEJ, but did not consider the temporal fluctuations in the soil moisture field. A subsequent GCM study (Taylor and Clark, 2001) examined the sensitivity of AEWs to the underlying land surface. They found increased synoptic variability in a simulation where a description of dense vegetation in the Sahel was replaced by a more realistic parameterisation of sparse vegetation. The latter produced increased day-to-day variability in surface fluxes, which, it was argued, enhanced synoptic variability in the atmosphere.

Taylor *et al.* (2005) examined the temporal variability in the surface energy balance using cloud-free thermal infrared imagery. They found strong synoptic-scale fluctuations in surface temperature across the Sahel driven by rainfall, with minima in regions of wet soil. The surface temperatures (and hence surface fluxes) were found to be well-organised at the synoptic scale, linked to the westward propagation of MCS and AEWs. They developed a conceptual model of the land–atmosphere interaction within an AEW, which is depicted schematically in Figure 2.26.

Considering an extensive, synoptic-scale dry zone such as depicted on the left (west) of Figure 2.26, strong horizontal gradients in temperature will develop in response

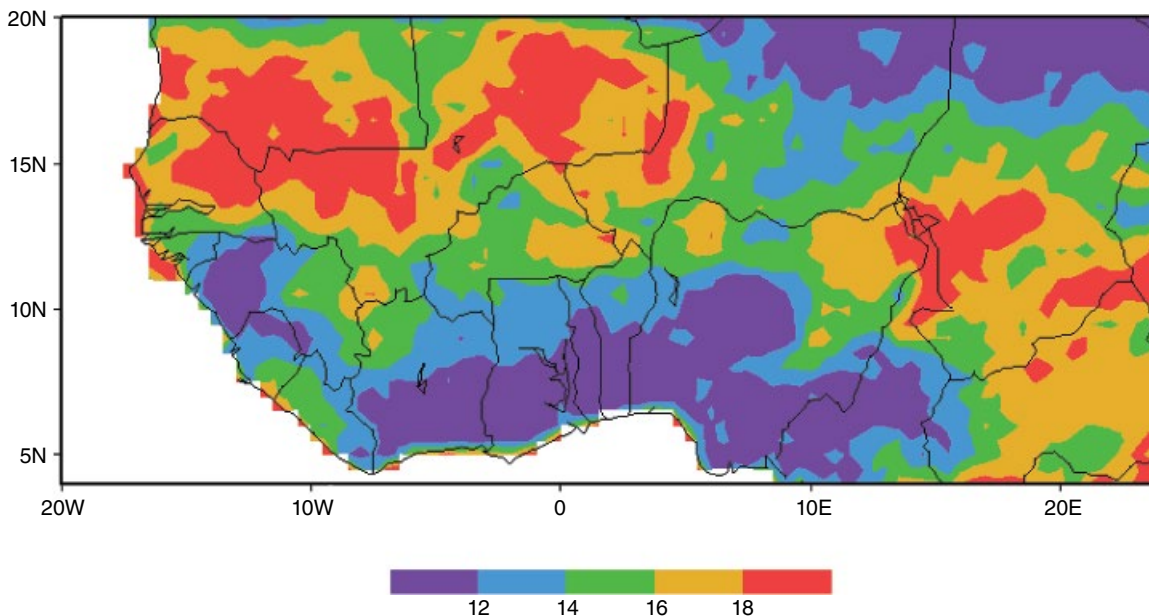


Figure 2.25 Standard deviation of sensible heat flux H (W m⁻²) averaged over July–September 2004–2007 from the ALMIP model ensemble (Boone *et al.*, 2009). The daily data have been filtered to remove variability with periods exceeding 10 days.

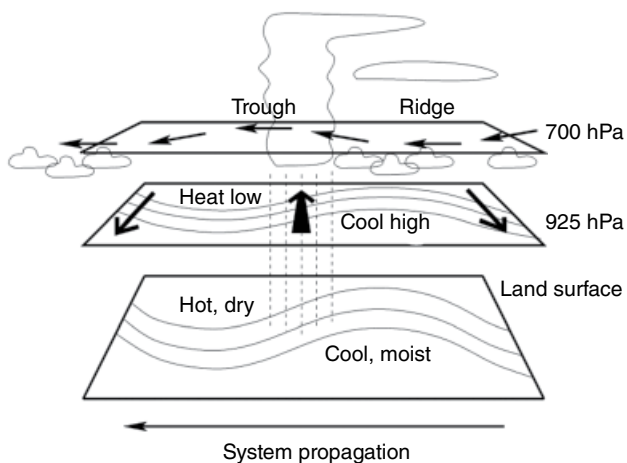


Figure 2.26 Schematic depicting land–atmosphere coupling within an AEW. The modulation of convection by a wave at 700 hPa creates synoptic variability in soil moisture, with wet soils favoured behind the trough. Zonal contrasts in availability of moisture for evapotranspiration drive sensible heat flux patterns, which perturb the isentropes at 925 hPa. In turn, this configuration favours maximum southerly flow between the dry and wet soils, enhancing new convection there. *Source:* Figure 7 from Taylor *et al.* (2005). Used with the permission of the Royal Meteorological Society.

to the daytime surface sensible heat flux contrasts. These perturb the climatological meridional gradient of temperature. Following Rácz and Smith (1999), during the day, when horizontal low-level flow is weak, a heat low anomaly tends to develop over the dry soil. Once the sun sets and coupling with the land surface effectively switches off (Section 4.1.3.2), the atmosphere responds to the thermal gradient generated during the day. This induces the development overnight of positive vorticity above dry soil, superimposed on the existing atmospheric dynamics. In the West African context, this flow favours enhanced southerly advection of moisture to the east of the dry soil, providing a favourable environment for new a MCS there (recalling from Section 2.1.3.6, that in the northern Sahel, where rainfall is limited by PW, rain occurs in the positive PW*, to the east of the low-level trough). As these systems propagate westward, they will tend to erode the dry anomaly from the east, in effect shifting the surface features westward. Similarly, on a timescale dictated by the drying of the top soil after rain (~2–3 days), the pre-existing wet soil to the east (right of Figure 2.26) will weaken in the absence of further rain. On top of this diabatic coupling, Parker (2008) explored the impact of adiabatic Rossby wave dynamics. Surface-induced zonal temperature anomalies embedded within the strong meridional gradient propagate westward through this mechanism. Analysis of a linear model showed that the fastest growing mode occurs when the lower atmosphere has a thermal anomaly to the east of a land surface temperature anomaly.

Modelling and observational evidence have been presented to illustrate how this form of coupling influences

monsoon dynamics on timescales of the order of 15 days (see Chapter 7 discussion of the Sahelian mode of intraseasonal variability). Wet sequences within the rainy season produce large-scale soil moisture features, which, via sensible heating, can feed back on the atmosphere. Taylor (2008) used passive microwave soil moisture data to estimate the modulations in surface heating across West Africa driven by soil moisture. By compositing wet and dry features, and examining the atmospheric state associated with large-scale soil moisture variability, that study was able to demonstrate that surface variability led (i.e. induced) variability in daytime PBL temperatures. These in turn amplified circulation anomalies considered important for this mode of variability (Janicot and Sultan, 2001), specifically low-level vorticity in the Sahel and southern Sahara. The data in Figure 2.27 illustrate temperature and wind anomalies at 925 hPa (derived from ECMWF analysis) associated with a wet phase of the mode. Negative anomalies in sensible heat flux drive negative PBL temperatures, which in turn produce anticyclonic vorticity.

This mechanism was subsequently explored in a GCM study (Lavender *et al.*, 2010). In simulations where soil moisture was imposed, heat low anomalies developed above dry soils and cool high anomalies developed above wet soils, and the associated modulation of moisture advection induced enhanced rainfall to the west of pre-existing wet soil regions, consistent with Taylor (2008). On the other hand, similar intraseasonal rainfall features were found in a simulation where soil moisture was held constant, though westward propagation of precipitation was less coherent. These results imply the atmosphere can support the Sahelian mode in the absence of surface hydrological feedback. However, analysis of the runs also showed how the atmospheric mode became phase locked with the imposed soil moisture, suggesting an important (though not primary) role for land feedbacks.

2.2 Operational Methods and Canonical Synoptic Patterns

2.2.1 Synoptic Fields and Main Inferences

In developing a weather forecast for a given location (or area) and time range, the forecaster needs to get an understanding of the three-dimensional structure and evolution of a given synoptic situation. This can be achieved through the use of various combinations of charts/fields that can best capture the situation.

Table 2.1 summarises the major parameters that may assist in analysis of the synoptic situation. How to use these parameters, as well as some proposed diagnostics to better detect and analyse the synoptic structures, is explained in Chapter 11.

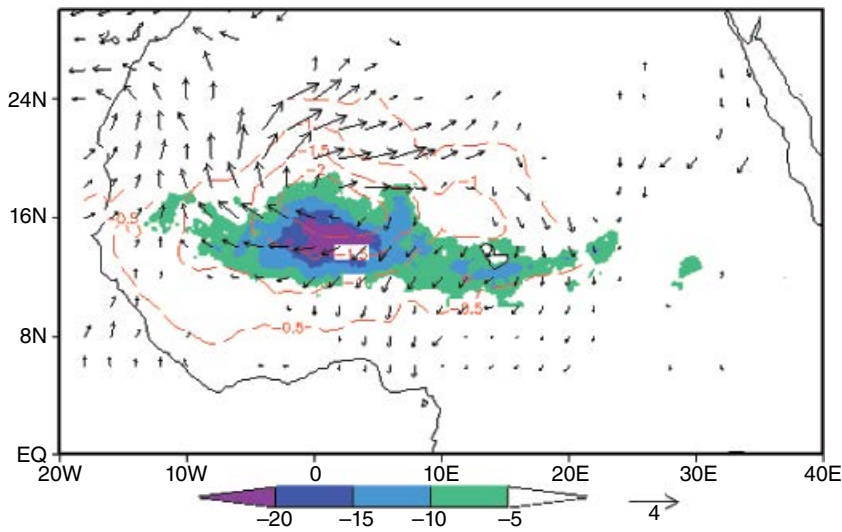


Figure 2.27 Differences in surface sensible heat flux (shaded; W m^{-2}), 925 hPa temperature differences (at 1800 UTC; dashed contour; K), and wind speed (at 0600 UTC the following day; vectors; m s^{-1}) between wet and dry surface intraseasonal composites. The wet (dry) composite is defined at day 0 by the minimum (maximum) in filtered daytime mean surface heat flux over a rectangle centred on 0°E , 15°N . Data are only plotted where they differ significantly from zero at the 95% level.

2.2.2 African Easterly Wave Case Studies and Canonical Structures

Training of forecasters on real-world case studies is a key step to assimilate the basic knowledge presented in this book. In particular, it is necessary to realise the high diversity of situations encountered in reality, which can sometimes be quite different from the conceptual models presented in Section 2.1. Therefore, we have developed a set of online case studies (see online link⁴). Some particular illustrations from these case studies, as well as some additional examples, are presented here to show canonical configurations of AEW structure and behaviour as a real-world complement to the idealised AEW structures shown in Figure 2.10.

2.2.2.1 An Archetypal African Easterly Wave Event: Case Study CS02⁴, 12–16 August 2012

This case shows many features that may be regarded as archetypes for AEW behaviour. The wave was first detected at 0000 UTC on 13 August (see online material). At this time, the detection of this new perturbation is not easy based on the 600 hPa meridional wind, but the major visible features are: the AEJ acceleration; wet anomalies over northern Chad as detected by the PW* field, associated with a large area of convective activity; and a strong northerly mean transport in the 925–600 hPa layer occurring in the 10–25°E band from the Mediterranean Sea to the Equator. By 1200 UTC (Figure 2.28 at $D_0 - 1.5$) the perturbation is well organised with all key

features in place; that is, the trough at 19°E, the AEJ core at its rear, the dry/wet dipole, the monsoon trough along 10°N, deep northerlies ahead and monsoon flux intensifying behind over south Sudan.

On 15 August at 0000 UTC (Figure 2.28 at D_0), the wave and the associated features, including deep convection, reach their maximum magnitude (Figure 2.29). The trough is tilted northeastward and shows the peak AEJ speeds to its east (as in Figure 2.10). The ITD shows a northward penetration corresponding to the moist phase of the wave behind (to the east of) the trough, and a southward ITD penetration in the dry phase, ahead of (west of) the trough. At 850 hPa (Figure 2.29b) there is a closed vortex at 0°E , 10°N , which is bringing strong southerly advection (Figure 2.29f) on its eastern side. Note also the well-defined SHL enhancement located at around 5°W , 23°N , ahead of the trough to the northwest, whose pressure gradient drives the monsoon burst (strong southerly winds in and ahead of the trough).

The following day the perturbation continues its westward progression toward the coast but slows down when arriving over the Fouta Djallon mountains on 16 August. At 1200 UTC (Figure 2.28 at $D_0 + 1.5$) the monsoon inflow from Guinea to the Liberian coast is deep and intense with a cyclonic centre C600_850 around Conakry. During this stage, the AEJ core for the first time precedes the trough. The monsoon burst reaches its maximum northward penetration as indicated by the ITD (in the numerical model data), reaching 28°N over southern Algeria. This moist region is cloudy, but the convection is less vigorous.

Table 2.1 Summary of the major parameters that may assist in analysis of the synoptic situation, and which are usually readily available to forecasters. Other chapters, particularly Chapters 3, 7, 9 and 11, have proposed additional diagnostics for synoptic analysis, including CAPE, CIN, wind shear, PW, monsoon depth and mean meridional transport, plus their anomalies from the mean seasonal cycle. The difficulty can be that NWP centres often provide only the basic variables as listed here. Forecasters need convenient and interactive tools to handle all these fields and superpose them.

Parameter	Useful levels	Application
MSLP		<p>The 1015 hPa line is a commonly used reference for the extent of southward push or retreat of the northerly high pressure influence. During the dry season, the inland ridge of the Azores High usually manifests itself as a closed ‘Libyan High’. A tightening of the pressure gradient on the southern flank of the Libyan High is usually a prelude to an outbreak of a widespread dust episode (see Chapter 5). This is also a crucial field to monitor the SHL activity (see Section 11.3) characterised by a large diurnal oscillation.</p> <p>Although the winds are influenced by the Coriolis force, especially in the north of the region, the geostrophic wind is not a good estimate of the low-level winds. Instead, winds typically flow toward low pressure, turned to the right by the Coriolis force. During the day, low-level wind speeds are much reduced by convective turbulent drag.</p>
Wind charts	Surface/10 m, 925 hPa, 950 hPa, 850 hPa, 700 hPa, 500 hPa, 300 hPa, 200 hPa, 150 hPa	<p>The low-level charts are of interest in determining the location of the ITD and hence the northward penetration of the monsoon flow (10 m to 925 hPa) and the location of vortices (10 m to 850 hPa). The middle levels (700 hPa) are examined for the strength and location of the AEJ, and for waves (AEWs), which may also be associated with low-level vortices at 850 hPa and the surface. At 300 hPa and above, extratropical troughs and the STJ are of interest.</p> <p>The 850 hPa level, lying close to the steering level of AEWs, can show distinct closed vortices and allows drawing of the monsoon trough.</p> <p>Streamline plots will suffice for most purposes, but commonly these do not show wind strength, which is useful for locating jet axis and for determining whether dust may be raised locally or at the main source regions.</p>
Temperature	Surface, 850 hPa and 700 hPa	<p>These charts are used in conjunction with humidity and winds to assess stability conditions and where the enhancement or suppression of convection may be favoured. They also help to identify the structure of AEWs below the AEJ level. The 850 hPa level is convenient to monitor the SHL (see Section 11.3).</p>
RH	Surface, 925hPa, 850 hPa, 700 hPa	<p>High values of low-level RH increase the CAPE of the column. Mid-level dryness (e.g. 700–500 hPa) can suppress convective initiation, but also can favour the organisation and maintenance of squall lines.</p>
Dew point temperature.	Surface, 925 hPa, 850 hPa, 700 hPa, 500 hPa	<p>The surface dew point temperature gradient (around 15 °C) is used among other criteria to locate the ITD (see Chapter 11).</p> <p>The humidity profile over West Africa from the surface through 850 hPa, 700 hPa and up to 500 hPa is used in forecasting the intensity and growth of thunderstorms. At 500 hPa, areas with dew point temperatures less than a threshold value are marked as areas of mid-level ‘dry air intrusion’. Such dry air intrusion zones, when located very close to very humid areas, can be associated with very violent thunderstorm activity.</p>
Vorticity	850 hPa, 700 hPa, 600 hPa, 500 hPa, 200 hPa	<p>From the surface to 700 hPa (even to 500 hPa), closed vortices can be associated with significant weather, in particular thunderstorm initiation.</p> <p>Vorticity is used at 850 hPa to define the monsoon trough, which also connects closed vortices.</p> <p>At upper levels, vorticity is an indicator of mid-latitude troughs.</p>

On 16 August at 1200 UTC (Figure 2.28 + 1.5 at $D_0 + 1.5$), while the AEW exits Africa over the Atlantic, a new one is growing at the Sudan–Chad frontier. As for the previous perturbation, the precursor detected a day before is a deep northerly flow organised from the Mediterranean Sea to 5°N, followed to the east by northward monsoon penetration. Again, we notice a reinforcement of the AEJ that can be detected before the appearance of the trough.

2.2.2.2 African Easterly Wave Breaking Events

AEW ‘breaking’ is here defined to occur when the curvature of the wave, seen in the 600 hPa streamlines for instance, becomes very steep, oriented north–south (or even in the northwest to southeast orientation), to the west of the wave trough. At the same time, the breaking wave becomes quite slow moving. Such events are important as they are favourable to high-impact weather systems with the possibility of flooding, and

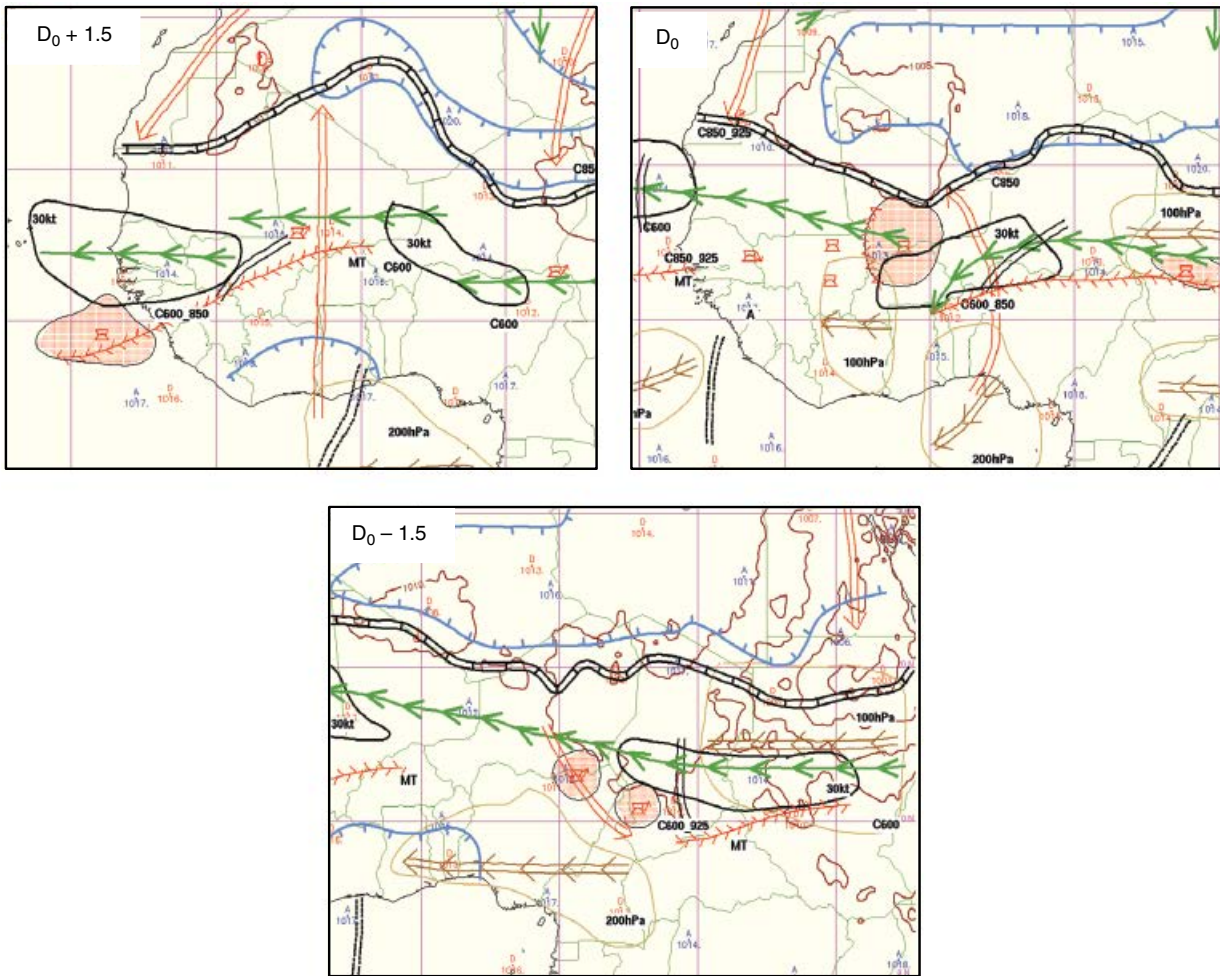


Figure 2.28 Sequence of West African Synthetic Analysis (WASA) charts showing the structure of the AEW of 12–16 August 2012. Day D_0 is 0000 UTC on 15 August 2012 corresponding to the mature and growing AEW stage. One and half day before ($D_0 - 1.5$) and later ($D_0 + 1.5$) correspond to the initiation stage and to its arrival at the coast. These charts may be compared with the conceptual model developed in Section 2.1.3.3 and Figure 2.10.

favour cyclogenesis when arriving at the coast. Owing to their strong vorticity signature, the predictability of breaking AEWs is relatively strong, but such events are not frequent.

Favourable factors for AEW breaking appear to be:

- 1) A *pre-existing significant monsoon penetration over the eastern Sahel, resulting in a larger wet spell* (positive PW*) over the Sahel, that propagates westward.
- 2) A *train of AEWs*. Indeed, it seems that a trough T2 can be reinforced by the previous trough T1 (with T1 to the west of T2) if the monsoon burst associated with this first trough T1 is intense and deep. A strong ridge develops between T1 and T2, with drier conditions, which slows down the propagation of the second

trough T2, allowing T2 to intensify, with the development of deep convection. This is consistent with the upstream propagation of the group velocity discussed in Diaz and Aiyver (2013).

- 3) An *intense AEJ core* associated with a growing trough.
- 4) *Intense deep convection* to the south of the AEJ core.
- 5) *Interaction with a deep and intense monsoon flow from the equatorial band*. This monsoon burst can be detected by the mean wind intensity in the surface to 600 hPa layer, reaching more than 7.5 m s^{-1} from the southwest sector.
- 6) *Forcing from mid-latitudes* can help the wave breaking, although the forcing from the equatorial band (the deep monsoon burst) appears as a more important ingredient for this scenario.

Two examples of AEW breaking are shown in Figures 2.30 and 2.31, both exhibiting these six favourable factors. Figure 2.30 illustrates the AEW ‘breaking case’ that occurred on 7 August 2012, well defined by the north–south orientation of the blue streamlines at 600 hPa to the west of the trough (around 0°E, 10°N). The AEJ core is stronger than 30 kt at the rear of an intense MCS around 2°W, 13°N, moving toward the southwest. Note the development of an intense ridge between the previous trough over the Atlantic Ocean and the breaking wave. This case illustrates factors (2) (train of AEWs) and (5) (forcing by the equatorial band), from the list of favourable factors above. For a detailed analysis of this case refer to case study CS01⁴.

The second case corresponds to the Ouagadougou flood event that occurred on 1 September 2009 with a maximum of precipitation of 263 mm accumulated in less than 12 h. Figure 2.31 illustrates the formation of the breaking, in terms of the curvature of streamlines at 600 hPa (around 0°E, 10°N on 1 September). A first strong trough T_1 passes over Benin and west Niger on 29 August. As this moves to the west there is strong southerly flow from the equatorial band behind it, bringing dry air (see weak T_d (green and blue) areas around 5°W on 31 August) into the region of the ridge at 600 hPa. In the lee of the first trough T_1 , a second trough T_2 is detected on 29 August in the Lake Chad region. Owing to the previous ridge intensification, T_2 slows its westward propagation and intensifies to form a closed circulation over northeast Nigeria on 31 August. Then T_2 moves faster and intensifies until on 1 September it is overturning, with the winds northwesterly on its western side. Owing to the pre-existing large wet spell (positive PW^* – favourable factor (1)), intense precipitation occurs over Burkina Faso a few degrees to the west of the vortex in a wet environment where northerlies are maximum. It is worth noticing that the rainfall in this case is not a squall line system, as no cold pool was generated due to a lack of rain evaporation in this wet environment.

2.2.2.3 Coastal Development of African Easterly Waves

There are two AEW tracks over West Africa: one to the south and the other to the north of the AEJ (Section 2.1.3.2). The interactions between these waves at the coast and eventually their merging can have important impacts on the weather and give rise to tropical cyclogenesis (Chen *et al.*, 2008; Hanks *et al.*, 2015; Section 2.1.3.7). When arriving at the coast, often the AEWs amplify and change their structure with two possible configurations, corresponding to a reinforcement of either

(configuration A) the southern vortex, or (configuration B) the northern vortex at 850 hPa. In general, the AEWs reach their maximum amplitude at the coast for all variables associated with their signature, such as oscillation of the streamfunction, meridional wind perturbation, vorticity and PW^* . Also, the eastward vertical tilt of the trough below the AEJ level (600–700 hPa) is reduced near the coast.

2.2.2.3.1 Summary of Configuration A: Reinforcement of the Southern Vortex

Favourable conditions for this configuration are:

- 1) A strong AEJ core (~ 45 kt, or more than 20 m s^{-1}) coupled with a strong southern vortex.
- 2) Very humid air in the column associated with a very strong and deep monsoon surge and strong onshore flow south to west of the vortex.

In addition, the interaction and merging with a northern vortex can contribute to reinforce the southern vortex. In the case of strong northerlies from mid-latitudes along the west coast, the northern vortex is blocked; it is forced to move southward, so as to meet the southern vortex and merge with it.

When passing over the Fouta Djallon the southern vortex is reinforced and deepened by the enhancement of convection. The effect is maximum if the southern vortex arrives over Fouta Djallon around 1800 UTC. The vortex then moves northwest toward Dakar and leaves the coast south of Dakar.

This type of situation is more typical around the end of July, into August. It is favourable to intense precipitation in the vicinity of the trough and to the north of the vortex. The slower propagation of the vortex than previously, over the continent, can explain large accumulations of precipitation. If other factors are favourable, cyclogenesis can occur in such situations. The 1–10 September 2014 period provides two nice examples of configuration A, driven by the ‘southern vortex’. This period is characterised by the passage of an ‘AEW train’ triggered east of 20°E in mid-August and moving westward over the whole domain at about 9 m s^{-1} , with the AEWs amplifying over West Africa to reach their maximum over the ocean both in terms of PW^* and vorticity anomalies. Figure 2.32 summarises the evolution of the synoptic situation during the 2–4 September period. On 2 September two trough axes T_{N1} and T_{S1} are well identified, north and south respectively, of the AEJ core located over Burkina. In agreement with the schematic (Figure 2.10), the trough axis T_{N1} is well defined between the dipole of PW^* over Mauritania, whereas the moist anomaly is in phase and ahead of T_{S1} , associated with a strong vortex over northern Ghana. Also, two ridge axes

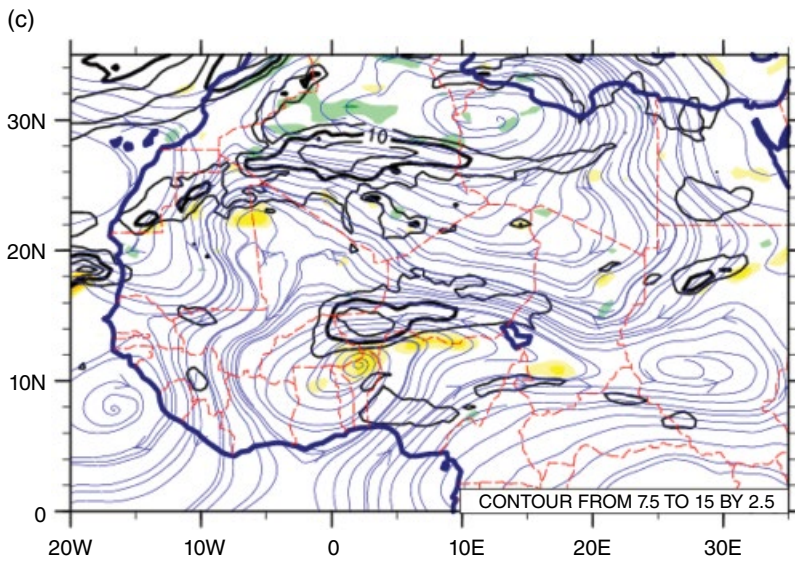
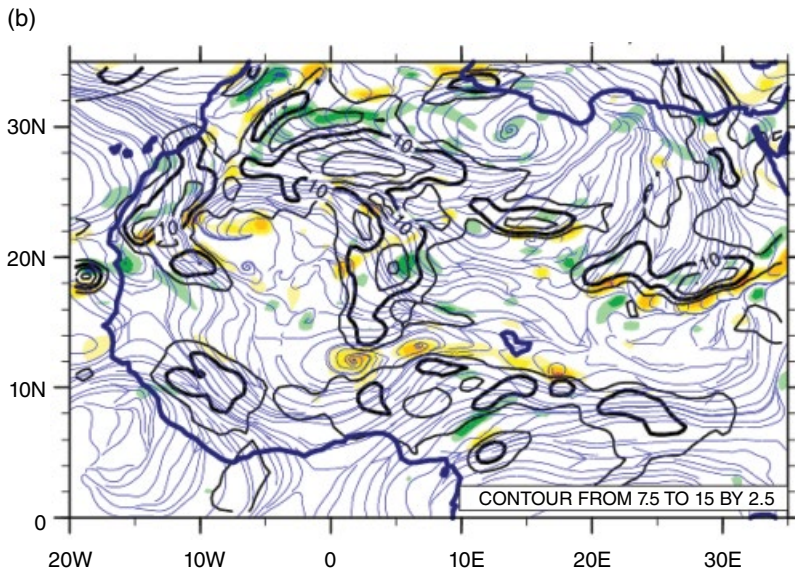
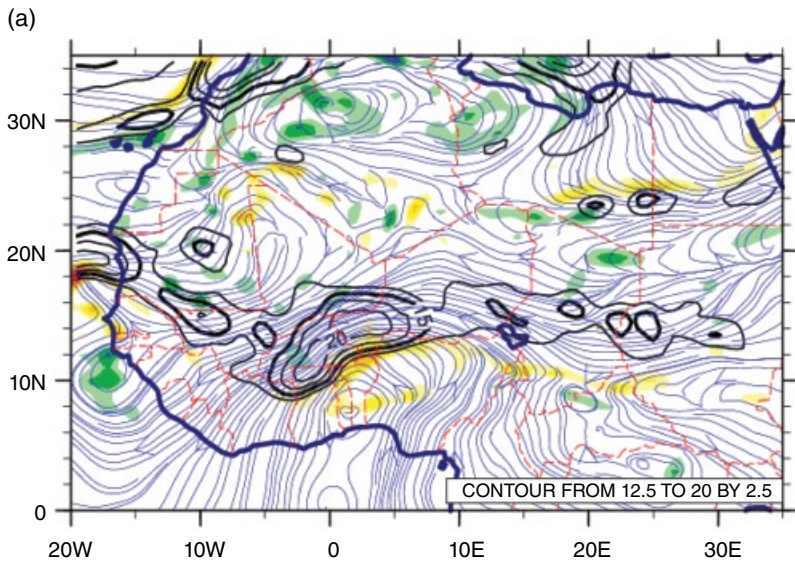
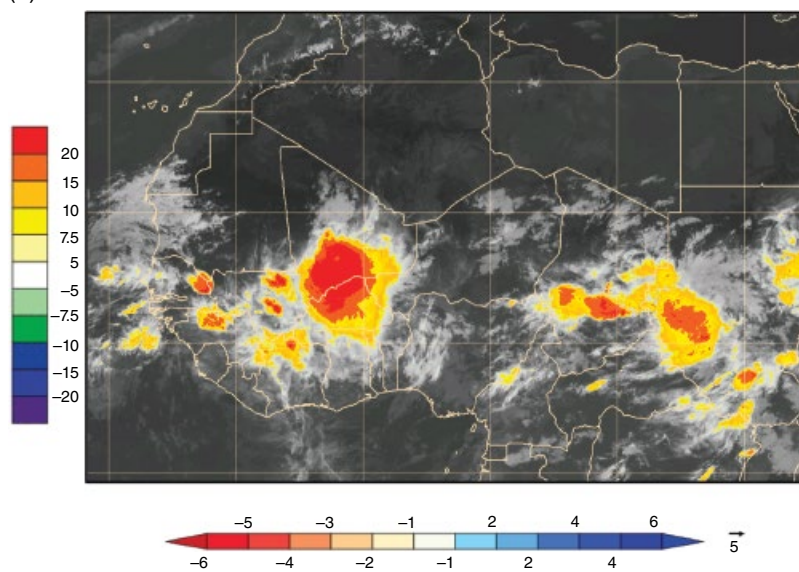


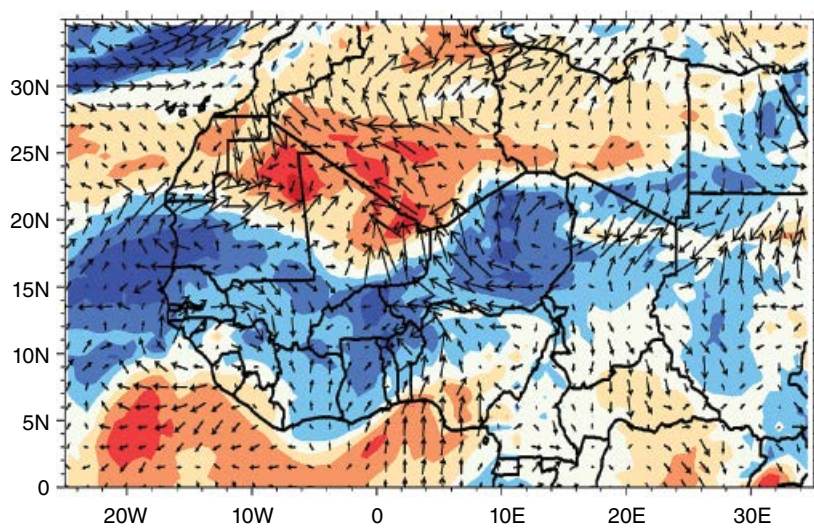
Figure 2.29 Example of an archetypal AEW from 15 August 2012, 0000 UTC. Streamlines (blue) are shown at (a) 600 hPa, (b) 850 hPa and (c) for the mean flow in the 950–600 hPa layer, with mean horizontal wind intensity (isolines, m s^{-1}) and vorticity (colour, 10^{-5} s^{-1}); (d) shows the infrared Meteosat image with yellow and red colours for coldest clouds (less than -40°C and -65°C respectively); (e) shows PW* (colour, mm) and 925 hPa horizontal wind anomalies (m s^{-1}); (f) shows mean meridional wind in the 925–600 hPa layer (colour, m s^{-1}) and mean horizontal wind vector in the 925–850 hPa layer. The WASA map for this case is in Figure 2.28 (time D_0).

Figure 2.29 (Cont'd)

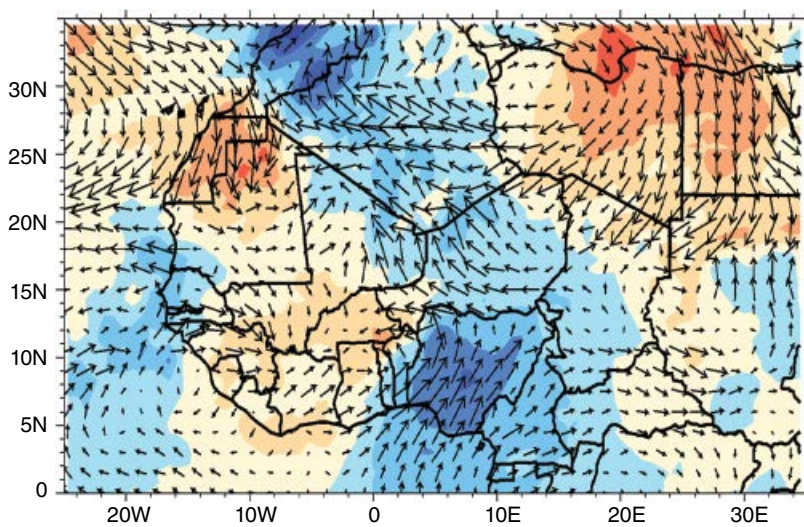
(d)



(e)



(f)



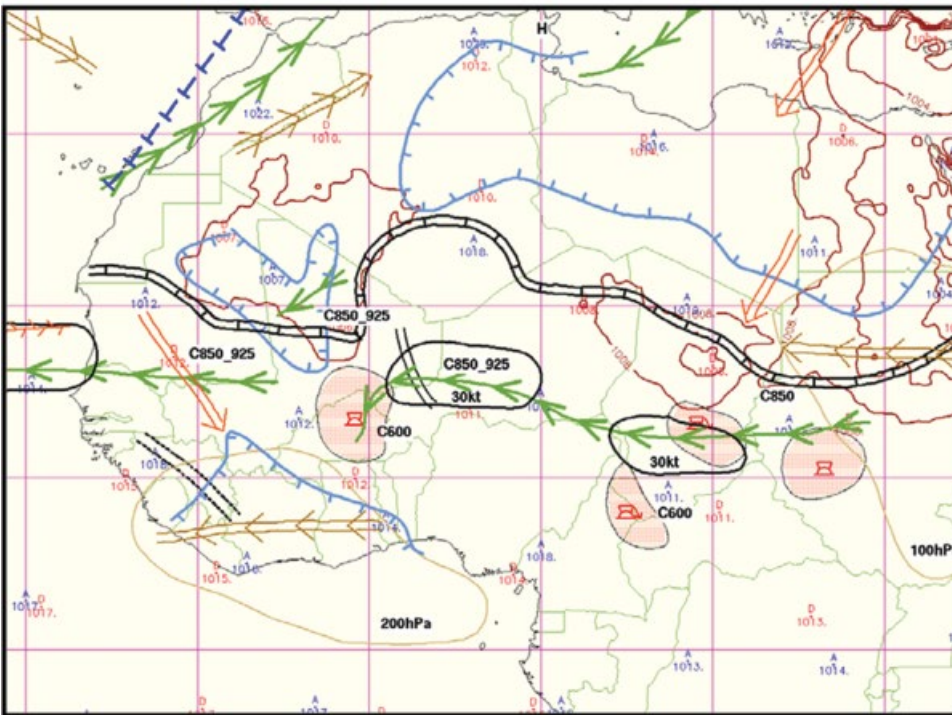
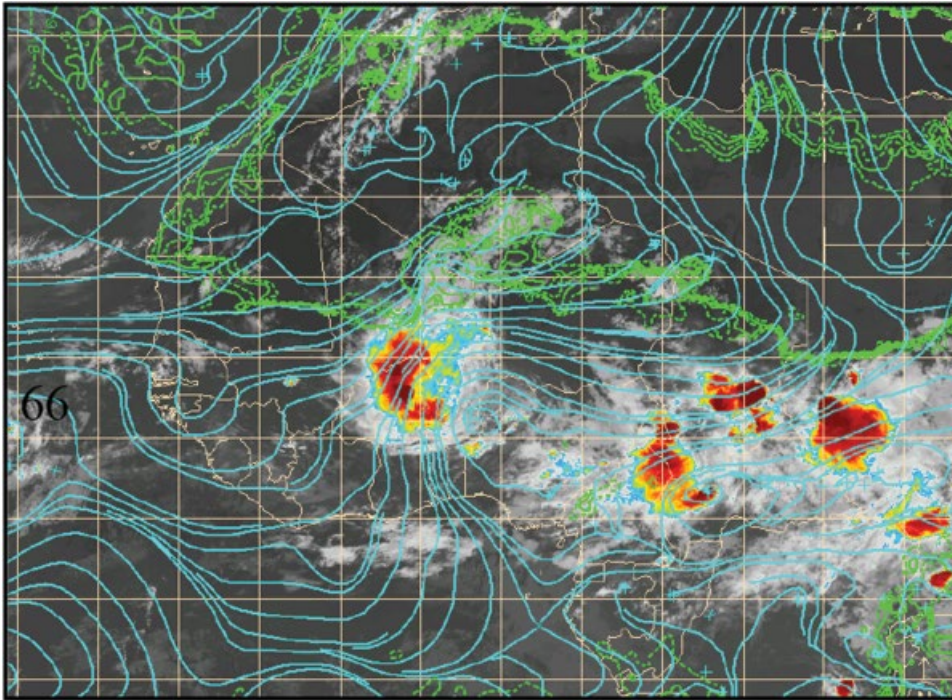


Figure 2.30 Example of an AEW 'breaking case' on 7 August 2012 at 0000 UTC (case study CS01⁴). Upper panel shows the infrared image with superposition of streamlines at 600 hPa and T_d at the surface (green isolines to visualise the ITD); lower panel shows the WASA. Note that the breaking of the AEW is identified by the north–south orientation of the streamlines to the west of the trough.

are identified (dashed black lines), one over the ocean and the other crossing Niger and Nigeria, indicating the strength of the AEW train south of the AEJ. One day later (Figure 2.32, second row), the previous structure has moved westward and amplified. However, owing to strong northerlies (trade winds) over the eastern Atlantic,

the propagation of the northern vortex associated with T_{N1} is blocked over Mauritania, whereas the T_{S1} axis has moved toward the coast and caught up with T_{N1} to form a continuous trough axis. In addition to this merging process, the occurrence of intense convection over the Guinea Highlands during the previous night and day has

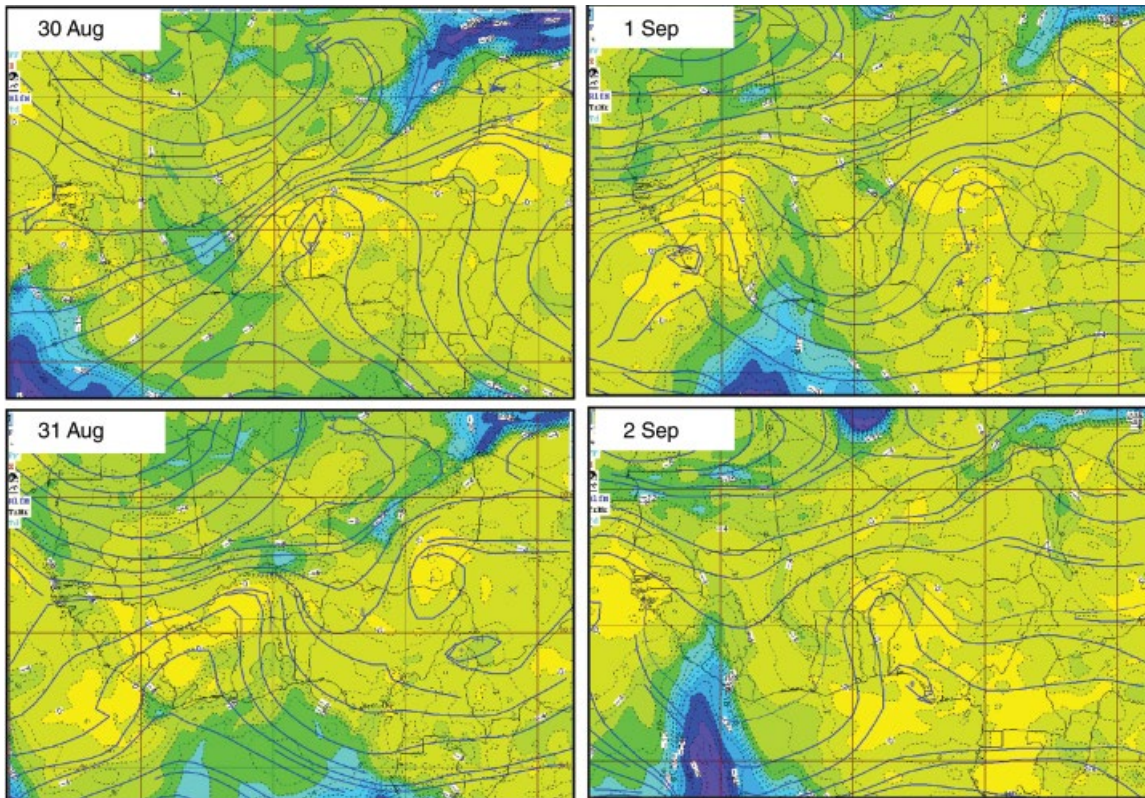


Figure 2.31 Illustration of the Ouagadougou flood case (case study CS04⁴) showing streamlines and dew point, T_d (colour) at 600 hPa on 30 August–2 September 2009 at 0000 UTC.

contributed also to the intensification of the southern vortex. The following day the merging and convection processes continue to result in an intense, moist vortex reaching the west coast, first moving northward along the coast and then leaving the continent westward (Figure 2.32, last row). Behind this, we have the merging and amplification of the north and south ridges, as observed for the troughs, helping the development of a second trough to the east over Nigeria. The following evolution scenario was very similar to that shown in Figure 2.32, but the resulting southern vortex was stronger and moister due to its earlier development and a trajectory a little more to the south. This second AEW reached a stronger magnitude, allowing the triggering of tropical cyclone Edouard (11–19 September 2014).

2.2.2.3.2 Summary of Configuration B: Reinforcement of the Northern Vortex

This situation is very common, representing perhaps 50% of cases in July. Favourable conditions are:

- 1) A northern vortex at 850 hPa is localised in the vicinity of the ITD and connected with the heat low reinforcement.
- 2) The northern vortex amplification could result from an interaction with mid-latitudes, in particular strong northerlies along the west coast blocking the

propagation of the northern vortex. As with configuration A, northerlies along the west coast seem to support the development, but in this case they have a better connection and continuity with northerlies at mid-latitudes.

- 3) A weaker southern vortex can favour reinforcement of the northern vortex.

This type of situation is favourable for significant dust lifting over Mauritania, and export of the dust over the Atlantic Ocean. Convection can occur close to the ITD that penetrates far to the north, but over the ocean precipitation is shifted to the south along the ITCZ. This situation is not favourable to tropical cyclogenesis.

2.2.3 Dry-season Thunderstorms in West Africa

The dry season in West Africa is dominated by dry northeasterly winds that transport Harmattan dust haze across West Africa. However, thunderstorms do sometimes occur during the dry season. When this happens, it usually sparks off interest amongst the public, with impacts ranging from agriculture to ground water conservation.

A common configuration for such dry-season storms is the interaction of a low-pressure system or trough over West Africa, with a low over the North African region. The favourable interaction of these systems can lead to

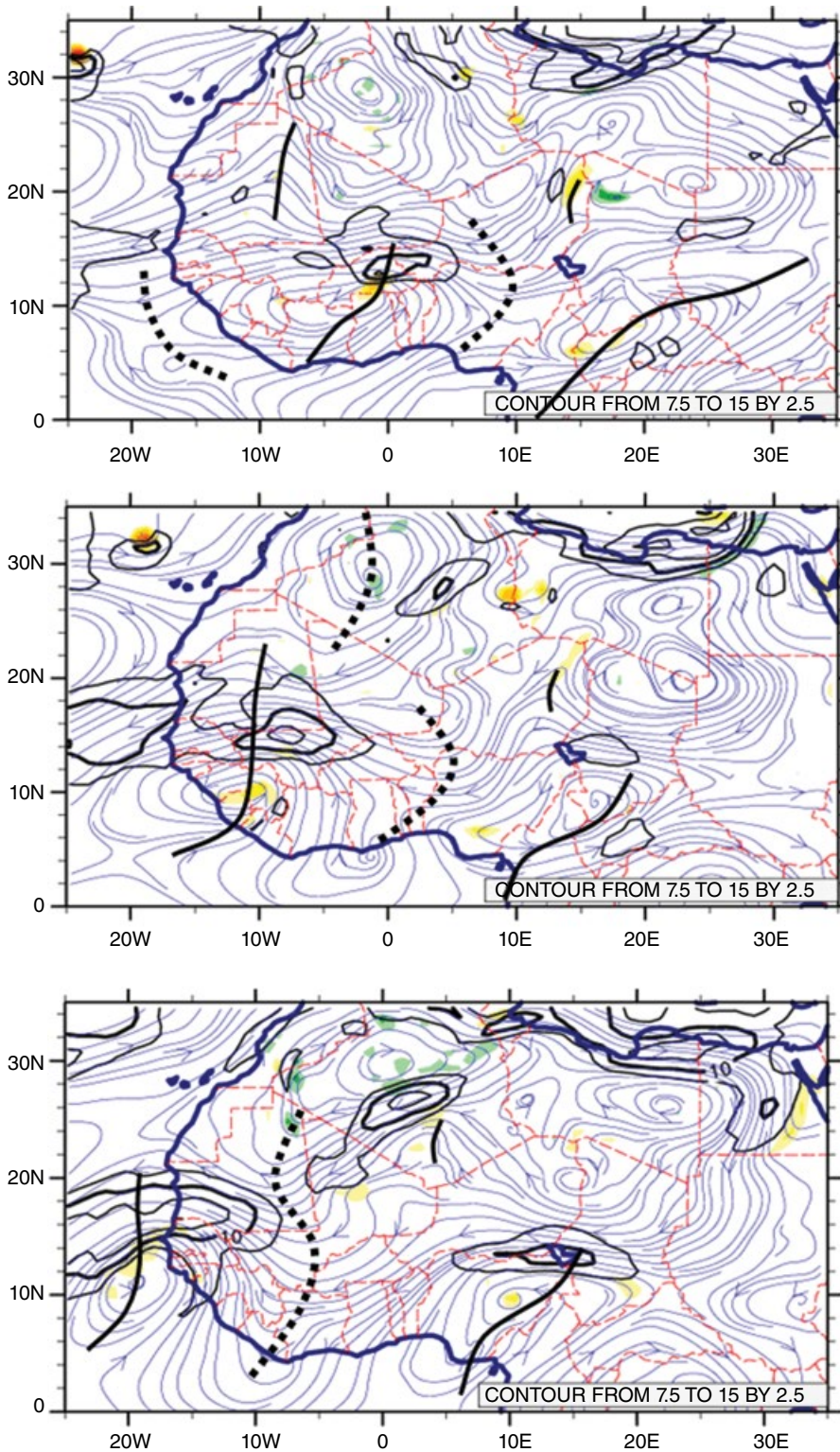


Figure 2.32 Evolution of the synoptic situation on 2, 3 and 4 September 2014 (first, second and third rows respectively) as depicted by the ECMWF analysis at 1200 UTC. Left column: streamlines, horizontal wind intensity (2.5 m s^{-1} isoline contours above 7.5 m s^{-1}) and vorticity (colour, 10^{-5} s^{-1}) for the mean flow averaged in the 950–600 hPa layer. Right column: PW* (colour, mm) and 925 hPa horizontal wind anomalies. Trough and ridge axes as detected by the above diagnostics are superposed by black solid and dashed lines respectively.

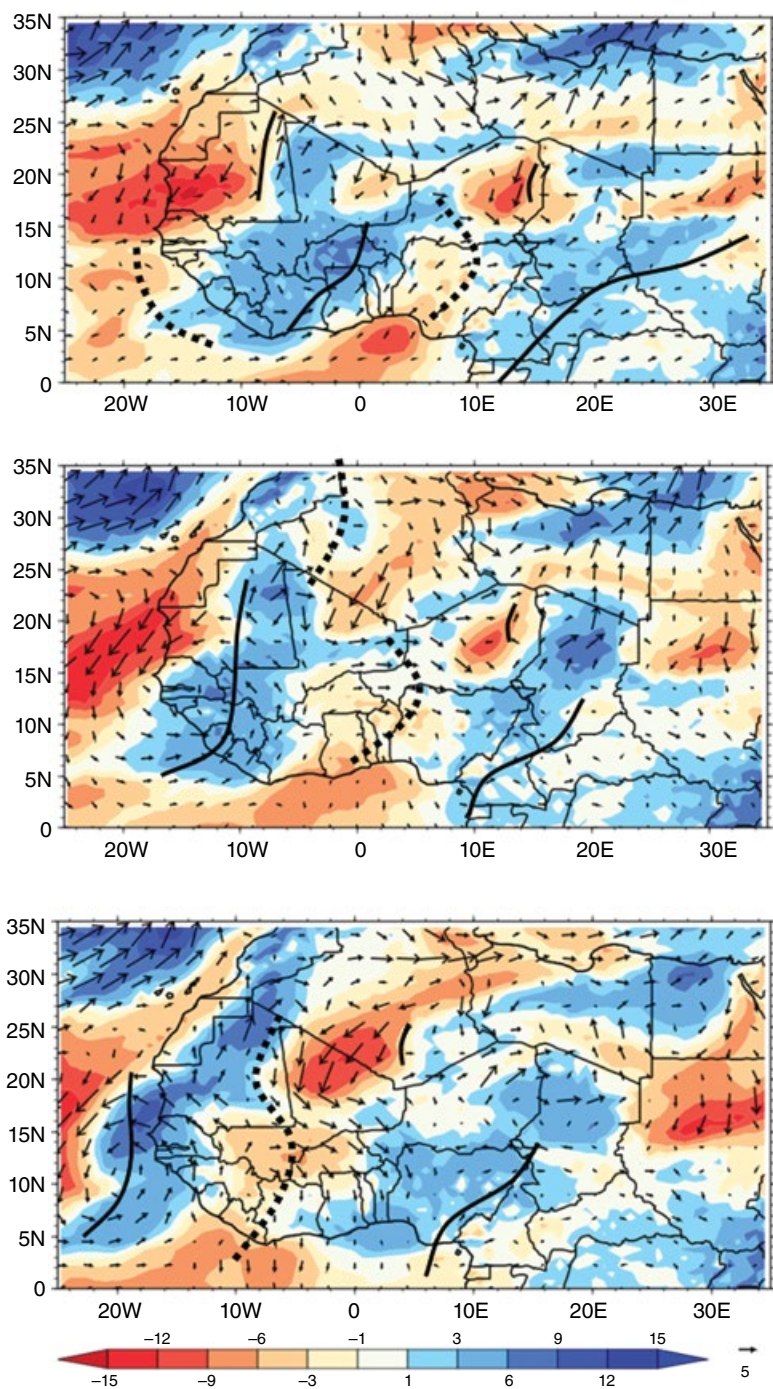


Figure 2.32 (Cont'd)

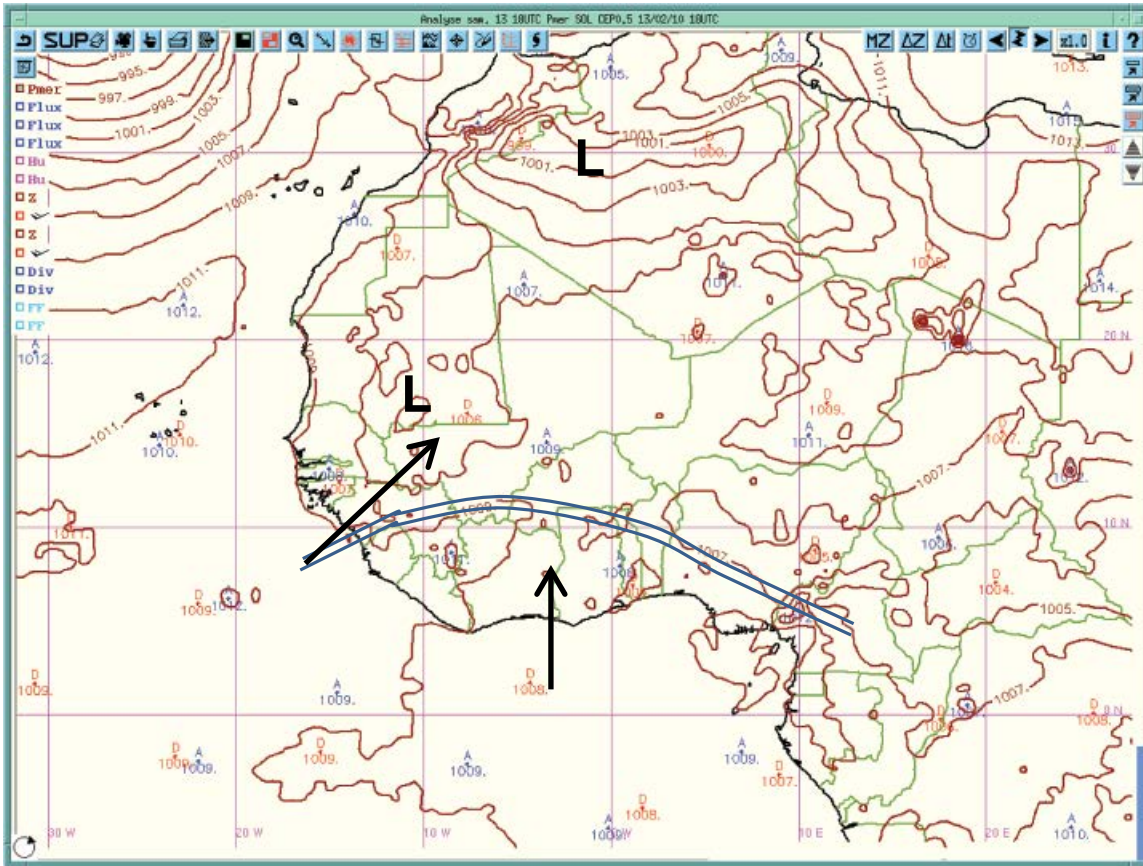
strong inland moisture transport from the west and Guinea coasts, supporting rainfall. Figure 2.33 illustrates an example, in the case of the thunderstorms that affected many coastal areas of West Africa during the period of 13–15 February 2010.

A mid-latitude trough that had been advancing eastward across the North Atlantic was penetrating deep into West Africa by the 12 February. There was significant

interaction between the tropical and extratropical systems (Figure 2.33a).

This situation created a favourable environment for penetration of moisture-laden southwesterlies far inland, and the MSLP and humidity (not shown) charts show evidence of a poleward shift of the ITD: on the 12 February, the ITD was at about 9°N, while by 1200 UTC on the 13 February it had shifted to about

(a)



(b)

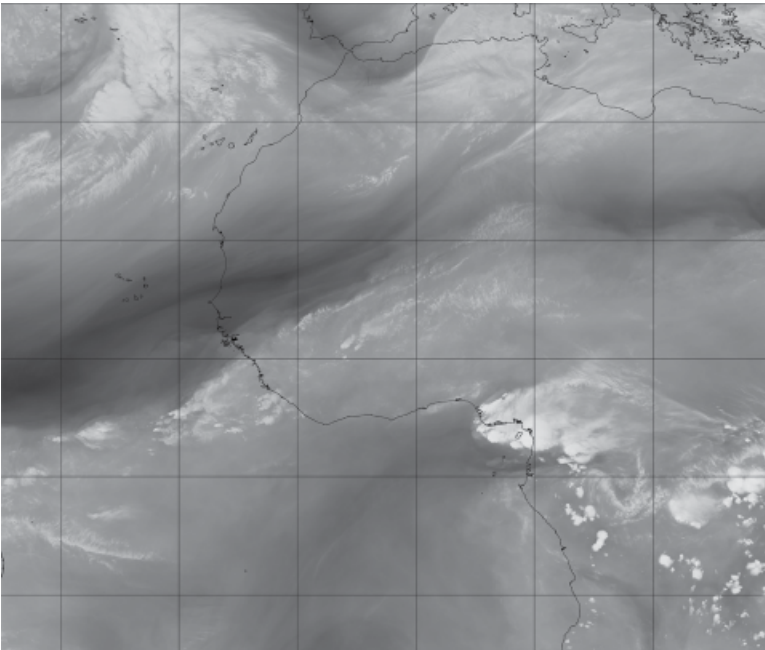


Figure 2.33 (a) Synoptic situation at 1200 UTC on 13 February 2010, indicating ITD, low-level winds (schematic vectors) and trough connecting low-pressure systems over Algeria and southern Mauritania, and Meteosat SEVIRI water vapour imagery (b) at 1200 UTC 13 February and (c) at 0000 UTC 15 February 2010. Panel (a) original to authors. Source: panels (b) and (c) courtesy of NEODAAS/University of Dundee.

(c)

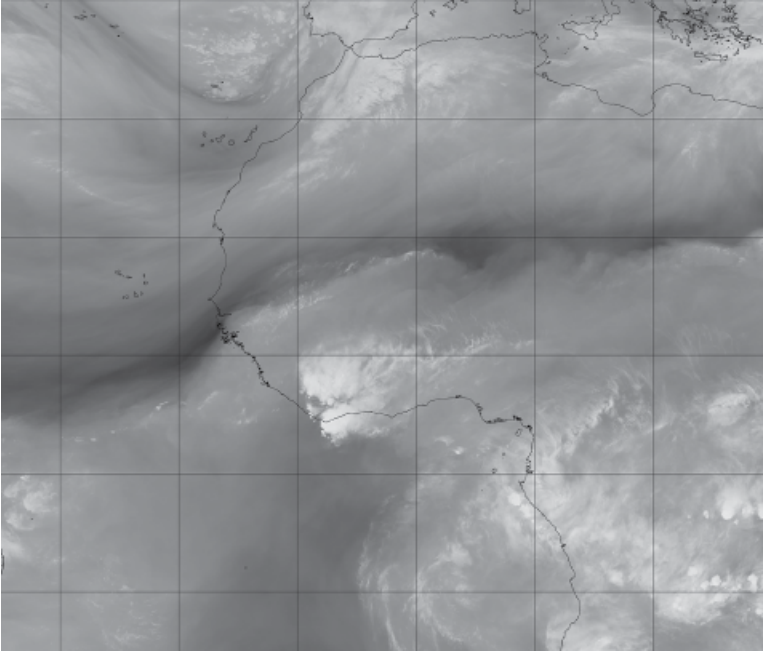


Figure 2.33 (Cont'd)

10.5°N (Figure 2.33a). A moist environment is an important component that is conducive for thunderstorm development. The trough is also dynamically favourable for thunderstorm initialisation since it generates vertical motion.

By 0200 UTC on 13 February, convective cloud clusters were observed over southeastern coastal areas of Nigeria as well as coastal areas of southwest Cameroon. The clusters became organised, with a distinct leading edge, and by 0900 UTC the system had covered much of southeastern parts of Nigeria. Westward propagation of the system ensued, and by around 1800 UTC (Figure 2.33b), the system had metamorphosed into a massive mesoscale convective complex. Around this time, the system was contiguous with deep convection all along the coast, south from Nigeria and Cameroon, and as far as Angola (Figure 2.33b). It is possible that some dynamical effects of this line of deep convection along the coast (presumably supported by local sea breezes) helped to intensify the system over Nigeria.

The storm continued to propagate westward and affected southern parts of Ghana, Togo and Benin. By 0000 UTC on 15 February (Figure 2.33c), the massive MCS had covered most parts of Ivory Coast. Finally, by 1100 UTC on 15 February the system showed consistent decay over Liberia. The organisation and westward propagation of the MCS suggests that the easterlies observed at 850 hPa over the coastal areas of West Africa

could have played a significant role in their kinematics. Indeed, it is likely that the northward push of cool oceanic air, moving with the ITD, is associated with easterly thermal-wind shear (as it is in the rainy season), which can help to organise storms.

Interaction between tropical and extratropical systems is fundamental to thunderstorm development during the dry season. Forecasters in the countries of the Guinea Coast look for these patterns, where a West African trough couples with a North African low, as a sign of likely thunderstorm activity in the coming days.

Acknowledgements

We are grateful to the ECMWF for providing the ERA Interim data used in this study and to Meteosat for providing the Meteosat data used in the satellite images shown in Sections 2.1 and 2.2. We are also grateful to the COMET MetEd programme for Figure 2.15 (from Laing and Evans (2011)).

Appendix: Acronyms

AEJ	African easterly jet
AEW	African easterly wave
ALMIP	AMMA Land Model Intercomparison Project

AMMA	African Monsoon Multidisciplinary Analysis	NLLJ	night-time low-level jet
CAPE	convective available potential energy	NWP	numerical weather prediction
CIN	convection/convective inhibition	OLR	outgoing longwave radiation
ECMWF	European Centre for Medium-Range Weather Forecasts	PBL	planetary boundary layer
GCM	general circulation model	PV	potential vorticity
GFS	Global Forecast System	PW	precipitable water
ITCZ	intertropical convergence zone	PW*	precipitable water anomaly
ITD	intertropical discontinuity	SAL	Saharan air layer
ITF	intertropical front	SHL	Saharan heat low
MCS	mesoscale convective system	SST	sea surface temperature
MCV	mesoscale convective vortex	STJ	subtropical jet
MJO	Madden–Julian oscillation	TEJ	tropical easterly jet
MSLP	mean sea-level pressure	UTC	Universal Time Coordinated
NCEP	National Centers for Environmental Prediction	WAM	West African monsoon

Notes

- Figure 2.8 is a temporal composite, so, as the AEW is westward propagating, times before the trough passage correspond to locations west of the trough.
- In fact, theoretical analysis has shown that both ‘downshear’ and ‘upshear’ tilts can be associated with ‘baroclinic’ wave growth: upshear – when the AEJ is narrow compared with the scale of the AEW; downshear – when the AEJ is broad compared with the scale of the AEW (Methven *et al.*, 2005).
- Note that the classical definition of AEW structure is in terms of winds, and in some cases AEWs may be dry.
- http://www.cnrm.meteo.fr/waf_handbook_casestudies/.
- By the same token, it should be recognised that perhaps 40% of squall lines are *not* associated with AEWs, and the presence of a large area of organised convection does not automatically indicate the presence of an AEW.
- Forecasters have also used this term for some time.

References

- Acheampong PK. 1982. Rainfall anomaly along the coast of Ghana – its nature and causes. *Geogr. Ann. A* **64**: 199–211.
- Agudelo P, Hoyos CD, Curry J, Webster PJ. 2011. Probabilistic discrimination between large-scale environments of intensifying and decaying African easterly waves. *Clim. Dyn.* **36**: 1379–1401.
- Avila LA, Pasch RJ. 1992. Atlantic tropical systems of 1991. *Mon. Weather Rev.* **120**: 2688–2696.
- Bain CL, Parker DJ, Taylor CM, *et al.* 2010. Observations of the nocturnal boundary layer associated with the West African monsoon. *Mon. Weather Rev.* **138**(8): 3142–3156.
- Bain CL, Parker DJ, Dixon N, *et al.* 2011. Anatomy of an African easterly wave in July 2006. *Q. J. R. Meteorol. Soc.* **137**: 923–933.
- Berry GJ, Thorncroft CD. 2005. Case study of an intense African easterly wave. *Mon. Weather Rev.* **133**: 752–766.
- Berry GJ, Thorncroft CD. 2012. African easterly wave dynamics in a mesoscale numerical model: the upscale role of convection. *J. Atmos. Sci.* **69**: 1267–1283.
- Berry GJ, Thorncroft CD, Hewson T. 2007. African easterly waves during 2004 – analysis using objective techniques. *Mon. Weather Rev.* **135**: 1251–1267.
- Blackadar AK. 1957. Boundary layer wind maxima and their significance for the growth of nocturnal inversions. *Bull. Am. Meteorol. Soc.* **38**: 283–290.
- Boone A, de Rosnay P, Balsamo G, *et al.* 2009. The AMMA Land Surface Model Intercomparison Project (ALMIP). *Bull. Am. Meteorol. Soc.* **90**: 1865–1880. doi: 10.1175/2009bams2786.1.
- Borgne JL. 1979. Un exemple d’invasion polaire sur la région mauritano–sénégalaise (An example of a polar intrusion into the Mauritanian–Sengalese region). *Ann. Géograph.* **489**: 521–548.
- Bou Karam D, Flamant C, Knippertz P, *et al.* 2008. Dust emissions over the Sahel associated with the West African monsoon intertropical discontinuity region: a representative case-study. *Q. J. R. Meteorol. Soc.* **134**(632): 621–634. doi: 10.1002/qj.244.
- Bouniol, D, Couvreur F, Kamsu-Tamo P-H, *et al.* 2012. Diurnal and seasonal cycles of cloud occurrences, types, and radiative impact over West Africa. *J. Appl. Meteorol. Climatol.* **51**(3): 534–553. doi: 10.1175/JAMC-D-11-051.1.

- Brown RG, Zhang C. 1997. Variability of midtropospheric moisture and its effect on cloud-top height distribution during TOGA COARE. *J. Atmos. Sci.* **54**: 2760–2774.
- Buckle C. 1996. *Weather and Climate in Africa*. Longman; 312 pp.
- Burpee RW. 1972. The origin and structure of easterly waves in the lower troposphere of North Africa. *J. Atmos. Sci.* **29**(1): 77–90.
- Burpee RW. 1974. Characteristics of North African easterly waves during the summers of 1968 and 1969. *J. Atmos. Sci.* **31**: 1556–1570.
- Carlson TN. 1969a. Some remarks on African disturbances and their progress over the tropical Atlantic. *Mon. Weather Rev.* **97**: 716–726.
- Carlson TN. 1969b. Synoptic histories of three African disturbances that developed into Atlantic hurricanes. *Mon. Weather Rev.* **97**: 256–276.
- Cecelski SF, Zhang D-L. 2013. Genesis of Hurricane Julia (2010) within an African easterly wave: low-level vortices and upper-level warming. *J. Atmos. Sci.* **70**(12): 3799–3817.
- Charney JG, Stern ME. 1962. On the stability of internal baroclinic jets in a rotating atmosphere. *J. Atmos. Sci.* **19**: 159–172.
- Chauvin F, Roehrig R, Lafore J-P. 2010. Intraseasonal variability of the Saharan heat low and its link with midlatitudes. *J. Climate* **23**: 2544–2561.
- Chen TS, Wang SY, Clark AJ. 2008. North Atlantic hurricanes contributed by African easterly waves north and south of the African easterly jet. *J. Clim.* **21**: 6767–6776.
- Chong M, Hauser D. 1989. A tropical squall line observed during the COPT 81 experiment in West Africa. Part II: water budget. *Mon. Weather Rev.* **117**: 728–744.
- Chou C, Neelin JD, Su H. 2001. Ocean–atmosphere–land feedbacks in an idealized monsoon. *Q. J. R. Meteorol. Soc.* **127**: 1869–1891.
- Cifelli R, Lang T, Rutledge SA, Guy N, *et al.* 2010. Characteristics of an African easterly wave observed during NAMMA. *J. Atmos. Sci.* **67**: 3–25.
- Cook KH. 1999. Generation of the African easterly jet and its role in determining West African precipitation. *J. Climate* **12**: 1165–1184.
- Cornforth RJ, Hoskins BJ, Thorncroft CD. 2009. The impact of moist processes on the African easterly jet–African easterly wave system. *Q. J. R. Meteorol. Soc.* **135**: 894–913.
- Davis J, Knippertz P, Fink AH. 2012. The predictability of precipitation episodes during the West African dry season. *Q. J. R. Meteorol. Soc.* **139**: 1047–1058. doi: 10.1002/qj.2014.
- Deme A, Roca R. 2008. Subjective analysis of African easterly waves during the 2006 monsoon: comparison to other methods. AMMA-EU Deliverable 2.1.C.g. Available from the AMMA Bureau.
- Diallo I, Bain CL, Gaye AT, *et al.* 2014. Simulation of the West African monsoon onset using the HadGEM3-RA regional climate model. *Clim. Dyn.* **43**, 575–594. doi: 10.1007/s00382-014-2219-0.
- Diaz ML, Aiyyer A. 2013. Energy dispersion in African easterly waves. *J. Atmos. Sci.* **70**: 130–145. doi: 10.1175/JAS-D-12-019.1.
- Dickinson M, Molinari J. 2000. Climatology of sign reversals of the meridional potential vorticity gradient over Africa and Australia. *Mon. Weather Rev.* **128**: 3890–3900.
- Diedhiou A, Janicot S, Viltard A, *et al.* 1999. Easterly wave regimes and associated convection over West Africa and tropical Atlantic: results from the NCEP/NCAR and ECMWF reanalyses. *Clim. Dyn.* **15**(11): 795–822. doi: 10.1007/s003820050316.
- Dunion JP, Velden CS. 2004. The impact of the Saharan air layer on the Atlantic tropical cyclone activity. *Bull. Amer. Meteorol. Soc.* **85**: 353–365.
- Duval J-P. 1990. Convection over tropical Africa and the Atlantic Ocean during northern summer. Part II: modulation by easterly waves. *Mon. Weather Rev.* **118**(9): 1855–1868.
- Eldridge RH. 1957. A synoptic study of West African disturbance lines. *Q. J. R. Meteorol. Soc.* **83**: 303–314.
- Fall S, Niyogi D, Mohanty UC, Kumar A. 2007. Application of weather prediction models for hazard mitigation planning: a case study of heavy off-season rains in Sénégal. *Nat. Hazards* **41**: 227–243. doi: 10.1007/s11069-006-9033-x.
- Fink AH, Reiner A. 2003. Spatio-temporal variability of the relation between African easterly waves and West African squall lines in 1998 and 1999. *J. Geophys. Res.* **108**(D11): 4332. doi: 10.1029/2002JD002816.
- Fink AH, Vincent DG, Ermert V. 2006. Rainfall types in the West African Soudanian zone during the summer monsoon 2002. *Mon. Weather Rev.* **134**: 2143–2164.
- Fink AH, Paeth H, Ermert V, *et al.* 2010. Meteorological processes influencing the weather and climate of Benin. In: *Impacts of Global Change on the Hydrological Cycle in West and Northwest Africa*, P Speth, M Christoph, B Dieckrüger, *et al.* (eds). Springer; pp. 135–149.
- Fink AH, Agustí-Panareda A, Parker DJ, *et al.* 2011. Operational meteorology in West Africa: observational networks, weather analysis and forecasting. *Atmos. Sci. Lett.* **12**: 135–141. doi: 10.1002/asl.324.
- Flamant C, Chaboureaud J-P, Parker DJ, *et al.* 2007. Airborne observations of the impact of a convective system on the planetary boundary layer thermodynamics and aerosol distribution in the inter-tropical discontinuity region of the West African monsoon. *Q. J. R. Meteorol. Soc.* **133**: 1175–1189. doi: 10.1002/qj.97.
- Flamant C, Knippertz P, Parker DJ, *et al.* 2009. The impact of a mesoscale convective system cold pool on the northward propagation of the intertropical discontinuity over West Africa. *Q. J. R. Meteorol. Soc.* **135**(638): 139–159. doi: 10.1002/qj.357.
- Fröhlich L, Knippertz P. 2008. Identification and global climatology of upper-level troughs at low latitudes.

- Meteorol. Z.* **17**(5): 565–573. doi: 10.1127/0941-2948/2008/0320.
- Fröhlich L, Knippertz P, Fink AH, Hohberger E. 2013. An objective climatology of tropical plumes. *J. Climate* **26**: 5044–5060. doi: 10.1175/JCLI-D-12-00351.1.
- Garcia-Carreras L, Marsham JH, Parker DJ, *et al.* 2013. The impact of convective cold pool outflows on model biases in the Sahara. *Geophys. Res. Lett.* **40**: 1647–1652. doi: 10.1002/grl.50239.
- Gaye AT, Fongang S, Garba A, Badiane D. 1994. Study of Heug rainfall in Sénégal using conventional data and Meteosat imagery. *Veille Climatique Satellitaire* **49**: 61–71 (available from Ministre de la Coopération–ORSTOM–Meteo-France, Lannion, France).
- Grams CM, Jones SC, Marsham JH, *et al.* 2010. The Atlantic inflow to the Saharan Heat low: observations and modelling. *Q. J. R. Meteor. Soc.* **136**: 125–140. doi: 10.1002/qj.429.
- Hall NMJ, Kiladis GN, Thorncroft CD. 2006. Three-dimensional structure and dynamics of African Easterly Waves. Part II: dynamical modes. *J. Atmos. Sci.* **63**: 2231–2245.
- Hankes I, Wang Z, Zhang G, Fritz C. 2015. Merger of African easterly waves and formation of Cape Verde storms. *Q. J. R. Meteor. Soc.* **141**(689): 1306–1319. doi: 10.1002/qj.2439
- Hopsch SB, Thorncroft CD, Hodges KI, Ayyer A. 2007. West African storm tracks and their relationship to Atlantic tropical cyclones. *J. Climate* **20**: 2468–2483.
- Hopsch SB, Thorncroft CD, Tyle KR. 2010. Analysis of African easterly wave structures and their role in influencing tropical cyclogenesis. *Mon. Weather Rev.* **138**: 1399–1419.
- Hoskins BJ, Ambrizzi T. 1993. Rossby wave propagation on a realistic longitudinally varying flow. *J. Atmos. Sci.* **50**: 1661–1671. doi: 10.1175/1520-0469(1993)050<1661:RWP OAR>2.0.CO;2.
- Hsieh JS, Cook KH. 2005. Generation of African easterly wave disturbances: relationship to the African easterly jet. *Mon. Weather Rev.* **133**: 1311–1327. doi: 10.1175/MWR2916.1.
- Iskenderian H. 1995. A 10-year climatology of Northern Hemisphere tropical cloud plumes and their composite flow patterns. *J. Climate* **8**: 1630–1637. doi: 10.1175/1520-0442(1995)008<1630:AYCONH>2.0.CO;2.
- Janicot S, Sultan B. 2001. Intra-seasonal modulation of convection in the West African monsoon. *Geophys. Res. Lett.* **28**: 523–526.
- Janicot S, Thorncroft CD, Ali A, *et al.* 2008. Large-scale overview of the summer monsoon over West Africa during the AMMA field experiment in 2006. *Ann. Geophys.* **26**: 2569–2595.
- Janiga A, Thorncroft CD. 2013. Regional differences in the kinematic and thermodynamic structure of African easterly waves. *Q. J. R. Meteor. Soc.* **139**: 1598–1614. doi: 10.1002/qj.2047.
- Jenkins G, Kucera P, Joseph E, *et al.* 2010. Coastal observations of weather features in Sénégal during the African Monsoon Multidisciplinary Analysis Special Observing Period 3. *J. Geophys. Res.* **115**: D18108. doi: 10.1029/2009JD013022.
- Jenkins GS, Pratt AS, Heymsfield A. 2008. Possible linkage between Saharan dust and tropical cyclone rain band invigoration in the eastern Atlantic during NAMMA-06. *Geophys. Res. Lett.* **35**: L08815. doi: 10.1029/2008GL034072.
- Joyce RJ, Janowiak JE, Arkin PA, Xie P. 2004. CMORPH: a method that produces global precipitation estimates from passive microwave and infrared data at high spatial and temporal resolution. *J. Hydrometeorol.* **5**: 487–503.
- Kamara SI. 1986. The origins and types of rainfall in West Africa. *Weather* **41**: 48–56.
- Karyampudi VM, Carlson TN. 1988. Analysis and numerical simulations of the Saharan air layer and its effect on easterly wave disturbances. *J. Atmos. Sci.* **45**: 3102–3136.
- Kiladis GN, Weickmann KM. 1997. Horizontal structure and seasonality of large-scale circulations associated with submonthly tropical convection. *Mon. Weather Rev.* **125**: 1997–2013. doi: 10.1175/1520-0493(1997)125<1997:HSASOL>2.0.CO;2.
- Kiladis GN, Thorncroft CD, Hall NMJ. 2006. Three-dimensional structure and dynamics of African easterly waves. Part I: observations. *J. Atmos. Sci.* **63**: 2212–2230.
- Kohler M, Kalthoff N, Kottmeier C. 2010. The impact of soil moisture modifications on CBL characteristics in West Africa: a case study from the AMMA campaign. *Q. J. R. Meteor. Soc.* **136**: 442–455. doi: 10.1002/qj.430.
- Knippertz P. 2005. Tropical–extratropical interactions associated with an Atlantic tropical plume and subtropical jet streak. *Mon. Weather Rev.* **133**: 2759–2776. doi: 10.1175/MWR2999.1.
- Knippertz P. 2007. Tropical–extratropical interactions related to upper-level troughs at low latitudes. *Dyn. Atmos. Oceans* **43**: 36–62. doi: 10.1016/j.dynatmoce.2006.06.003.
- Knippertz P, Fink AH. 2008. Dry-season precipitation in tropical West Africa and its relation to forcing from the extratropics. *Mon. Weather Rev.* **136**: 3579–3596. doi: 10.1175/2008MWR2295.1.
- Knippertz P, Fink AH. 2009. Prediction of dry-season precipitation in tropical West Africa and its relation to forcing from the extratropics. *Weather Forecast.* **24**: 1064–1084. doi: 10.1175/2009WAF2222221.1.
- Knippertz P, Martin JE. 2005. Tropical plumes and extreme precipitation in subtropical and tropical West Africa. *Q. J. R. Meteor. Soc.* **131**: 2337–2365. doi: 10.1256/qj.04.148.
- Knippertz P, Fink AH, Reiner A, Speth P. 2003. Three late summer/early autumn cases of tropical–extratropical interactions causing precipitation in northwest Africa. *Mon. Weather Rev.* **131**: 116–135.

- Knippertz P, Fink AH, Schuster R, *et al.* 2011. Ultra-low clouds over the southern West African monsoon region. *Geophys. Res. Lett.* **38**: L21808. doi: 10.1029/2011GL049278.
- Kwon HJ, Mak M. 1990. A study of the structural transformation of the African Easterly Waves. *J. Atmos. Sci.* **47**: 277–292.
- Lafore J-P, Moncrieff MW. 1989. A numerical investigation of the organization and interaction of the convective and stratiform regions of tropical squall lines. *J. Atmos. Sci.* **46**: 521–544. DOI:10.1175/1520-0469(1989)046<0521: ANIOTO>2.0.CO;2.
- Lafore J-P, Flamant C, Guichard F, *et al.* 2011. Progress in understanding of weather systems in West Africa. *Atmos. Sci. Lett.* **12**: 7–12. doi: 10.1002/asl.335.
- Laing A, Evans J-L. 2011. *Introduction to Tropical Meteorology*. UCAR/COMET. http://www.meted.ucar.edu/tropical/textbook_2nd_edition/ (accessed 16 October 2015).
- Laing AG, Carbone R, Levizzani V, Tuttle J. 2008. The propagation and diurnal cycles of deep convection in northern tropical Africa. *Q. J. R. Meteorol. Soc.* **134**: 93–109. doi: 10.1002/qj.194.
- Lavaysse C, Flamant C, Janicot S, *et al.* 2009. Seasonal evolution of the West African heat low: a climatological perspective. *Clim. Dyn.* **33**: 313–330.
- Lavaysse C, Flamant C, Janicot S, Knippertz P. 2010. Links between African easterly waves, midlatitude circulation and intraseasonal pulsations of the West African heat low. *Q. J. R. Meteorol. Soc.* **136**(S1): 144–158. doi: 10.1002/qj.555
- Lavender SL, Taylor CM, Matthews AJ. 2010. Coupled land–atmosphere intraseasonal variability of the West African monsoon in a GCM. *J. Climate* **23**: 5557–5571.
- Lebel T, Parker D, Flamant C, *et al.* 2010. The AMMA field campaigns: multiscale and multidisciplinary observations in the West African region. *Q. J. R. Meteorol. Soc.* **136**: 8–33. doi: 10.1002/qj.486
- Leppert KD II, Cecil DJ, Petersen WA. 2013a. Relation between tropical easterly waves, convection, and tropical cyclogenesis: a Lagrangian perspective. *Mon. Weather Rev.* **141**: 2649–2668.
- Leppert KD II, Petersen WA, Cecil DJ. 2013b. Electrically active convection in tropical easterly waves and implications for tropical cyclogenesis in the Atlantic and East Pacific. *Mon. Weather Rev.* **141**: 542–556.
- Leroux S, Hall NMJ. 2009. On the relationship between African easterly waves and the African easterly jet. *J. Atmos. Sci.* **66**: 2303–2316.
- Leroux S, Hall NMJ, Kiladis GN. 2010. A climatological study of transient–mean-flow interactions over West Africa. *Q. J. R. Meteorol. Soc.* **136**: 397–410. doi: 10.1002/qj.474.
- Leroux S, Hall NMJ, Kiladis GN. 2011. Intermittent African easterly wave activity in a dry atmospheric model: influence of the extratropics. *J. Climate* **24**: 5378–5396. doi: 10.1175/jcli-d-11-00049.1.
- Lin Y-L, Robertson KE, Hill CM. 2005. Origin and propagation of a disturbance associated with an African easterly wave as a precursor of Hurricane Alberto (2000). *Mon. Weather Rev.* **133**: 3276–3298.
- Lin Y-L, Liu L, Tang G, *et al.* 2013. Origin of the pre-Tropical Storm Debby (2006) African easterly wave–mesoscale convective system. *Meteorol. Atmos. Phys.* **120**: 123–144. doi: 10.1007/s00703-013-0248-6.
- Lothon M, Saïd F, Lohou F, Campistron B. 2008. Observation of the diurnal cycle in the low troposphere of West Africa. *Mon. Weather Rev.* **136**: 3477–3500.
- Mapes BE, Zuidema P. 1996. Radiative–dynamical consequences of dry tongues in the tropical troposphere. *J. Atmos. Sci.* **53**: 620–638.
- Marsham JH, Parker DJ, Grams CM, *et al.* 2008. Uplift of Saharan dust south of the intertropical discontinuity. *J. Geophys. Res. Atmos.* **113**(D21): D21102. doi: 10.1029/2008JD009844.
- Marsham JH, Dixon N, Garcia-Carreras L, *et al.* 2013. The role of moist convection in the West African monsoon system – insights from continental-scale convection-permitting simulations. *Geophys. Res. Lett.* **40**: 1843–1849. doi: 10.1002/grl.50347.
- Mathon V, Laurent H, Lebel T. 2002. Mesoscale convective system rainfall in the Sahel. *J. Appl. Meteorol.* **41**: 1081–1092.
- Mekonnen A, Rossow WB. 2011. The interaction between deep convection and easterly waves over tropical North Africa: a weather state perspective. *J. Climate* **24**: 4276–4294. doi: 10.1175/2011jcli3900.1.
- Mekonnen A, Thorncroft CD, Aiyyer AR. 2006. Analysis of convection and its association with African Easterly Waves. *J. Climate* **19**: 5405–5421.
- Meier F, Knippertz P. 2009. Dynamics and predictability of a heavy dry-season precipitation event over western Africa – sensitivity experiments with a global model. *Mon. Weather Rev.* **137**: 189–206. doi: 10.1175/2008MWR2622.1.
- Methven J, Hoskins BJ, Heifetz E, Bishop CH. 2005. The counter-propagating Rossby wave perspective on baroclinic instability. Part IV: nonlinear life cycles. *Q. J. R. Meteorol. Soc.* **131**: 1425–1440.
- Mounier F, Kiladis GN, Janicot S. 2007. Analysis of the dominant mode of convectively coupled Kelvin waves in the West African monsoon. *J. Climate* **20**(8): 1487–1503.
- National Hurricane Center (2015). Best Track Data (HURDAT2). <http://www.nhc.noaa.gov/data/#hurdat> (accessed 23 July 2016).
- Omotosho JB. 1985. The separate contribution of line squalls, thunderstorms and the monsoon to the total rainfall in Nigeria. *J. Climatol.* **5**: 543–552.
- Parker DJ. 2008. A simple model of coupled synoptic waves in the land surface and atmosphere of the northern Sahel. *Q. J. R. Meteorol. Soc.* **134**: 2173–2184. doi: 10.1002/qj.343.

- Parker DJ, Thorncroft CD, Burton RR, Diongue-Niang A. 2005a. Analysis of the African easterly jet, using aircraft observations from the JET2000 experiment. *Q. J. R. Meteorol. Soc.* **131**: 1461–1482. doi: 10.1256/qj.03.189.
- Parker DJ, Burton RR, Diongue-Niang A, *et al.* 2005b. The diurnal cycle of the West African monsoon circulation. *Q. J. R. Meteorol. Soc.* **131**: 2839–2860.
- Parsons DB, Yoneyama K, Redelsperger JL. 2000. The evolution of the tropical western Pacific atmosphere–ocean system following the arrival of a dry intrusion. *Q. J. R. Meteorol. Soc.* **126**: 517–548.
- Payne SW, McGarry MM. 1977. The relationship of satellite inferred convective activity to easterly waves over West Africa and the adjacent ocean during phase III of GATE. *Mon. Weather Rev.* **105**: 413–420.
- Pierrehumbert RT. 1998. Lateral mixing as a source of subtropical water vapor. *Geophys. Res. Lett.* **25**: 151–154.
- Pierrehumbert RT, Roca R. 1998. Evidence for control of Atlantic subtropical humidity by large scale advection. *Geophys. Res. Lett.* **25**: 4537–4540.
- Piersig W. 1944[1936]. Variations of pressure and winds, a treatise on the weather of trade wind region of eastern North Atlantic. *Bull. Am. Meteorol. Soc.* **25**: 2–16. (English translation of parts 2 and 3 of ‘Schwankungen von Luftdruck und Luftbewegung, sowie ein Beitrag zum Wettergeschehen im Passatgebiet des östlichen Nordatlantischen Ozeans’, Archiv D, Deutschen Seewarte, Bd 54, No. 6, 1936.)
- Poan DE. 2013. Documentation and physical interpretation of the African monsoon intra-seasonal variability for improved weather forecasts. PhD thesis, Université Paul Sabatier, Toulouse, France.
- Poan DE, Roehrig R, Couvreux F, Lafore J-P. 2013. West African monsoon intraseasonal variability: a precipitable water perspective. *J. Atmos. Sci.* **70**: 1035–1052. doi: 10.1175/JAS-D-12-087.1.
- Poan DE, Lafore J-P, Roehrig R, Couvreux F. 2015. Internal processes within African easterly wave system. *Q. J. R. Meteorol. Soc.* **141**: 1121–1136. doi: 10.1002/qj.2420.
- Pytharoulis I, Thorncroft CD. 1999. The low-level structure of African easterly waves in 1995. *Mon. Weather Rev.* **127**: 2266–2280.
- Rác Z, Smith RK. 1999. The dynamics of heat lows. *Q. J. R. Meteorol. Soc.* **125**: 225–252.
- Redelsperger JL, Parsons DB, Guichard F. 2002. Recovery processes and factors limiting cloud-top height following the arrival of a dry intrusion observed during TOGA COARE. *J. Atmos. Sci.* **59**: 2438–2457.
- Reed RJ, Norquist DC, Recker EE. 1977. The structure and properties of African wave disturbances as observed during phase III of GATE. *Mon. Weather Rev.* **105**: 17–33.
- Roca R, Lafore JP, Piriou C, Redelsperger JL. 2005. Extra-tropical dry air intrusions into the West African monsoon mid-troposphere: an important factor for the convective activity over Sahel. *J. Atmos. Sci.* **62**: 390–407.
- Roehrig R, Chauvin F, Lafore JP. 2011. 10–25-day intraseasonal variability of convection over the Sahel: a role of the Saharan heat low and midlatitudes. *J. Climate* **24**: 5863–5878. DOI:10.1175/2011JCLI3960.1.
- Ross RS. 1991. Energetics of African wave disturbances derived from the FSU Global Spectral Model. *Meteorol. Atmos. Phys.* **45**(3): 139–158. doi: 10.1007/BF01029651.
- Rowell DP, Milford JR. 1993. On the generation of African squall lines. *J. Climate* **6**: 1181–1193.
- Rowell S, Hodges KI, Cornforth RJ. 2016. Hurricane Katrina, August 2005 – an African easterly wave study. *Mon. Weather Rev.* in press.
- Schrage JM, Fink AH. 2007. Use of a rain gauge network to infer the influence of environmental factors on the propagation of quasi-linear convective systems in West Africa. *Weather Forecast.* **22**: 1016–1030.
- Schrage JM, Fink AH. 2012. Nocturnal continental low-level stratus over tropical West Africa: observations and possible mechanisms controlling its onset. *Mon. Weather Rev.* **140**: 1794–1809. doi: 10.1175/MWR-D-11-00172.1.
- Schuster R, Fink AH, Knippertz P. 2013. Formation and maintenance of nocturnal low-level stratus over the southern West African monsoon region during AMMA 2006. *J. Atmos. Sci.* **70**: 2337–2355. doi: 10.1175/JAS-D-12-0241.1.
- Seck A. 1962. Le Heug ou pluies de saison sèche au Sénégal (The Heug or dry season rainfall in Sénégal). *Ann. Géograph.* **385**: 225–246.
- Simpson RH, Frank N, Shideler D, Johnson HM. 1968. Atlantic tropical disturbances, 1967. *Mon. Weather Rev.* **96**: 251–259.
- Smith RK, Spengler T. 2011. The dynamics of heat lows over elevated terrain. *Q. J. R. Meteorol. Soc.* **137**: 250–263. doi: 10.1002/qj.737.
- Spengler T, Smith RK. 2008. The dynamics of heat lows over flat terrain. *Q. J. R. Meteorol. Soc.* **134**: 2157–2172.
- Spengler T, Smith RK, Reeder MJ. 2005. The dynamics of heat low in simple background flows. *Q. J. R. Meteorol. Soc.* **131**: 3147–3165.
- Stein THM, Parker DJ, Delanoe J, *et al.* 2011. The vertical cloud structure of the West African monsoon: a 4 year climatology using CloudSat and CALIPSO. *J. Geophys. Res. Atmos.* **116**(D22): D22205. doi: 10.1029/2011JD016029.
- Sultan B, Janicot S, Diedhiou A. 2003. The West African monsoon dynamics. Part I: documentation of intra-seasonal variability. *J. Climate* **16**: 3389–3406. doi: 10.1175/1520-0442(2003)016<3389:TWAMDP>2.0.CO;2.
- Taylor CM. 2008. Intraseasonal land–atmosphere coupling in the West African monsoon. *J. Climate* **21**: 6636–6648.
- Taylor CM, Clark DB. 2001. The diurnal cycle and African easterly waves: a land surface perspective. *Q. J. R. Meteorol. Soc.* **127**: 845–867.
- Taylor CM, Parker DJ, Lloyd CR, Thorncroft CD. 2005. Observations of synoptic scale land surface variability and its coupling with the atmosphere. *Q. J. R. Meteorol. Soc.* **131**: 913–938.

- Thorncroft CD, Blackburn M. 1999. Maintenance of the African easterly jet. *Q. J. R. Meteorol. Soc.* **125**: 763–786. doi: 10.1002/qj.49712555502
- Thorncroft CD, Flocas HA. 1997. A case study of Saharan cyclogenesis. *Mon. Weather Rev.* **125**: 1147–1165.
- Thorncroft, CD and Hoskins, BJ. 1994. An idealized study of African easterly waves. *Part I: a linear view.* *Q. J. R. Meteorol. Soc.* **120**: 953–982.
- Thorncroft CD, Parker DJ, Burton RR, *et al.* 2003. The JET2000 Project – aircraft observations of the African easterly jet and African easterly waves. *Bull. Am. Meteorol. Soc.* **84**: 337–351. doi: 10.1175/BAMS-84-3-337.
- Thorncroft CD, Hall NMJ, Kiladis GN. 2008. Three-dimensional structure and dynamics of African easterly waves. Part III: genesis. *J. Atmos. Sci.* **65**: 3596–3607.
- Tomas RA, Webster PJ. 1994. Horizontal and vertical structure of cross-equatorial wave propagation. *J. Atmos. Sci.* **51**: 1417–1430. doi: 10.1175/1520-0469(1994)051<1417:HAVSOC>2.0.CO;2.
- Tyner B, Ayyer A. 2012. Evolution of African easterly waves in potential vorticity fields. *Mon. Weather Rev.* **140**: 3634–3652. doi: 10.1175/MWR-D-11-00170.1.
- Van der Linden R, Fink AH, Redl R. 2015. Satellite-based climatology of low-level continental clouds in southern West Africa during the summer monsoon season. *J. Geophys. Res. Atmos.* **120**: 1186–1201. doi: 10.1002/2014JD022614.
- Ventrice MJ, Thorncroft CD. 2013. The role of convectively coupled atmospheric Kelvin waves on African easterly wave activity. *Mon. Weather Rev.* **141**: 1910–1924. doi: 10.1175/MWR-D-12-00147.1.
- Ventrice MJ, Thorncroft CD, Janiga MA. 2012. Atlantic tropical cyclogenesis: a three-way interaction between an African easterly wave, diurnally varying convection, and a convectively coupled atmospheric Kelvin wave. *Mon. Weather Rev.* **140**: 1108–1124.
- Walker J, Rowntree PR. 1977. The effect of soil moisture on circulation and rainfall in a tropical model. *Q. J. R. Meteorol. Soc.* **103**: 29–46.
- Waugh DW, Polvani LM. 2000. Climatology of intrusions into the tropical upper troposphere. *Geophys. Res. Lett.* **27**: 3857–3860. doi: 10.1029/2000GL012250.
- Webster PJ, Holton JR. 1982. Cross-equatorial response to middle-latitude forcing in a zonally varying basic state. *J. Atmos. Sci.* **39**: 722–733. doi: 10.1175/1520-0469(1982)039<0722:CERTML>2.0.CO;2.
- Wernli H, Sprenger M. 2007. Identification and ERA-15 climatology of potential vorticity streamers and cutoffs near the extratropical tropopause. *J. Atmos. Sci.* **64**: 1569–1586. doi: 10.1175/JAS3912.1.
- Wu M-LC, Reale O, Schubert SD. 2013. A characterization of African easterly waves on 2.5–6-day and 6–9-day time scales. *J. Climate* **26**: 6750–6774. doi: 10.1175/JCLI-D-12-00336.1.
- Zipser EJ, Twohy CH, Tsay S-C, *et al.* 2009. The Saharan air layer and the fate of African easterly waves – NASA's AMMA field study of tropical cyclogenesis. *Bull. Am. Meteorol. Soc.* **90**: 1137–1156.

Repository KITopen

Dies ist ein Postprint/begutachtetes Manuskript.

Empfohlene Zitierung:

Cornforth, R.; Mumba, Z.; Parker, D. J.; Berry, G.; Chapelon, N.; Diakaria, K.; Diop-Kane, M.; Ermert, V.; Fink, A. H.; Knippertz, P.; Lafore, J. P.; Laing, A.; Lepape, S.; Maidment, R.; Methven, J.; Orji, B.; Osika, D.; Poan, E.; Roca, R.; Rowell, S.; Smith, R.; Spengler, T.; Taylor, C. M.; Thorncroft, C.; Vincendon, J.-C.; Yorke, C.; Thorncroft, C.

[Synoptic Systems](#).

2017. Meteorology of Tropical West Africa : The Forecasters' Handbook.

Ed.: D. Parker, John Wiley and Sons.

doi: [10.5445/IR/1000067805](https://doi.org/10.5445/IR/1000067805)

Zitierung der Originalveröffentlichung:

Cornforth, R.; Mumba, Z.; Parker, D. J.; Berry, G.; Chapelon, N.; Diakaria, K.; Diop-Kane, M.; Ermert, V.; Fink, A. H.; Knippertz, P.; Lafore, J. P.; Laing, A.; Lepape, S.; Maidment, R.; Methven, J.; Orji, B.; Osika, D.; Poan, E.; Roca, R.; Rowell, S.; Smith, R.; Spengler, T.; Taylor, C. M.; Thorncroft, C.; Vincendon, J.-C.; Yorke, C.; Thorncroft, C.

[Synoptic Systems](#).

2017. Meteorology of Tropical West Africa : The Forecasters' Handbook.

Ed.: D. Parker, 40–89, John Wiley and Sons.

doi: [10.1002/9781118391297.ch2](https://doi.org/10.1002/9781118391297.ch2)

Lizenzinformationen: [KITopen-Lizenz](#)